Ministero dell'Istruzione, dell'Università e della Ricerca

UNIVERSITY OF SALERNO

Department of Civil Engineering

PhD course in
Risk and Sustainability in Civil Engineering, Architecture and Environmental Engineering Systems

Cycle XXXII (2016-2019)

A NEW METHOD FOR CHARACTERIZING AND FORECASTING THE EVOLUTION OF SLOPE MOVEMENTS

Maria Rosaria Scoppettuolo

Supervisor
Prof. Leonardo Cascini

Coordinator
Prof. Fernando Fraternali

Co-supervisor
Dr. Enrico Babilio

Index

List of Figures

List of Tables

Sommario

La caratterizzazione e la previsione dell'evoluzione dei movimenti di versante sono temi ampiamente studiati a causa delle possibili conseguenze delle frane su edifici, infrastrutture ed in termini di perdite umane. La letteratura scientifica internazionale fornisce analisi e modellazioni dettagliate di specifici fenomeni, mentre è mancante una procedura generalizzata volta ad identificare proprietà comuni delle frane.
In questa tesi è presentato uno schema generale per la comprensione di andamenti tipici dei movimenti di versante, con l'obiettivo di classificare le fasi di attività delle frane e predire la loro evoluzione nel tempo. A questo scopo, si sono raccolti i dati di monitoraggio di spostamenti di molteplici casi studio presenti in letteratura che differiscono per materiali, geometria e fattori innescanti. Questi dati sono analizzati riferendosi a singole fasi di attività, selezionate sulla base delle proprietà geometriche delle serie di dati e delle variazioni delle cause innescanti.
Successivamente, sono stati costruiti diagrammi adimensionali di spostamento, permettendo l'identificazione di alcuni trend, ciascuno caratterizzato da comuni leggi di crescita relative solo allo stadio evolutivo indipendentemente dalle specifiche caratteristiche in termini di dimensioni, geometria, materiali e così via.
I trend adimensionali sono analizzati tramite le derivate della funzione di spostamento fino al terzo ordine, ossia velocità, accelerazione e jerk. Segno e crescita delle derivate permette di identificare caratteristiche comuni nell'evoluzione delle frane. Quindi, si è introdotta una opportuna funzione interpolante dei dati di spostamento al fine di sviluppare un algoritmo di previsione capace di stabilire livelli di allerta utili in sistemi di preallarme.
Tale algoritmo è applicato ai casi di letteratura e alla frana di La Saxe (Courmayeur, Valle d'Aosta, Italy) per cui sono disponibili dati di monitoraggio continuo, con una frequenza di acquisizione di un'ora. Si sono ottenuti trend adimensionali in termini di spostamento, velocità e jerk, mostrando una correlazione soddisfacente con la reale evoluzione temporale dei movimenti franosi. Inoltre, l'algoritmo di previsione è applicato ad un'importante collasso che ha coinvolto localmente la frana di La Saxe e ad alcune instabilità in una miniera a cielo aperto, mostrando la capacità del metodo nello stabilire utili livelli di allarme.

Abstract

Characterizing and forecasting the evolution of slope movements are highly studied topics due to the possible consequences of landslides on buildings, infrastructures and in terms of loss of life. The international scientific literature provides detailed analysis and modelling of specific phenomena, whereas a generalized procedure aimed at identifying common properties of landslides is lacking.
In this thesis a general framework for understanding typical behaviours of slope movements is presented, with the aim of classifying stages of activity of landslides and predicting their time evolution. For this purpose, monitoring displacement data are collected for several case studies from literature that differ in materials, geometry and triggering factors. These data are analysed referring to single activity stages, selected on the basis of geometric properties of data series and on variations of triggering causes. Thereafter, displacement dimensionless diagrams are constructed, allowing the identification of some trends, each characterized by common growth properties related only to the evolutive stage not depending on the specific characteristics in terms of dimensions, geometry, materials and so on.
Dimensionless trends are analysed through the derivatives of displacement function up to the third order, namely velocity, acceleration and jerk. Sign and growth properties of derivatives allow identifying common characteristics in the evolution of landslides. Hence, an appropriate interpolating function of displacement data is introduced in order to develop a forecasting algorithm able to establish alert levels useful in early warning systems.
This procedure is applied to the cases from literature and to La Saxe rockslide (Courmayeur, Valle d'Aosta, Italy) for which continuous monitoring data are available with a sampling frequency of one hour. Dimensionless trends are obtained in terms of displacements, velocities, accelerations and jerks, showing a satisfying correlation with actual time evolution of landslide motions. In addition the forecasting algorithm is applied to an important failure that locally involved La Saxe rockslide and to some instabilities in an open pit mine, showing the capability of the method in establishing useful alert levels.

Acknowledgements

At the end of this PhD course I would like to thank the people who were part of it.

First of all I would like to thank my supervisor, Professor Leonardo Cascini, for being a precious guide for me in these years and for the important lessons I learned from him. I also want to acknowledge my co-supervisor Enrico Babilio for his precious support, suggestions and encouragements during the development of this research.

I would like to thank Dr. Davide Bertolo and Eng. Patrick Thuegaz of the Geological Survey of Regione Valle d'Aosta (RVDA) and Prof. Nicola Casagli of University of Florence (UniFi) for providing the data used for the validation of the method.

I want to thank all the professors, researchers, PhD students and technicians of Geotechnical Laboratory, for advice, discussions, experiences and all the valuable moments we spent together.

I am very grateful to my parents for their constant support and comprehension throughout all my university studies and especially in this particular and difficult period. Thank you to my brothers, Mauro and Pasquale, for being always present during these years with their jokes and their kindness.

Sincere thanks to my PhD friends Giuseppe and Maria Grazia for the strange discussions, the advice and especially for the laughs. Thank you to Adele, Mirella and Mario for all the moments we shared in these years, firstly in Fisciano and now on Whattsapp.

Finally, the most special thanks to Nicola, always on my side, from my first day as a PhD student until today. Thank you for believing in me and in my work, for your patience, for your engineering point of view and, above all, for your love. This thesis is for you.

About the Author

Maria Rosaria Scoppettuolo graduated in July 2016 in Land and Environmental Engineering – Soil conservation - at University of Salerno with 110/110 cum laude. In November 2016 she started her PhD course in Risk and Sustainability in Civil, Architectural and Environmental Engineering (Cycle XXXII) at University of Salerno. During her PhD course she deals with modelling kinematic evolution of slope movements, analysing a large variety of phenomena. She deepened these themes attending several courses within the PhD programme, among which LARAM school (LAndslide Risk Assessment and Mitigation). She published some of the achieved results on an International Journal and presented her work in some conferences, such as IARG (Incontro annuale dei ricercatori di Geotecnica) in 2017, in which she was a relator.

Maria Rosaria Scoppettuolo si è laureata in Ingegneria per l'Ambiente ed il Territorio – Difesa del suolo – all'Università degli Studi di Salerno con la votazione di 110/110 e lode. A Novembre 2016 inizia il corso di dottorato in Rischio e sostenibilità nei sistemi dell'ingegneria civile, edile ed ambientale (XXXII ciclo) all'Università degli Studi di Salerno. Durante il suo corso di dottorato si è occupata della modellazione dell'evoluzione cinematica dei movimenti di versante, analizzando una grande varietà di fenomeni. Ha approfondito questi temi frequentando diversi corsi all'interno del corso di studi, tra cui la scuola LARAM (LAndslide Risk Assessment and Mitigation). Ha pubblicato parte dei risultati conseguiti su Rivista Internazionale ed ha presentato il suo lavoro in alcune conferenze, come lo IARG (Incontro annuale dei ricercatori di Geotecnica) nel 2017, in cui è stata relatrice.

1. Introduction

Landslides are natural phenomena widespread all over the world and the related consequences strictly depend on the kinematic evolution of the slope movement.
Slow moving landslides cause essentially economic losses with damages to structures and infrastructures, whereas fast slope movements can generate more dangerous effects, often causing casualties.
Indeed, the study of the kinematic evolution of slope movements represents a crucial topic, widely discussed in the scientific literature. Moreover, forecasting displacements and displacement rates of landslides is a relevant goal for any modern society, mainly to assure the safety of people directly impacted.
The aim of this Thesis is to present a method that, through the analysis of displacement data, is able to characterize the movement typology and to forecast the future evolution, establishing alert levels, useful in early warning procedure.
To this aim Chapter 2 introduces main concepts about landslides, starting from the collection of data about the diffusion and the causes of these phenomena. Then, from the analysis of the Scientific Literature, most commonly used classification systems are briefly described.
In Chapter 3, after a brief description of creep phenomena, some forecasting methods are presented. Among these Fukuzono-Voight proposal (Fukuzono 1985, Voight, 1988) is analysed in detail, focusing on its applicability in early warning systems and its limitations.
In Chapter 4 a dimensional analysis of several case studies selected from the Scientific Literature is developed, observing that common behaviours in displacement data series are identifiable using a normalization procedure (Grimaldi, 2008). In fact, obtained dimensionless diagrams preliminary allow recognizing common growth properties of different activity stages, independently from material composition, dimensions and geometry of the moving body of landslides.
In Chapter 5, derivatives of displacement data are computed up to the third order, obtaining the behaviour of velocity, acceleration and jerk, that represents the derivative of the acceleration over time. The analysis of the derivatives allows obtaining a mechanical description of landslide evolution, which is useful both for phenomenon interpretation and forecasting. Particularly, acceleration is directly

proportional to the system of forces acting on the landslide body, whereas jerk is associated to the variation of these forces over time.

In Chapter 6 a descriptive parameter is introduced for studying, in a concise way, kinematic characteristics of the landslide movement through the use of an interpolation function. This leads to the development of an approach to forecast landslide failure and to fix alert thresholds based on the new parameter. The procedure is preliminarily validated referring to La Saxe rockslide (Valle d'Aosta, Italy) and to an undisclosed open pit mine (Carlà et al., 2017) for which continuous monitoring data are available.

In Chapter 7 a perspective for describing physical mechanisms underlying trends is presented. To this aim, stability theory of dynamic systems, according to Lyapunov' study (1892), is applied to a simplified scheme of slope, highlighting the role played by the different physical quantities acting on the landslide body for active slow movements.

Finally, in Chapter 8, concluding remarks are presented summarizing the potential and limitations of the proposed method.

2. Slope movements

Landslides are natural phenomena, widespread all over the world, that Cruden (1991) defined as “the movement of a mass of rock, earth or debris down a slope”.
This is a general definition, very impressive but not comprehensive, since it does not give specific information about important features as dimensions and geometry of the moving body, mechanical properties of the materials, shape of the surface along which the landslide motion develops. For this reason, the use of a classification is required to better specify the type of the considered phenomenon.
In this chapter, firstly a series of data from some datasets and inventories are presented, with the aim of understanding the dimension of the problem.
Secondly, a description of the main causes of landslides is reported with indications about their distribution on the Italian territory.
Then, the main classification systems proposed in the scientific literature are described with the aim of introducing a general framework about landslides.
Finally, focusing on translational and rotational slides, some models used in describing the dynamic of slopes are presented.

2.1 Diffusion

To better understand the diffusion of the phenomena, it is possible to refer to several studies in the international literature that provide datasets and inventory maps.
Datasets enumerate landslide events referring to global, continental and national scales, whereas inventory maps localize these events over smaller areas.
From a global point of view, we can refer to international datasets, as for example NatCatSERVICE (Natural catastrophe statistics online – Munich Re, 2018) that records a total number of 7,355 hydrological events, such as floods and landslides, corresponding to 251,157 victims in the period 1980-2018.
Petley (2012) enumerated 2,620 non seismic fatal landslides during the period from 2004 to 2010, causing a total of 32,322 victims, on the basis of analysis from government statistics, aid agency reports and research papers. According to the Authors, events are mostly concentrated in Asia, in particular on the Himalayan Arc and in China, the Philippines and Indonesia.

More recently, Froude and Petley (2018) updated the study of Petley (2012) carrying out a new analysis, identifying 4,862 fatal landslides associated with 55,997 people for the period from January 2004 to December 2016. Spatial distribution of these events are presented by the Authors in Figure 2.1, with the indication of the number of landslides.

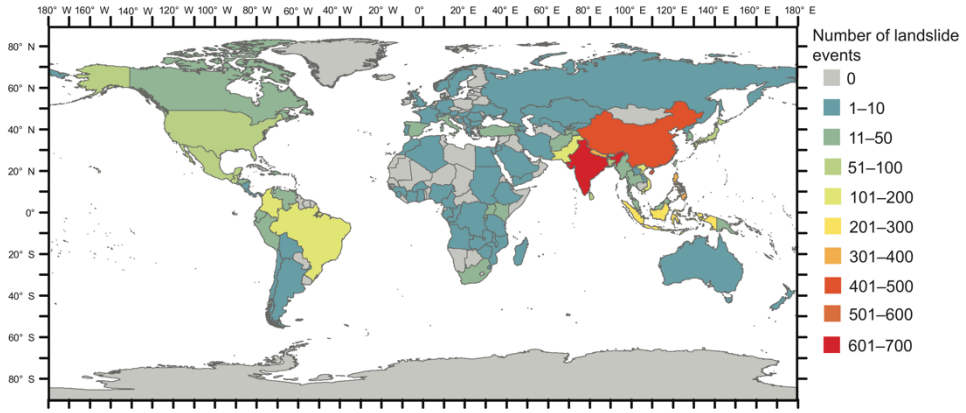

Figure 2.1: Number of non-seismically induced landslides for country in the period between January 2004 and December 2016 (Froude and Petley, 2018)

Kirschbaum et al. (2015) presented a global landslide catalogue (GLC), based on media reports, online datasets and other sources. They counted 5,741 landslides in the period 2007-2013, mainly occurring in Asia and North America, during the period from July to September. In addition, they recorded about 20,500 fatalities in correspondence of 1,827 events (~30% of the total number of enumerated landslides).

Regarding to the European situation, Haque et al. (2016) counted 476 fatal landslides, associated with 1,370 deaths and 784 injuries, recorded in the period from 1995 to 2014 in 27 European countries. Actually, they analysed a total of 49 states 37 of them affected by non-fatal landslides. The most hit countries were: Turkey, Italy, Russia and Portugal.

Landslide susceptibility in Europe is testified by several maps that assesses the typology, volume (or area) and spatial distribution of landslides which exist or potentially may occur in an area.

Günther et al. (2013) proposed a landslide susceptibility map which covers 27 EU countries excluding Cyprus and adding Norway, Switzerland and the Balkan states, using an heuristic approach based on geoenvironmental information available from public sources (Figure 2.2).

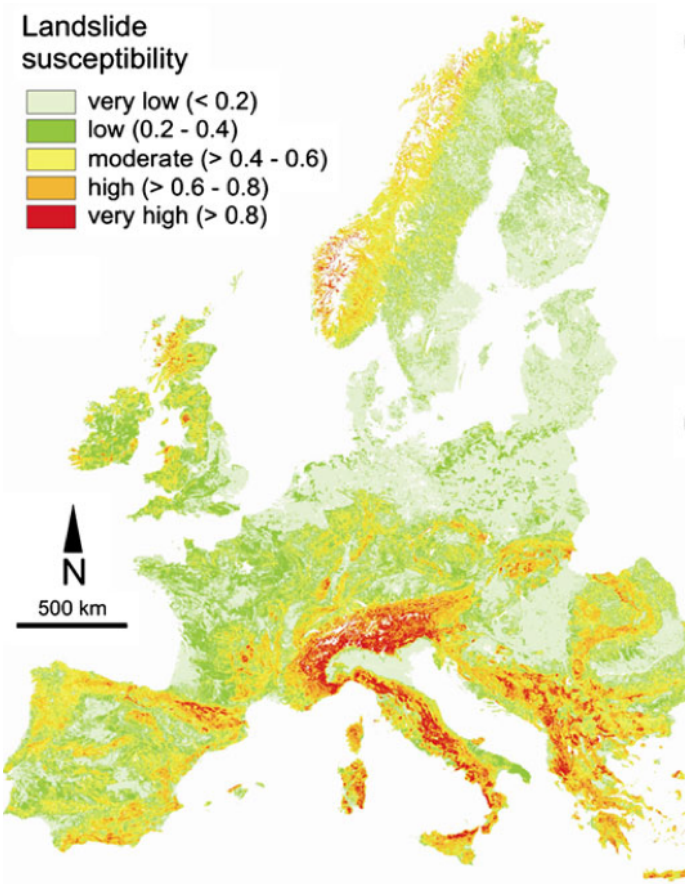

Figure 2.2: Landslide susceptibility in Europe (Günther et al., 2013)

Focusing on Italy, we can refer to the AVI project (Guzzetti et al. 1994) - the acronym of "Aree Vulnerate Italiane"- that is the catalogue of Italian areas affected by landslides and floods, developed by the CNR ("Consiglio Nazionale della Ricerca"). For the period 1918-1994, the project enumerated a total of 9,086 catastrophic events and produced a map, reporting 2,608 areas affected periodically by landslides.

A more recent inventory is the one proposed by ISPRA ("Istituto Superiore per la Protezione e la Ricerca Ambientale"), the so-called IFFI project ("Inventario dei Fenomeni Franosi in Italia"), that gives a general framework on the distribution of landslides in Italy. Currently, the total number of the recorded phenomena is 620,808, involving an area of 23,700 km^2, corresponding to 7.9% of the Italian territory. Figure 2.3 shows the map, reporting the landslides density (in Italian "indice di franosità") defined as the ratio between landsliding and total areas, computing on a square of 1 km^2 .

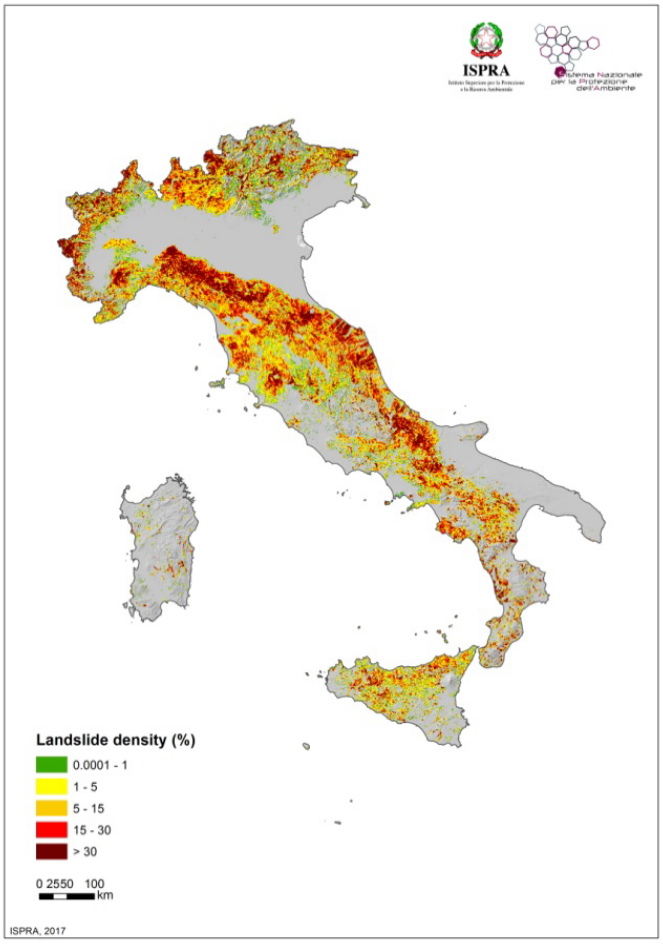

Figure 2.3: Landslide density for Italy (ISPRA, 2018)

Calvello and Pecoraro (2018) developed *FraneItalia* catalogue, enumerating 8,931 landslides, in the period from January 2010 to December 2017. The phenomena, divided in areal landslide events (938) and single landslide events (4,231), are mainly diffused in the mountainous areas, in correspondence of Alpes and Apennines.
All the mentioned studies testify the large diffusion of the landslides in the world, causing large economic damages and, in the case of catastrophic events, important economic damages and less frequent human loss.

2.2 Landslide causes

An important role in analysis and mostly in definition of mitigation measures for a landslide phenomenon is represented by the knowledge about the causal factors that

lead to movement. Several Authors try to classify the different typologies of causes affecting a slope.
According to Terzaghi (1950) the factors which control slope instability can be divided in internal and external ones. Internal factors, that correspond to a decrease in shear strength, are: geo-structural setup (lithology, morphology, tectonic structures), mechanical behaviour of the materials (strength and stiffness), hydraulic regime of the slope. External factors, that lead to an increase in shearing stresses, are: rainfalls, earthquakes, anthropic actions and morphological evolution.
Landslide causes are commonly divided in preparatory or predisposing factors, that increase the probability that the slope suffers a movement, and triggering factors, that cause the actual beginning of the movement. Popescu (1994) proposed four classes of causal factors (Figure 2.4), three of which can be defined both preparatory and triggering.

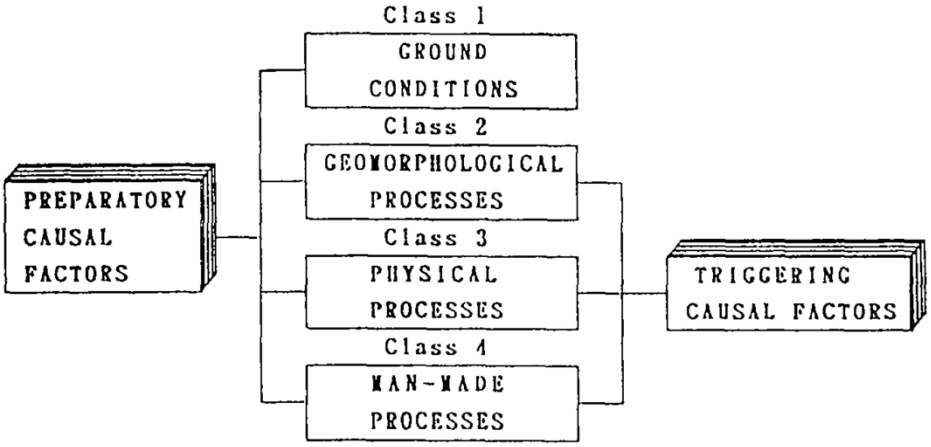

Figure 2.4: Classification of preparatory and triggering factors (Popescu, 1994)

Ground conditions are intrinsic mechanical characteristics of involved materials and they cannot be triggering factors; geomorphological processes are represented by tectonic or volcanic uplift, erosion, piping, vegetation removal etc; physical processes are related to climatic conditions such as rainfalls, snowmelt, freeze and thaw weathering or earthquakes and volcanic eruptions; man-made processes are related to human actions on the slope such as excavations, loadings on the crest of the slope, deforestations.
An interesting description of the major landslide causes has been proposed by U.S. Geological Survey (2004) that distinguishes between geological, morphological and human causes (Table 2.1).

Table 2.1: Landslide causes (USGS, 2004)

Geological causes	Morphological causes	Human causes
a. Weak or sensitive materials	a. Tectonic or volcanic uplift	a. Excavation of slope or its toe
b. Weathered materials	b. Glacial rebound	b. Loading of slope or its crest
c. Sheared, jointed, or fissured materials	c. Fluvial, wave, or glacial erosion of slope toe or lateral margins	c. Drawdown (of reservoirs)
d. Adversely oriented discontinuity (bedding, schistosity, fault, unconformity, contact, and so forth)	d. Subterranean erosion (solution, piping)	d. Deforestation
e. Contrast in permeability and/or stiffness of materials	e. Deposition loading slope or its crest	e. Irrigation
	f. Vegetation removal (by fire, drought)	f. Mining
	g. Thawing	g. Artificial vibration
	h. Freeze-and-thaw weathering	h. Water leakage from utilities
	i. Shrink-and-swell weathering	

IFFI project, the special report on landslides in Italy (ISPRA 2008) has highlighted the typology of causes for the about 52,000 recorded phenomena, without distinguishing between predisposing and triggering factors (Figure 2.5). Summarizing IFFI data, aimed to defining some macro-categories (Berti 2015), it is possible to conclude that in Italy:

- 35% of landslides is caused by rainfalls, both intense short period and prolonged in time;
- 9% is related to fluvial erosion of at the toe of a slope or in correspondence of the lateral margins;
- 9% is associated to temperature variations due to freeze-and-thaw cycle;
- 8% is caused by human activities.

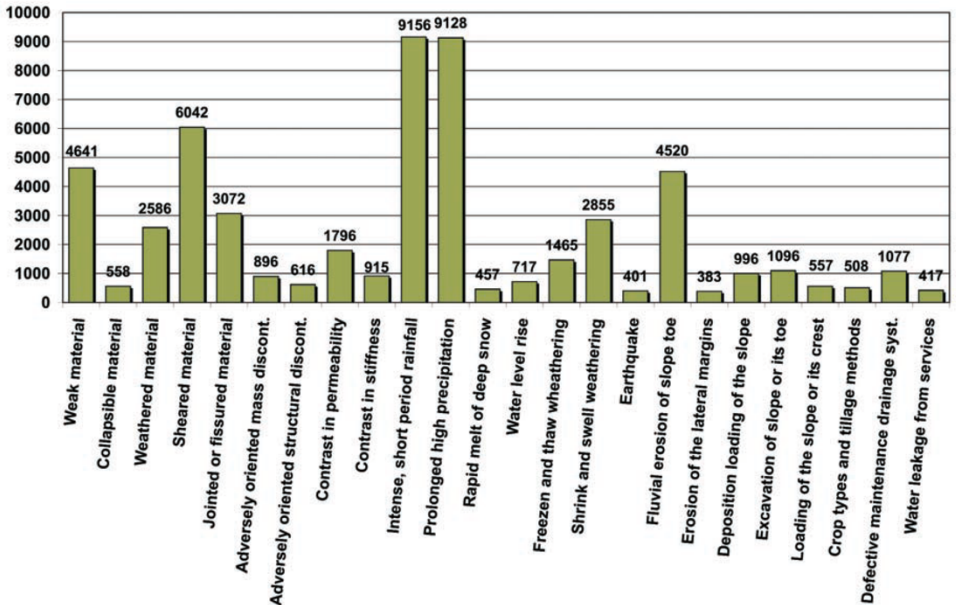

Figure 2.5: Predisposing and triggering factors for landslides in Italy (ISPRA 2008)

2.3 Classifications

With the aim of simplifying landslide study and creating a summarizing framework, landslide classification systems are proposed by several Authors in the international literature (Skempton 1953, Blong 1973, Varnes 1978, Hutchinson 1988, Cruden and Varnes 1996, Leroueil et al. 1996, Hungr et al. 2014), essentially to simplify landslide studies and to create a summarizing framework.

Evidently, there are a lot of features that can be used for classifying landslides and it is not possible to define an unique way to catalogue the different phenomena present in nature. Walker et al. (1987) observed that the large number of existing classifications is due to the fact that the "continuum landslide" can be divided in infinite ways; nonetheless, this heterogeneity in classifications does not allow obtaining a clear and unique terminology.

According to Hungr et al. (2014) a classification should be able to provide a framework useful to organize the main information about a specific class of landslides and to clearly communicate them to others, combined with flexibility in order to satisfy the needs of all the possible users.

The following sections present several classifications that are grouped according to the analysed characteristics, namely the type, the rate of movement and evolution stage of the landslides.

2.3.1 Typological classifications

With regard to typological and morphological classification, a first contribution was proposed by Skempton (1953) that developed a simple morphometric scheme to catalogue landslides in terms of relative depth, defined as the ratio between maximum thickness (D) and maximum length (L) of the landslide body. The Author defines thereby three categories: slumps, slides and flows (Table 2.2).

Table 2.2: Landslide type as function of the ratio D/L (Walker, 1987)

Landslide Type	D/L (%)
Slumps	15-30
Slides	5-10
Flows	0,5-3

Blong (1973) proposed a classification that distinguishes the landslides in translation slides, rotational slides, flows and falls. Translational slides are landslides with one or more slip surfaces that are rather parallel to the slope (velocity from the order of mm/s up to m/s); in rotational slides the slip surfaces are curved (velocity from the order of mm/d up to m/d); in flows the materials slide like a viscous fluid (velocity from the order of cm/min up to m/s); in falls the mass of material covers most of its movement in the air (velocity from the order of m/min up to m/s). Velocity ranges are attributed by Jahns (1978).

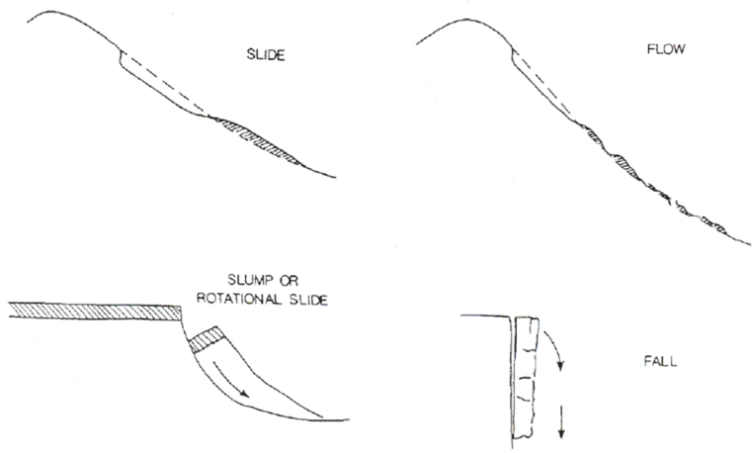

Figure 2.6: Landslide classification proposed by Blong (1973)

One of the most used classification is that proposed by Varnes (1978) who introduced some typologies of movement (falls, topples, rotational slides, translational slides, lateral spread, flow and combinations of these) associated to three different categories of material (rock, debris and earth), Table 2.3.

Table 2.3:Varnes classification system (1978)

Type of movement			Type of material		
			Bedrock	**Debris**	**Earth**
Falls			Rock fall	Debris fall	Earth fall
Topples			Rock topple	Debris topple	Earth topple
Slides	Rotational	Few units	Rock slump	Debris slump	Earth slump
	Translational	Few units	Rock block slide	Debris block slide	Earth block slide
		Many units	Rock slide	Debris slide	Earth slide
Lateral spread			Rock spread	Debris spread	Earth spread
Flow			Rock flow (deep creep)	Debris flow	Earth flow (soil creep)
Complex			Combination of two or more principal types of movement		

Falls are slope movements in which a mass detaches from a steep surface, without shear displacements; after the failure the mass drops moving in the air. Topple means the movement of a mass around a centre of rotation under the action of gravity forces. The term slide refers to the shear strain and displacement of a unit on a surface or several surfaces. When the surface propagates from a local failure, it represents a progressive failure.

Slides are defined rotational or translational depending on the shape of the sliding surface. If this is curved concavely upward, the landslide is usually defined slump and represents one of the most common slope movement.

In the translational slides the surface or the surfaces are planar or gentle undulatory. Lateral spreads consist in lateral extensions associated to shear or tensile fractures.

Flows are typical of unconsolidated materials, in wet or dry conditions. The Author uses the term creep with the meaning of deformation under constant stress (like in mechanics of materials); the velocity of deformation is usually very low, but in some cases reach higher rate of deformation close to the collapse stage. The term debris avalanche is referred to very rapid debris flows.

Finally, a landslide can be constituted by several types of movement, combined during different phases or in various parts of the body.

Regarding materials, Varnes identified three different types: bedrock, debris and earth. The term bedrock indicates hard rock, considered intact before the start of the motion. Debris and earth are defined by the Author as engineering soils, referring to loose and unconsolidated material; debris are coarse and superficial soil, earth includes materials from sand to clay.

This classification is used all over the world in many working field, even though with some modifications. The update proposed by Hungr et al. (2014) expands the original classification, reaching a total of 32 landslide types. The major

modifications concern the material terminology, that is extended introducing seven material types and a series of descriptors usable as supplementary characteristics. Regarding the types of movement, the Authors define six classes that are similar to the ones proposed by Varnes (fall, topple, slide, spread, flow) but adding slope deformations, which include soil creep. Finally, complex landslides are not present as class, attainable combining different types.
Another used classification system is the one proposed by Hutchinson (1988), that individuates 8 categories for slope movements, as indicated in Table 2.4. The Authors includes, for each category, some sub-categories to better describe characteristics of the landslides as geometry and materials.

Table 2.4: Hutchinson classification system (modified from Hutchinson, 1988)

Category	Slope movement
A	**Rebound**
1	Movements associated with man-made excavations
2	Movements associated with naturally eroded valley
B	**Creep**
1	Superficial, predominantly seasonal creep; mantle creep
2	Deep-seated, continuous creep; mass creep
3	Pre-failure creep; progressive creep
4	Post-failure creep
C	**Sagging of mountain slopes**
1	Single-sided sagging associated with the initial stages of landsliding
2	Single-sided sagging associated with the initial stages of double landsliding, leading to ridges spreading
3	Sagging associated with multiple toppling
D	**Landslides**
1	Confined failures
2	Rotational slips
3	Compound failures
4	Translational slides
E	**Debris Movements of Flow-like form**
1	Mudslides (non-periglacial)
2	Periglacial mudslides
3	Flow slides
4	Debris flows
5	Sturzstroms
F	**Topples**
1	Topples bounded by pre-existing discontinuities
2	Topples released by tension failure at rear of mass
G	**Falls**
1	Primary, involving fresh detachment of material; rock and soil falls
2	Secondary, involving loose materials, detached earlier; stone falls
H	**Complex slope movements**
1	Cambering and valley-bulging

2	Block-type slope movements
3	Abandoned clay cliffs
4	Landslides breaking down into mudslides or flows at the toe
5	Slides caused by seepage erosion
6	Multi-tiered slides
7	Multi-storeyed slides

To have an idea of the diffusion of these types of landslides, the special report of (ISPRA 2018) develops the statistics in Figure 2.7, highlighting that in Italy rotational and translational slides, followed by flow-type landslides, are the most diffused instability phenomena.

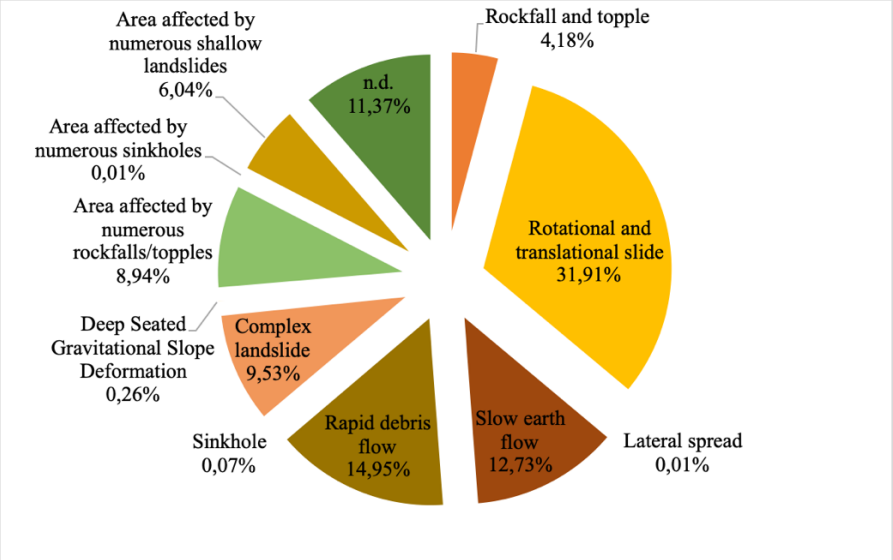

Figure 2.7: Type of movement for landslides in Italy (ISPRA, 2018)

2.3.2 Classification based on rate of movement

Rate of movement is an important parameter for a landslide because it can be related to its destructiveness. In particular, Cruden and Varnes (1996) identified seven classes, from extremely slow (16 mm/year) to extremely rapid (5 m/s) with information about the probable destructive significance, expressed in terms of expected damages (Table 2.5).

An example of the usefulness of this type of classification is provided by Cascini et al. (2005) who identified the intensity of a landslide with its maximum velocity in order to develop susceptibility maps to be used for proper territorial planning.

Table 2.5: Velocity classes for landslides (Cruden and Varnes, 1996)

Class	Description	Probable Destructive Significance	Typical velocity	Velocity (m/s)
7	Extremely rapid	Catastrophe of major violence; buildings destroyed by impact of displaced material; many deaths; escape unlikely.	5 m/s	5
6	Very rapid	Some lives lost; velocity too much to permit to the persons to escape.	3 m/min	$5 \cdot 10^{-2}$
5	Rapid	Escape evacuation possible; structures, possessions, and equipment destroyed.	1.8 m/hr	$5 \cdot 10^{-4}$
4	Moderate	Some temporary or little damageable structures can be temporarily maintained.	13 m/mounth	$5 \cdot 10^{-6}$
3	Slow	Remedial construction can be undertaken during movement; intensive structures can be maintained with frequent maintenance work if total movement is not large during a particular acceleration phase.	1.6 m/year	$5 \cdot 10^{-8}$
2	Very slow	Some permanent structures cannot be damaged from the movement	16 mm/year	$5 \cdot 10^{-10}$
1	Extremely slow	Imperceptible without monitoring instruments; construction possible with precaution.	<16 mm/year	$<5 \cdot 10^{-10}$

2.3.3 Classifications based on evolution stage

Several papers in scientific literature deal with classifications based on the evolution of slope movements, including information about state of activity, distribution, style. Cruden and Varnes (1996) formalized the glossary defined in three different Working Party on the World Landslide Inventory (WP/WLI 1990, 1991, 1993) with the aim of defining a common vocabulary for landslides.
In particular, in WP/WLI (1993) landslides are described in terms of the state of activity as (Figure 2.8):

- **Active** landslides when they are moving, both first-time motions and reactivations (1);

- **Reactivated** landslides when they are active after a period in which they have been inactive, usually sliding on pre-existing slip surface with residual strength parameters (2);
- **Suspended** landslides are those that are not currently moving but have been active during the last annual cycle (3);
- **Inactive** are called the landslides that have not moved in more than one annual seasonal cycle (4). This category includes **dormant** landslides (5) if they can be reactivated by the original trigger or others, **abandoned** landslides (6) if they are no more affected by the original cause of movement, **stabilized** landslides (7) if they are stopped by artificial measures, **relict** landslides (8) if the climatic or geomorphological conditions are considerably changed by the ones under which the slides developed.

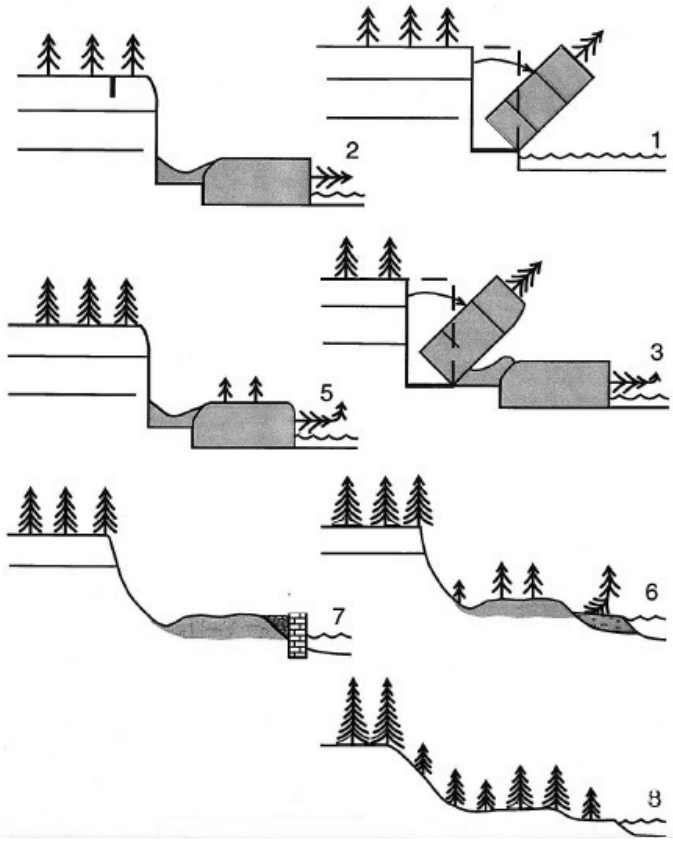

Figure 2.8: States of activity of a landslide: 1) Active landslide; 2) Suspended landslide; 3) Reactivated landslide; 5) Dormant landslide; 6) Abandoned landslide; 7) Stabilized landslide; 8) Relict landslide. (WP/WLI, 1993)

The landslides are also classified in terms of distribution:

- **Advancing** when the rupture surface propagates in the direction of movement;
- **Retrogressive** when the rupture surface propagates in the opposite direction respect the motion of the landslide;
- **Enlarging** when the rupture surface moves in more than one directions;
- **Diminishing** when the mobilized mass diminishes its volume;
- **Confined** when it is possible to detect a scarp but no presence of rupture surface is visible at the foot of the landslide.
- **Moving** when the mass moves without any visible variation in slip surface or volume;
- **Widening** when the rupture propagates in one or both flanks of the landslide body.

Furthermore, some indications are given also for style of movement:

- **Complex** are the landslides in which two or more types of movements are present in sequence;
- **Composite** landslides are characterized by two or more types of movements that occur simultaneously in different parts of the mass;
- A **successive** landslide has movements of the same type of a nearby, earlier landslide, but do not compart with it materials or rupture surface;
- A **single** landslide is a single movement of the mass;
- **Multiple** landslides are characterized by the repetition of the same type of movement.

Leroueil et al. (1996) proposed a framework consisting in a 3-D matrix for the characterization of landslides (Figure 2.9). The three axis represent activity stages, materials and movement types, extended respect the ones proposed by Varnes (1978).

The main point defined by the Authors represents a qualitative relationship for displacement rate over time, highlighting four activity stages for slope movements, regardless of the materials involved in the landsliding.

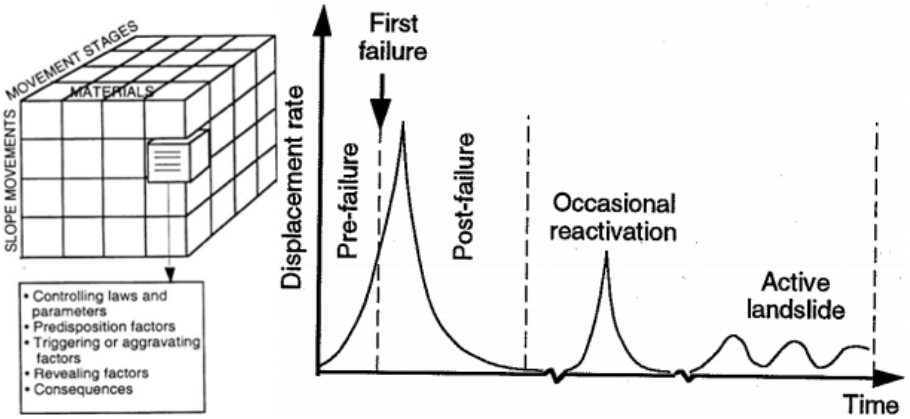

Figure 2.9: Landslides classification and activity stages for slope movements (Leroueil et al., 1996)

According to the Authors, pre-failure stage is related to intact soils before the formation of the shear band that characterizes the failure stage. This is followed by the post-failure stage that ends when the mass stops. Finally, the reactivation stage occurs when the soil mass moves along a pre-existing shear surface. The first three stages usually characterize the geological evolution of natural slopes and, engineered slopes threatened by anthropogenic factors. In all cases displacement rate and displacements are relevant in failure and post-failure stage. The reactivation stage consists of two different stages respectively related to recurrent, as seasonal rainfall, or unusual triggering factors, as earthquakes. The first ones originate the so-called active landslides that systematically suffer negligible displacements. The second ones cause an occasional reactivation of an existing landslide that suffers significant displacements not changing the original slope configuration. The reactivation stages usually involve existing landslides that suffered a first failure over a geological time.

2.4 Dynamic modelling of landslides

Motion of landslide body can be reproduced through various and more or less sophisticated models. Focusing on translational and rotational slides, sliding block analysis is largely applied. If slope keeps its basic shape during the movement, as in the case of slow landslides, the model of a rigid block on an inclined plane can be adopted. This schematization, introduced by Heim (1932), has been used by various authors in scientific literature (Helmestetter et al., 2004; Corominas et al., 2005; Secondi et al., 2011; Alonso et al., 2016).

In more complex situations, especially in the cases in which large displacements occur, a one-block scheme is not the most suitable to simulate the slope motion. In

such cases, a model representing two interacting blocks sliding on two different planes can be adopted, taking into account the changes in geometry of slope during the motion.

Such a model has been proposed by Ferrari et al. (2011) for analysing the effects of mass accumulation in the stabilization of Vallcebre landslide and by Alonso et al. (2010) for simulating the collapse of Vajont landslide. A model based on the interaction of more than two blocks have been proposed by Crosta et al. (2014) that suggested discretizing La Saxe rockslide into several rigid parts for reproducing the three dimensional geometry of the slope.

This models allow writing dynamic equations, introducing the forces acting on the landslide body, simulating triggering causes.

Dynamic equation of a single block was enhanced by Scoppettuolo and Cascini (2017) introducing a strain-rate-dependent friction angle, to take into account a variation of strength associated to sliding velocity:

$$tan\varphi' = tan\varphi'_0 + (tan\varphi'_1 - tan\,\varphi'_0)(1 - e^{-a\,v(t)}) \qquad (2.1)$$

where φ'_0 is the residual friction angle, φ'_1 is the maximum mobilized friction angle and a is a parameter of the model, whose physical dimension is TL^{-1}.

Such a dependence is testified by several experimental studies in scientific literature. La Gatta (1970, 1971), through ring shear tests, recorded a variation from -8% to +18% of the friction coefficient with an applied displacement rate from 0.0048 up to 2.4 mm/min to clays and shales samples. Bucher (1975) measured, also using ring shear tests, an increase of the friction coefficient up to +24% in clays. A synthesis of other experimental studies on the phenomenon is reported in Tika et al. (1996), that also analysed several samples in a ring shear tests, concluding that three different effects - neutral, positive and negative – are possible on the friction coefficient due to the displacement rate, depending on the characteristics of the soils. Analytical relationships between frictional coefficient and velocity have been proposed by Dieterich (1978), Ruina (1983), Davis et al. (1993), Alonso et al. (2016).

Presented studies are only a few part of existing contributions aimed at describing the dynamic mechanisms that occur inside landslide body determining the evolution of displacement behaviour, that is discussed in depth in this thesis.

3. Forecasting landslide evolution at slope scale

Chapter 2 stresses that landslides represent one of the most diffused natural hazards, causing both human losses and considerable economic damages to structures and infrastructures.
Indeed, forecasting landslide evolution and eventually the collapse of the slope represents an important task, in order to mitigate the related risk. Temporal forecasting models link evolution of landslide to some monitored quantity. Among others, displacement monitoring represents an effective tool, particularly for rockslides.
This chapter analyses the most used forecasting models proposed in the Scientific Literature, starting from a brief description of creep phenomena in soil and rock.
Afterwards, some applications of forecasting models to early warning systems are highlighted, showing both their potential and limitations.

3.1 From creep to failure

Varnes (1978) states that the term creep is used in different engineering fields as material science and earth science. However, the term assumes different meanings depending on the context in which it is used, and also in the same discipline several definitions are provided by Scientific Literature.
Mechanics of materials assumes that creep is a deformation with time under constant stress (Varnes 1978, Fell et al. 2000).
Laboratory tests show that the creep in cohesive soils is similar to the one observed for continuum materials.
Creep curve is usually described as composed by three phases namely primary, secondary and tertiary creep as shown in Figure 3.1a (Singh 1966, Emery 1971, 1979). Actually the points of separation between the different phases are not always easily identifiable, but the scheme is useful to describe the behaviour of deformation.

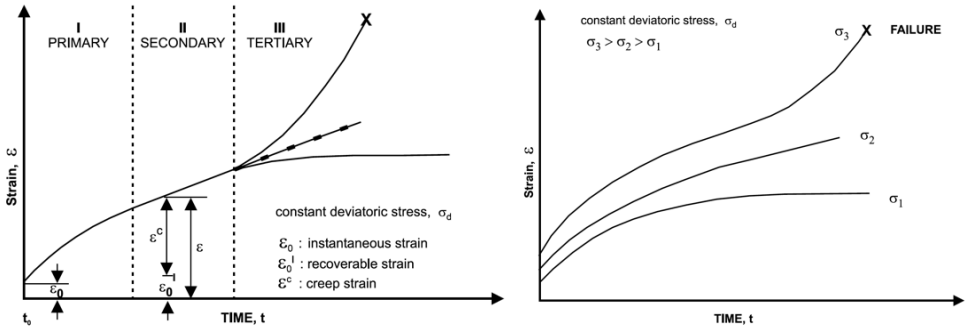

a) b)

Figure 3.1: Creep behaviour for with the indication of the three phases (a) and creep curves for different values of applied deviatoric stress (b) (Crosta and Agliardi, 2003)

Under a constant deviatoric stress, the material shows first a concave downward curve, corresponding to the so called primary or transient creep during which strain rate decreases in time. Secondary creep corresponds to a linear reach, with a strain rate that remains constant in time. Finally tertiary creep, that is the most alarming, shows an upward concave curve, corresponding to an accelerating phase that can lead to the failure. Tertiary creep and the consequent failure are not always observed in laboratory tests, depending on the value of applied stress (Figure 3.1b).

Referring to slopes, Terzaghi (1950) defined creep as "a continuous movement which proceeds at an average rate of less than a foot per decade", that can be associated to class 1 and 2 of Cruden and Varnes classification (1996).

Hutchinson (1988) defined four different categories of creep phenomena:

- superficial, predominantly seasonal creep or mantle creep, that is a typical definition of geomorphologic approach;
- deep-seated, continuous creep or mass creep, that occurs at constant stress lower than the strength of the material;
- pre-failure creep or progressive creep, in which an accelerating behaviour is recorded before the collapse;
- post-failure creep, related to reactivation occurring along an existing sliding surface.

Another interesting definition is proposed by Emery (1971) who defined slope creep as "slow, more or less continuous deformation or flow of natural and excavated slopes involving soil, rock, ice or combination materials which takes place under gravity and external loadings".

Referring to active landslides, in which pore water pressure variations are the major triggering factors, it is important to well interpret the displacements. The ones associated with creep are related to constant stress and boundary conditions,

independently from hydrological seasons. Usually, the actual movement of a landslide is the result of creeping behaviour and a seasonal trend directly associated to hydrological conditions of the slopes, not present when the water table is below the failure surface.
The study of the factors that can lead to transition between slow creeping movement to fast and dangerous evolution (tertiary creep) is a thoroughly discussed topic in Literature. Alonso et al. (2016) described the effect of high temperature generated during the sliding, that leads to a pressurization of pore water pressure, causing a loss of strength along the shear band.
Di Prisco and Flessati (2019) studied this phenomenon through a strain softening elastic–viscoplastic constitutive relationship and a simplified scheme of infinite slope, that was used to assess both the local response of a single layer and the global system in correspondence of groundwater level variation. Authors observed that local instability, associated with the increase of strain rate along the shear band, always anticipates the global one with a time interval depending on geometry and constitutive parameters, such as viscosity. This suggests that strain measurements along shear band could provide an useful forecasting tool.
In conclusion, creep phenomena in geological materials have been described with different approaches in Scientific Literature. The micro-mechanistic approach, mainly developed for thermally activated processes, tries to describe creep by studying the atomic scale of the material and by defining strain rate equations useful to describe the time-dependent deformations (Mitchell et al. 1968). Rheological or phenomenological approaches interpret creep phenomena through linear or non-linear models (using springs, dashdots, sliders and related constants) able to represent the mechanical behaviour of the real material. In the empirical approach, empirical or semi-empirical relationships are developed on the basis of laboratory tests aimed to relate strain or strain rate to physical parameters such as time, stress and temperature. The following section focuses on these latter models.

3.2 Forecasting time of failure of slopes

By analysing the creep phenomena that occur in natural and man-made slopes consisting of soils and/or rock, some Authors defined the time of failure through empirical functions that describe the deformations preceding slope collapse.
The first contribution aimed at giving a phenomenological method for failure prediction is provided by Saito and Uezawa (1961) and Saito (1965). By analysing secondary, steady-state creep in triaxial tests, these Authors defined an empirical

relationship between time of failure t_f, expressed in minutes, and strain rate $\dot{\eta}$, expressed in 10^{-4} minutes.

$$\log t_f = 2.33 - 0.916 \log \dot{\eta} \pm 0.59 \tag{3.1}$$

This result, that was not suitable to properly describe tertiary creep stage, was extended by Saito (1969), that modified previous relationship as:

$$\log(t_f - t) = \log a - \log \dot{\eta} \tag{3.2}$$

in which t is an optional time, $\dot{\eta}$ is the strain rate at time t and a is a constant.
Rearranging the equation and assuming the strain rate equal to zero at time $t = t_0$ and the strain equal to $\varepsilon = {\Delta l}/{l_0}$, the Author obtained:

$$\Delta l = a\, l_0 \log \frac{t_f - t_0}{t_f - t} \tag{3.3}$$

Δl is the relative displacement between two different measures and l_0 is the initial displacement between two different measures: moving toward the failure value of Δl increases if acquisition time is constant.
The equation (3.3), that includes three unknown constants, has been analytically and graphically solved by the Author. Choosing three points, with equal difference of displacement between each other, it is possible to delete the constants a, l_0 and, following simple steps, the time of failure t_f as function of the time t_1, t_2, t_3. The graphical procedure, that is particularly convenient, is shown in Figure 3.2.

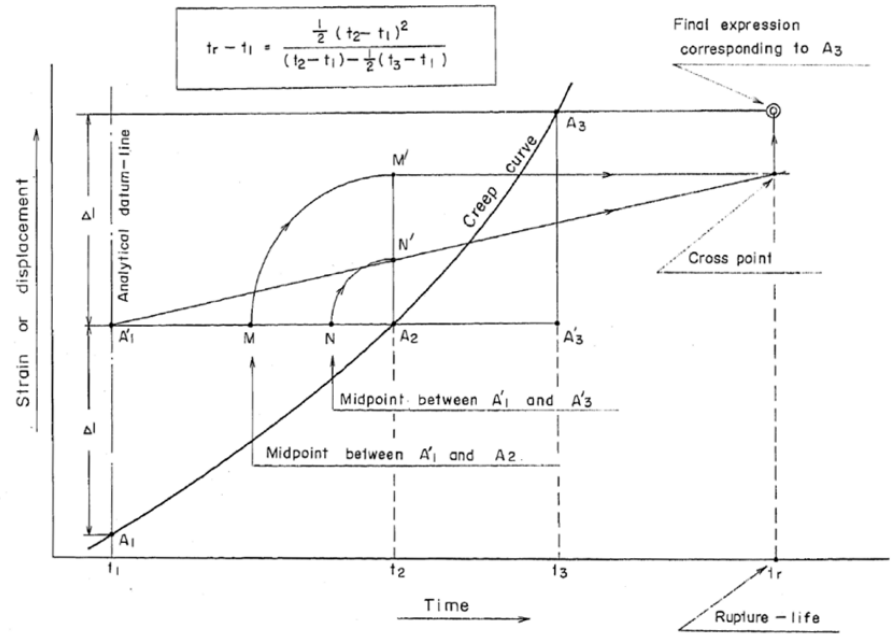

Figure 3.2: Graphical procedure to compute time of failure of landslides according to Saito (1969)

Hayashi et al. (1988) divide tertiary creep in two subsequent stages, the first one immediately after the secondary creep curve and the second one, relative to the collapse, coincident with the accelerating stage identified by Saito (1965). The method proposed by the Authors aims to obtain information of time of failure analysing the first stage of tertiary creep, and thus earlier than Saito's method. In particular, first and second stages are analysed considering the different relationships between displacement l, velocity v and time t, through observations both in indoor models and in real slopes. The proposed procedure starts from the observation that the higher is the velocity at the beginning of the first stage the closer is the failure. This concept has been expressed measuring the time Δt required for reaching a fixed displacement Δl. The relationship between Δt and time of collapse t_f is:

$$t_f = a\,\Delta t^n \tag{3.4}$$

in which a and n are two constants, respectively equal to 2.13 and 1.6 for actual slopes if $\Delta l = 10\ cm$.

Figure 3.3a shows the behaviour of displacements over time for the failures of Agoyama and Jizukiyama landslides. Figure 3.3b reports Δt as function of t_f for real slopes, fixing $\Delta l = 10\ cm$.

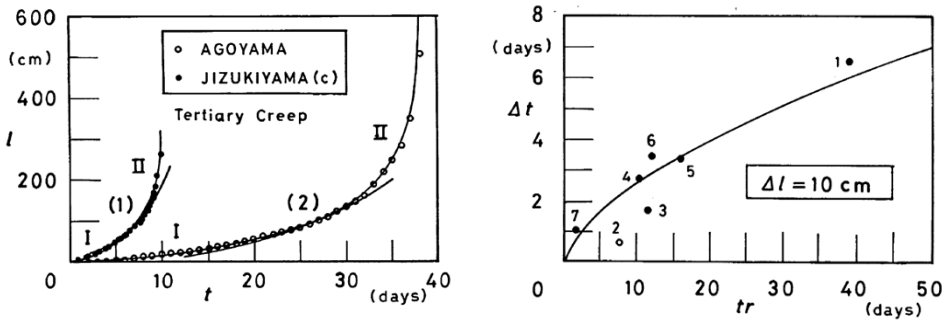

a) b)

Figure 3.3: a) Displacement over time in tertiary creep for the failure of Agoyama and Jizukiyama landslides; b) Relationship between elapsed time and time of failure for slope failures (Hayashi et al., 1988)

Asaoka (1978) analysed the final step of edometric tests with a graphical approach, that Azimi (1988) applied to forecast the collapse of slopes. After the plot of displacements in time, according to the procedure, the curve is divided in equal displacement intervals Δd. The series of time values $(t_0, t_1, .., t_i, ... t_n)$ associated to each displacement point is plotted in a diagram with t_{i-1} and t_i as axes. The point indicating the failure time is detected when regression line of these points and the line corresponding to the plane bisector $(t_i = t_{i-1})$ intersect.

Fukuzono (1985, 1990) carried out experimental studies on a scale model of a slope, with a height of 5 meters, a width of 4 meters and with a soil layer with a thickness of 1 meter. The Author induced failure on the model through an artificial rainfall and monitored the displacements during the process. Analysing the measures, it was possible to obtain a proportional relationship between the logarithm of displacement rate $(\dot{\eta})$ and the logarithm of acceleration $(\ddot{\eta})$ that is possible to express as:

$$\ddot{\eta} = A\,\dot{\eta}^{\alpha} \tag{3.5}$$

in which A and α are two empirical constants.

This relationship was theoretically studied and extended by Voight (1988, 1989) to different types of natural phenomena. For volcanic eruptions, the Author stated that the quantity η, which represents displacement in the original formulation, can be replaced with other physical quantities, such as geodetic or geochemical observations or seismic quantities.

The relationship (3.5) can be integrated in time, obtaining an expression of the quantity $\dot{\eta}$, that rewritten in term of the inverse of the velocity is:

$$\frac{1}{\dot{\eta}} = [A(\alpha - 1)(t_f - t) + \dot{\eta}_f^{1-\alpha}]^{\frac{1}{\alpha-1}} \tag{3.6}$$

Equation (3.6) is valid for $\alpha > 1$, that is a characteristic of the 80% of measured displacement in landslides and particularly it is equal to 2 in the 50% of cases (Fukuzono, 1990; Varnes, 1983). For which concerns parameter A, it is larger than zero considering increasing strain and has a strict correlation with α (Cornelius and Scott, 1993). Both the constants can be derived from a calibration on data series of velocity vs. time.
Finally, time of failure is obtained assuming an infinite value of $\dot{\eta}$ at this time, a condition that is only ideal and not physically possible, but useful in the forecasting procedure.
Equation (3.6) can be solved graphically with the aim of obtaining the unknown time of failure. The procedure varies depending on the value of the parameter α. The case relative to $\alpha = 2$ is reported in Figure 3.4: in such a case the curve representing experimental points is linear.

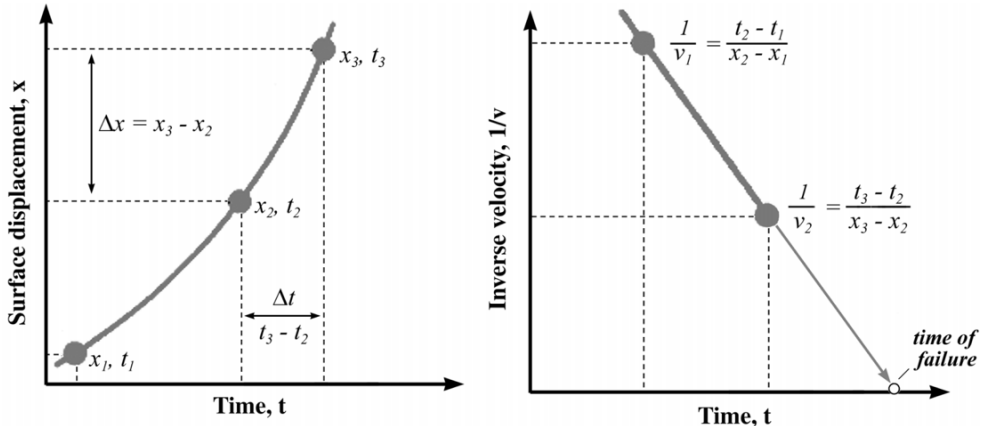

Figure 3.4: Graphical procedure to compute time of failure of landslides according to Fukuzono (1985, 1990) (figures from Eberhardt, 2008)

For different values of the parameter α the theorical curve can assume concave ($1 < \alpha < 2$) or convex shape ($\alpha > 2$).
Petley et al. (2002) and Kilburn and Petley (2003) correlated the shape of the curve of the inverse velocity over time with the crack propagation along the shear surface for translational and rotational slides. By correlating rate of movement with the crack nucleation and growth in the shear zone, they introduced the following equation:

$$\dot{\eta} = \dot{\eta}_0 e^{\psi(\eta - \eta_0)} \tag{3.7}$$

in which η_0 and $\dot{\eta}_0$ are displacement and velocity at the time in which crack propagation first becomes greater than crack nucleation, ψ is a parameter, expressed

as an inverse length, that depends on material properties, geometry and applied stress.
Equation (3.7) can be rearranged to obtain a relationship in terms of inverse velocity:

$$\frac{1}{\dot{\eta}} = \frac{1}{\dot{\eta}_0} - \psi(t - t_0) \tag{3.8}$$

According to Petley et al. (2002), equation (3.8) returns a linear behaviour when crack growth is predominant, whereas in the processes involving crack nucleation the inverse of velocity asymptotically tends to zero, showing a concave shape.
These observations have been demonstrated firstly referring to the Selborne slope-cutting experiment representing a first time failure, in which the collapse of the slope has been triggered by increasing pore water pressure (Cooper et al., 1998). In this case, that represent a first failure phenomenon, it is possible to observe a linear behaviour in the curve $1/\dot{\eta}$ vs. time (Figure 3.5a).
On the other hand, Authors analysed some landslides moving on pre-existing shear surfaces, showing a non-linear behaviour (see the example of Tessina landslide, Figure 3.5b).

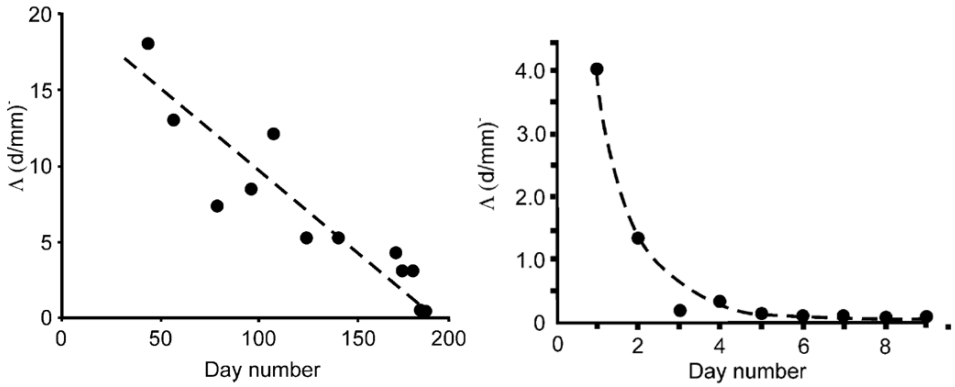

Figure 3.5: Inverse velocity Λ vs. time for the first failure of Selborne slope-cutting experiment (a) and for a movement on pre-existing shear surface, Tessina landslide (Petley et al., 2002)

Federico et al. (2012) analysed the relation between the last measured acceleration and rate of movement for thirty slope failures, with the aim of defining a variation law, useful when time series of displacement data are not available. They found a relationship similar to the Fukuzono's proposal:

$$\ddot{\eta} = 0.052\,\dot{\eta}^{1.5} \tag{3.9}$$

This relationship can be plotted in a log-log diagram obtaining the straight line, reported in Figure 3.6, in which the markers indicate the points corresponding to the collected case studies.

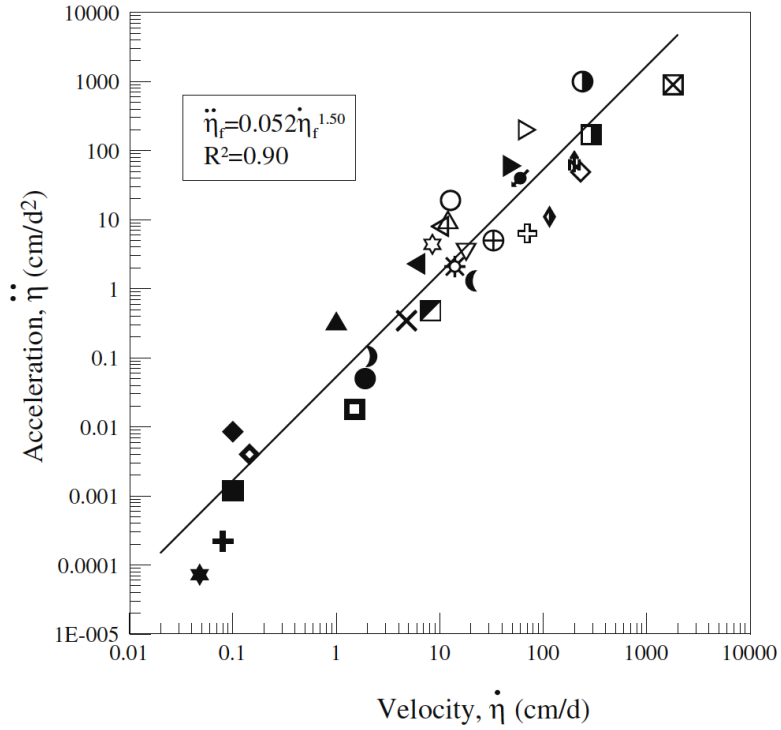

Figure 3.6: Relationship between acceleration and rate of movement for 30 slope failure (Federico et al., 2012)

3.3 Fukuzono-Voight method in early warning systems

3.3.1 Early warning systems and alert parameters

Considering the risk as composed by three different terms (Varnes, 1984) – Hazard, Vulnerability and Element at risk - mitigation measures can work on one or more of these terms through structural or non-structural actions. Structural actions decrease the hazard or the vulnerability of existing elements at risk through engineering works (e.g. drainage, vegetation, ground improvements, barriers, walls). Non-structural actions consist in reducing the consequences acting on the presence of elements at risk (e.g. retreat from hazard, land-use planning, early-warning, emergency plans) (SafeLand, 2012). Among these actions, early warning systems (EWS), at regional

and local scale, represent a cost effective alternative, applicable even to landslide too large to be stabilized (Intrieri et al. 2012).

Calvello (2017) identifies three different components: landslide model, that corresponds to the definition of functional relationships between landslide causes and events; warning model, that consists in the development of alert procedures; warning system, that includes all the actions required for the application of the emergency plan.

It is clear that, in designing of an EWS, a crucial part is represented by the used forecasting methodology.

Focusing on temporal forecasting models, it is possible to consider different approaches, depending on the monitored parameter used as input information.

Pecoraro et al. (2019) presents an interesting review on slope-scale strategies, showing a statistics about the parameters used for defining alert criteria (Figure 3.7).

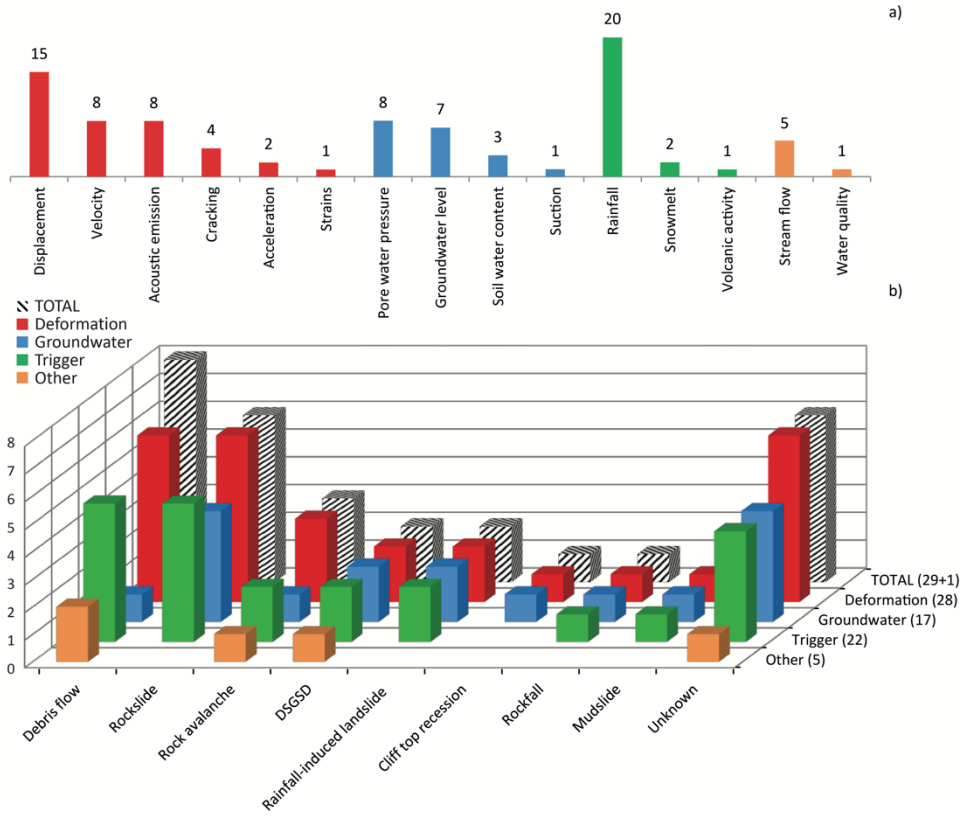

Figure 3.7: a) Alert parameters used in early warning systems; b) Correlation between landslide types and alert parameters (Pecoraro et al. 2019)

Referring to the 29 analysed cases, the Authors showed that the most used parameters are the deformations – including displacements, velocity, acoustic emission, cracking, acceleration, strains – especially for rock landslides.
Examples of landslide and warning models are presented in the following section, with particular reference to methods based on deformation measurement, focusing on Fukuzono-Voight proposal.

3.3.2 Landslide and warning model: applications

Crosta and Agliardi (2003) proposed an interesting application to Ruinon landslide (Valfurva, Central Alps, Italy), defining velocity alert thresholds, used in emergency plan of the civil protection of Regione Lombardia, that are based on inverse velocity method of Fukuzono-Voight.
Ruinon landslide is a rockslide located in the lower sector of *Cima di Saline* slope, involves 20 Mm^3 of material and is composed by rock in the upper scarp whereas the lower scarp is constituted by debris and disintegrated rock. Rainfall are among the most relevant triggering factor during the summer season, while snow melting at the end of the winter season.
Ruinon rock slide is active since 1960, but the more important movements are recorded after 1980. For this reasons, the slope has been equipped over the years with a large monitoring system constituted by 14 boreholes with inclinometers and piezometers. Starting from 1997 the system was expanded with 25 wire extensometers, 17 GPS, optical targets and distometers, 2 borehole inclinometers, a borehole multibase extensometer and other tools, as GB-InSAR radar interferometry (Alberti, 2019).
Crosta and Agliardi (2003) analysed the behaviour of the rockslide for a period of 5 years (from 1997 to 2001). The Authors developed *characteristic velocity curves* starting from the proposal of Voight. In particular, integrating equation (3.5), it is possible to obtain the following expression of rate of movement (for α>1) :

$$\dot{\eta} = [A(\alpha - 1)(t_f - t) + \dot{\eta}_f^{1-\alpha}]^{\frac{1}{1-\alpha}} \tag{3.10}$$

Equation (3.10) requires the definition of the parameters A, α and t_f to be used for velocity modelling. To this aim, equation (3.10) is again integrated, obtaining the value of displacement η as:

$$\eta = \frac{1}{A(\alpha-2)}\left\{[A(\alpha - 1)t_f + \dot{\eta}_f^{1-\alpha}]^{\frac{2-\alpha}{1-\alpha}} - [A(\alpha - 1)(t_f - t) + \dot{\eta}_f^{1-\alpha}]^{\frac{2-\alpha}{1-\alpha}}\right\} \tag{3.11}$$

This relationship is used for calibrating the parameters, fitting the displacement data recorded in the considered period through nonlinear estimation analysis (Figure

3.8a). The first value of time of failure is obtained from the inverse velocity plot, according to the procedure of Fukuzono-Voight. It is worth noting that displacement data used in the calibration are referred to the whole data series, without considering seasonal behaviours.

Finally, the characteristic velocity curves are reported in Figure 3.8b for five monitoring stations, equipped with distometers.

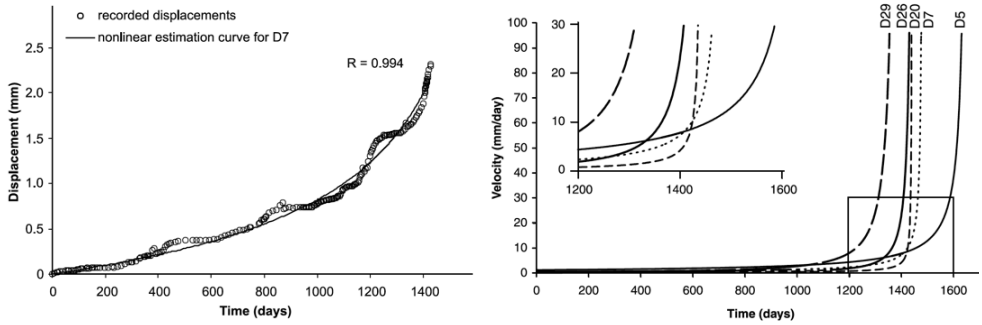

a) b)

Figure 3.8: Ruinon rockslide: a) Nonlinear estimation for displacement curve; b) Characteristic velocity curves for distometers D5, D7, D20, D26, D29 (Crosta and Agliardi, 2003)

Once obtained, *characteristic velocity curves* allow to define some velocity thresholds. The Authors proposed to set three warning levels, corresponding to different stages in the emergency management:

- *Pre-alert* threshold, that is reached 30 days before the potential time of failure, indicates the necessity of a check of the conditions of the slope and of the monitoring devices;
- *Alert* threshold, that corresponds to the velocity reached 15 days before the failure, requires the increase in the monitoring;
- *Alarm* threshold, that is defined 7 days before the failure, indicates the achievement of the final stage of the landslide, suggesting the application of emergency measures.

Segalini et al. (2018) proposed a similar procedure to define alert thresholds. Starting from equation (3.10), the calibration of the parameters A, α and t_f is obtained plotting $\frac{1}{\dot{\eta}}$ over time and firstly computing t_f using values of A, α corresponding to linear interpolation ($\alpha = 2$). Afterwards, these two parameters are calibrated minimizing the root-mean-square error between modelled velocity - through equation (3.10) - and monitoring data. Clearly, the procedure is updated when new monitoring data are available. It was observed that the values of A and α remain almost constant during the accelerating phase.

Finally, the Authors compute normalized-velocity $\dot{\eta}_n$ defined as:

$$\dot{\eta}_n = \frac{\dot{\eta} - \mu_v}{\sigma_v} \tag{3.12}$$

in which μ_v is the mean value and σ_v the standard deviation of the curve $\dot{\eta} - t$.
Applying this relationship to several failure case studies from the scientific literature and plotting the resulting curves over time, Authors obtained the diagrams reported in Figure 3.9, where the last 30 days before the failure are considered. The procedure of normalization allows to obtain a generalized criterion to define alert thresholds suitable for all the analysed case studies.

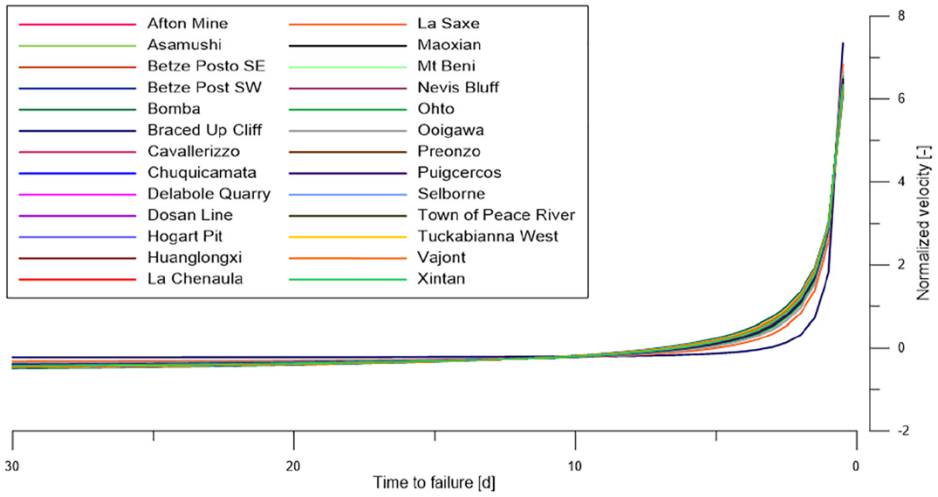

Figure 3.9: Normalized velocity curves (Segalini et al., 2018)

Another interesting proposal is developed by Carlà et al. (2017a) that, after the evaluation of the time of failure computed with the Fukuzono-Voight method, defined two alert thresholds to use in warning systems.
With the aim of using the graphical method, the Authors proposed to use some smoothing techniques, in order to compare the results obtained with raw data and those obtained with filtered ones. In particular, they used:

- moving average of the velocity at time t:

$$\overline{v_t} = \frac{v_t + v_{t-1} + \cdots + v_{t-(n-1)}}{n} \tag{3.13}$$

  with $n = 3$ at short-term (SMA) and $n = 7$ at long-term (LMA);
- exponential smoothing function (ESF):

$$\overline{v_t} = \beta v_t + (1 - \beta) v_{t-1} \tag{3.14}$$

The inverse velocity method has been applied to four case studies: Mount Beni rockslide, Vajont landslide, a roto-translational slide on a volcanic debris talus (Stromboli) and also to the collapse of a section of medieval wall built on unstable terrain.
The results in terms of time of failure show that in the cases in which is not possible to clearly recognize the accelerating trends (the last two analysed case studies), smoothing techniques are necessary to apply the method.
Summarizing, the Authors suggest using smoothing techniques when low velocity are recorded in the landslide - because in these cases the beginning of the accelerating trend is not easily identifiable- and when the noise of the data is high. In cases in which noise is low or displacement rate is high, the use of smoothing techniques does not increase the quality of the results.
After this examination on the procedure of application of the Fukuzono-Voight method, the Authors introduced two alarm thresholds. The first one level of alarm can be defined in correspondence of the point in which the accelerating behaviour starts (so-called Onset Of Acceleration - OOA). The identification of this point clearly is clearly related with the expertise of the user. The second alarm threshold is defined on the basis of the time of failure obtained with moving average on displacement data. This threshold is represented by an interval of time in which failure is more probable. Supposing that $T_f(SMA) < T_f(LMA)$, the failure window is defined as:

$$\left[T_f(SMA) - \frac{\Delta}{2}; T_f(LMA) + \frac{\Delta}{2}\right] \tag{3.15}$$

In Figure 3.10 the procedure is presented for Mount Beni landslide, by way of example: data series plotted in blue are computed with LMA, those in violet with SMA; green arrow indicates the effective collapse time. The value of Δ is determined equal to 5 days between $T_f(SMA)$ and $T_f(LMA)$. It is possible to observe that the failure time is contained in the computed window.

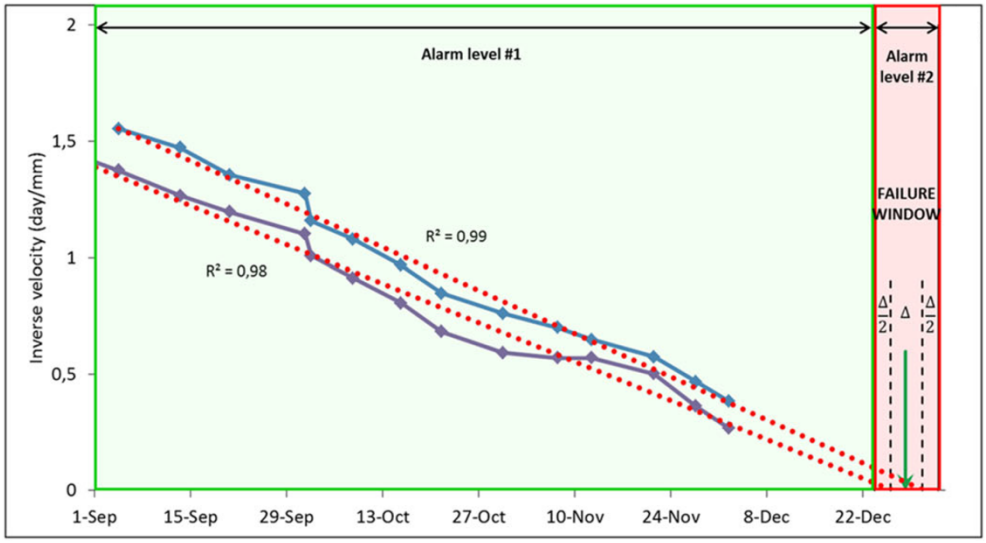

Figure 3.10: Alarm thresholds for Mount Beni landslide (Carlà et al., 2017a)

3.3.3 Limitations of the method

In the previous section the capability of Fukuzono-Voight method in forecasting landslide collapse has been presented, showing some applications presented in International Literature. The strength of the method probably lies in its ease of use and in the reliability of the results that are sometimes obtained.

However, this phenomenological method allows to obtain only information about the collapse time, for failures that occur according to creep theory, without giving a description of the previous movement stages.

Furthermore, the inverse-velocity method is based on the assumption that the failure occurs when $1/\dot{\eta} = 0$, thereby when the velocity reaches an infinite value. Actually, Newcomen and Dick (2015) observed that not only displacement rate at failure is not infinite, but its value depends on the characteristics of the landslides, such as materials, geometry, movement type.

The main difficulty in the procedure is probably the identification of the beginning of the accelerating stage, which is not evident. Dick et al. (2014) focused on the determination of the OOA, highlighting that the methodology requires the presence of an user, making the procedure subjective and depending on the expertise and judgement. To better understand the relevance of the selection of OOA in computation of time of failure, Authors carried out a sensitive analysis showing that choosing OOA later provides a more conservative result rather than an earlier OOA. Rose and Hungr (2007) applied the method to 4 case studies regarding to open pit mines, emphasizing the possibility of generating false alarms, due to the fact that the

method is based on the assumption that the displacement trend is uniform towards the failure. In fact, some factors can work on the landslide body, inducing unexpected deceleration. To reduce this type of mistakes, Authors suggest to use the method coupled with monitoring of other quantities related to the slope stability, such as stress and groundwater regime.

Carlà et al. (2017b) also studied the reliability of the inverse velocity method in open pit mines. They analysed several points of a brittle rock mine, studying both failure and not failure movements, that are characterized by planar and wedge sliding and toppling. They firstly observed that tertiary creep occurs also in hard rock materials showing very rapid evolution, of the order of some hours. Clearly, this is an aspect to consider in monitoring systems referring to measurement frequency.

Thereafter, Authors applied the method in two cases with an accelerating phase followed by a deceleration: as shown in Figure 3.11 the use of inverse velocity leads to the computation of a time of failure that did not occur in the practice. The red lines reported in the Figure 3.11a,b indicate the points in which, in a near real time system, the failure time can be computed, while the actual evolution involves a deceleration and a subsequent stabilization. For this reason, the use of the procedure can cause false alarms considering that acceleration is not always a precursor of failure, affecting the capability of planning a reliable early warning system.

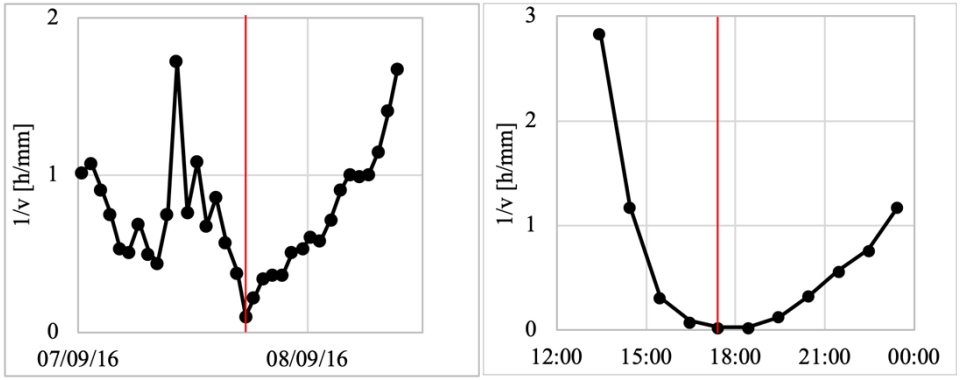

a) b)

Figure 3.11: Inverse velocity over time for two instabilities in open pit mine; red lines indicate the failure time improperly computed during the accelerating phases that not leads to real collapse (modified from Carlà et al., 2017b)

To reduce errors and false alarms, a proper characterization of activity phases of movement is recommendable. For this purpose, the construction of a method able to describe all the landslide history and not only the failure stage can be a valid tool. Furthermore, the study of physical quantities associated to the dynamic of the slope movement can allow to distinguish between accelerating stages that lead to failure

and those that are only transient losses of equilibrium. In addition, the analysis of other features related to landslide evolution can represent a support for the identification of the point in which the accelerating phase starts.
In the following chapters a new method is presented, aimed at characterizing and then forecasting displacement behaviour of slope movements on the basis of a procedure that is developed starting from the observation of real case studies and then formalized with a consistent mathematical approach.

4. Finding common trends in landslide displacements

(Based on: *Scoppettuolo, M.R., Cascini, L., Babilio, E. (2020). Typical displacement behaviours of slope movements. Landslides)*

Grimaldi (2008), Cascini et al. (2014, 2019), analysing well-documented landslides in the Scientific Literature, remapped their heterogeneous displacements in a dimensionless diagram. This allowed recognizing that different phenomena exhibit common displacement characteristics that could be framed in a quantitative and general framework able to describe the displacements of active and occasionally reactivated landslides.
In this chapter, the method proposed by these Authors is extended to an expanded database containing a much larger number of well-documented case studies that include all the landslide stages defined by Leroueil et al. (1996) and involve different materials.
The results obtained for the eighteen landslides in the database reinforce the already proposed framework and allow to obtain insights on the landslides that suffer or can suffer a catastrophic failure.
After the description of the landslides in the database, the adopted procedure is presented and applied firstly to three explanatory case studies – Bindo Cortenova, La Clapiere, Vajont – and then to all the eighteen landslides in the dataset.

4.1 The landslide dataset

The eighteen analysed landslides, in some cases composed of multiple landslide bodies, have been chosen among those better documented in the scientific literature as it concerns quality and completeness of data, including the relationships between triggering factors and landslide displacements. Location, monitoring stations, length of the main landslide body, materials and triggering causes of any analysed phenomenon are collected in Table 4.1.

Table 4.1: Landslides dataset with the indication of location, monitoring stations, length, maximum depth, volume of the main body, materials, movement type and main triggers.

	Landslide	References	Location	Considered monitoring station*	L (m)	D (m)	V (10^6 m^3)	Materials	Movement type	Trigger
a)	**Bindo-Cortenova**	Secondi et al. 2011	Valsassina, Lecco, Italy	B17 optical target	1000	50	-	Rock block in a gravely sand matrix	Translational slide	Rainfall
b)	**Castelrotto**	Simeoni and Mongiovì 2007	Bolzano, Italy	T8 inclinometer	390	64	2.5	Debris, tuff	Complex slide	
c)	**Fosso San Martino**	Bertini et al. 1986	Teramo, Italy	B inclinometer	340	20	-	Silty and marly clay	Slide	
d)	**Montaldo di Cosola**	Lollino et al. 2006	Alessandria, Italy	AIS inclinometer	1250	36	-	Clay	Complex slide	
e)	**Ohto**	Suwa et al. 2010	Japan	7 extensometer	2000	-	-	Rock	Avalanche	
f)	**Porta Cassia**	Tommasi et al. 2006	Orvieto, Italy	O4 inclinometer	550	20	-	Volcanic grains, toufaceus block and softened clay	Slide	
g)	**Vallcebre**	Corominas et al. 2005	Pyrenees, Spain	S2 extensometer	1200	34	20	Stiff clays with shale and gypsium layers	Translational slide	
h)	**La Frasse**	Tacher et al. 2005	Aigle, Switzerland	A inclinometer	2000	110	73	Sandstones, clay schists	Slide	
i)	**Rosone**	Binet et al. 2007	Orco river valley, Turin, Italy	B1 inclinometer	1500 **	100	20.5	Granitic ortho-gneisses	Complex slide	
j)	**Xintan**	Keqiang and Sijing 2006	China	A3 surface marker	-	-	-	Debris	Slide	
k)	**Val Pola**	Crosta et al. 2004	Valtellina, Sondrio, Italy	ES2 extensometer	900	100	34 – 43	Debris	Avalanche	
l)	**La Saxe**	Crosta et al. 2014	Courmayeur, Aosta, Italy	B4 optical target	550	90	8	Rock	Slide	Snow melt
m)	**Kunimi**	Shuzui 2001	Japan	BV60 – 1 inclinometer	1000	9.6	-	Clay-with-breccia type		
n)	**Ragoleto**	Musso 1997	Licodia Eubea, Catanzaro, Italy	B surface markers	500**	-	-	Debris, silt, marl limestone	Rotational slide	Fluctuation in reservoir level
o)	**Vajont**	Nonveiller 1987	Erto and Chiasso, Pordenone, Italy	4 surface marker	1200 **	250	270	Clays and marls, limestone	Slide	

p)	**La Clapière**	Helmstetter et al. 2004	Southern Alpes, France	10 surface marker	900**	200	55	Rock mass in gneisses	Flexural toppling/ rotational slide	Fluctuation in river flow
q)	**Ruinon**	Crosta and Agliardi 2003	Valtellina, Sondrio, Italy	D7 distometer	550	70	13-20	Rock	Roto-translational slide	Rainfall, snow melting and creep of rock mass
r)	**Chuqui-camata**	Voight and Kennedy 1979	Andes, Chile	F-2 (5) Crackmeters	500**	-	11 - 14	Metamorphic rock	Slide	Excavation earthquake

* Names of monitoring stations indicated in the references.

** Length, not reported in the relevant references, but deduced by the authors of the present contribution on the basis of the information presented therein.

Notice that all the landslides in the dataset, with the exception of Chuquicamata case study, are characterized by the presence of a partially or totally developed shear surface and are triggered by an increase in pore water pressure, mainly due to weather conditions (i.e., rainfall, snow melt or a combination of both) or fluctuations in water level, when located on a river shore or a reservoir. In contrast, the data from Chuquicamata are related to a first failure phenomenon triggered in a pit mine by excavation and detonation activities.

Information collected in Table 4.1 clearly shows that the analysed landslides are different in terms of the involved materials (e.g., rock, debris, clays, silt, limestone) and size of the body undergoing motion, with lengths in a large range, spanning from 340 m up to 2000 m. Monitoring stations indicated in Table 4.1 are also equipped with different techniques; most of the displacement data originate from superficial measurements, such as total station optical targets, other represent deep measurements, as in the case of inclinometers. Certainly, these techniques have different meanings, but the collected data are all considered representative of the landslide motion in the quoted references. Indeed, they were implemented as input data in the proposed method.

The cumulate displacements versus time for the landslides in the dataset are plotted in Figure 4.1, exhibiting a behaviour that is different for each case study, probably due to the different characteristics of the materials involved in the landsliding.

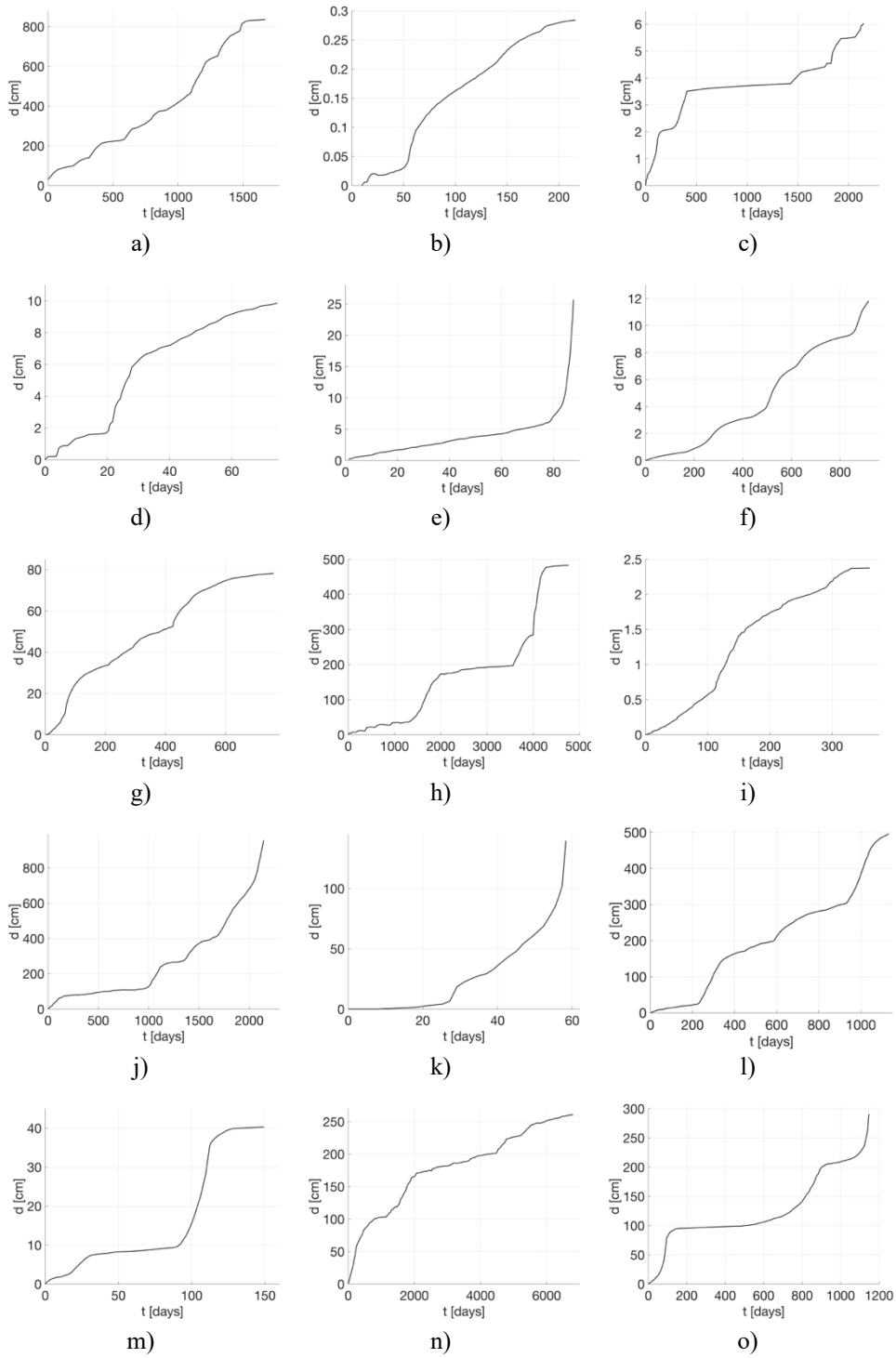
d [cm]
t [days]
a)
b)
c)
d)
e)
f)
g)
h)
i)
j)
k)
l)
m)
n)
o)

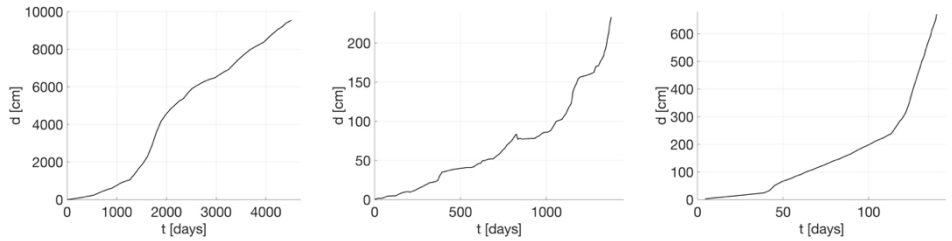

p) q) r)

Figure 4.1: Graphs of cumulate displacements vs. time for the landslides in the database.

4.2 Typical displacement trends

The diagrams in Figure 4.1, despite the clear differences, highlight common characteristics for landslide displacements. Indeed, all the data are arranged according to linear and concave or convex curves, similar to those described by Singh (1966) and Emery (1979) to introduce primary, secondary and tertiary creep. Moreover, typical landslide evolutions can be partitioned in ordered sequences, as those sketched in Figure 4.2, where an active landslide (a), an occasional reactivation (b) and a phenomenon evolving towards a catastrophic stage (c) are qualitatively shown.

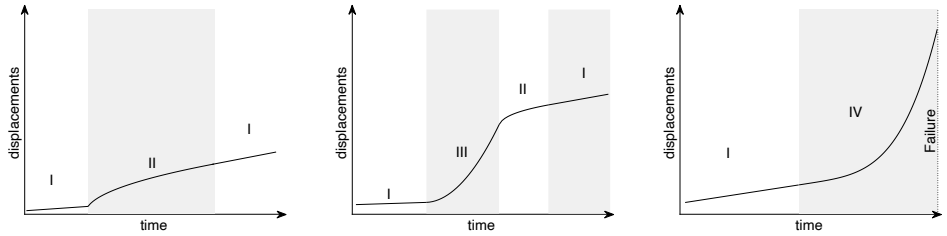

a) b) c)

Figure 4.2: Main typical sequences of displacement trends for: an active landslide, sistematically reactivated by recurrent triggering factors, in between two steady states (a); a lanslide reactivated by an occasional event (e.g. earthquake) in between a steady state and a Trend II followed by a steady state (b); evolution to failure from a steady state (c). Roman number indicate the different trend types present in the sequences.

We can argue that data with a linear behaviour indicates a stable condition of the landslide, whose motion is characterized by a constant velocity at zero acceleration. In such a case, the internal and external forces acting on the landslide are balanced. On adopting the nomenclature of Cascini et al. (2014), we call such a behaviour as Trend I. It is noteworthy that the slope of the trends still depends on several factors,

including the shape of shear surfaces, the materials composing the moving body and the materials along the shear surface, among many others.
Starting from an instantaneous and transient loss of equilibrium (where external forces overcome internal stabilizing forces) represented by an increase in the diagram slope, as the time advances, the system leaves the transient phase and evolves towards a new equilibrium that is reached when a linear Trend I is achieved once again (Figure 4.2a). We call the concave phase as the Trend II, and the whole process can be considered representative of an active landslides, as defined by Leroueil et al. (1996).
Trend II is also observable in Figure 4.2b with a different conceptual meaning. In this case, the process is initially characterized by data arranged along a convex curve, representing an acceleration in the landslide movement, followed by a concave branch: physically this alternance of shapes indicates perturbed state, caused by initially unbalanced force fields globally acting on the landslide, which evolves towards a new equilibrium configuration. The latter, again, is reached whenever a linear growth takes place provided that other new perturbations do not occur. Referring to Cascini et al. (2014), we call Trend III the convex curve. This is a typical feature of occasional reactivations, as defined by Leroueil et al. (1996), and the initial moderate perturbations are usually called occasional triggering factors.
Finally, we call Trend IV a phase characterized by data gathering along convex curve not likely reaching a stable state, that is a new linear phase. Such a behaviour is associated with a landslide undergoing, under some specific conditions, a catastrophic failure, essentially due to a largely unbalanced system of forces acting on the landslide (Figure 4.2c). Leroueil et al. (1996) call this behaviour as failure stage, that is the case of the Chuquicamata pit mine (Voight and Kennedy, 1979).
By critically observing the eighteen case studies in the dataset, we recognize that such an accelerative trend can likely also be observed in occasionally reactivated phenomena. This is, for instance, the case of the infamous Vajont landslide, started out by an occasional triggering factor of a particularly high intensity. Hence, trend IV actually seems to extend the classification proposed by Leroueil et al. (1996) to the occasional reactivations that evolve to a catastrophic ending.

4.2.1 Single-phase selection

Every sample of data in the dataset is a complicated assemblage of many single-activity phases. Kinks, steep gradients and concavity-convexity changes in the displacement curve must be identified to primarily distinguish the stages for any selected landslide. Then, a comparison among the obtained phases and the triggering factors can validate the interpretation of the displacement curve.

For what concerns Trend II, and specifically for a rainfall-induced landslide, modifying the original procedure described in Grimaldi (2008) and Cascini et al. (2014), we use the relationships among displacement rate, pore water pressure regime and seasonal rainfall trend. We take *i)* as the initial reference displacement that recorded in coincidence with the first increase in the pore water pressure diagram and *ii)* as the final displacement that corresponds to the end of the decreasing phase in pore water pressure. Initial and final times of any activity stage are taken accordingly. A similar procedure is followed for landslides systematically activated by different triggering factors.

A lack in correlation is likely a sign of an occasional reactivation, which usually calls for further investigation on the cause of the landslide motion and may result in some difficulties due to the heterogeneity in the triggering factors that are sometimes not properly monitored. However, the start and end points of the time interval can be properly defined referring to the displacement gradient, which is usually much steeper than that corresponding to active seasonal landslides.

4.2.2 Nondimensionalization of displacement trends

Once the whole displacement record of a landslide is properly partitioned, the next step is to re-map every stage in a suitable dimensionless space. To this aim, following the proposal of Grimaldi (2008) and Cascini et al. (2014), the dimensionless displacements are set as

$$D_{i,j} = \frac{d_{i,j} - d_{0,j}}{d_{n,j} - d_{0,j}}, \tag{4.1}$$

with:

$$d_{0,j} \leq d_{i,j} \leq d_{n,j}, \quad i \in [0, n], \quad j \geq 1$$

where $d_{i,j}$ and $D_{i,j}$ are the i^{th} cumulated and dimensionless displacement records, respectively, belonging to the j^{th} stage. Conventionally, the first element in the j^{th} stage is marked as "0,*j*", while the last is "*n*,*j*", that is, the *any* stage is a closed discrete set of n+1 elements. Note that equation (4.1) implies that the dimensionless displacement ranges from 0 to 1.

Accordingly, the dimensionless time is computed as

$$T_{i,j} = \frac{t_{i,j} - t_{0,j}}{t_{n,j} - t_{0,j}}, \tag{4.2}$$

with:

$$t_{0,j} < t_{i,j} < t_{n,j},$$

in which the dimensionless time $T_{i,j}$ goes from 0 to 1.

By using equations (4.1) and (4.2), the dimensionless diagram is readily constructed as a set of points $P_{i,j} \equiv \left(T_{i,j}; D_{i,j}\right)$ for any stage.

4.3 Explanatory applications

In order to clarify how the proposed procedure works, it is applied to three case studies, namely the Bindo-Cortenova, La Clapière and Vajont landslides, which are indeed representative of the whole dataset.

4.3.1 Bindo-Cortenova landslide

The active, translational Bindo-Cortenova landslide, located in Valsassina (northern Italy), is constituted by conglomeratic rock blocks in a gravely sand matrix that suffered two failures in December 2002 and May 2004, respectively involving 1.2×10^6 m^3 and 2.0×10^5 m^3 (Secondi et al. 2011). Thereafter, both the displacements and displacement rates have decreased and the slope has been affected by only a slow-moving behaviour strictly related to the pore water pressure regime (Crosta et al. 2006; Secondi et al. 2011).
Records of cumulated displacements taken with total stations are available in the literature for the period between January 2005 and December 2009. Water table levels measured in open-pipe piezometers instrumented with transducers are also available. Figure 4.3a shows a map, a stratigraphic section of the slope and the position of the analysed monitoring system that provides data for interpreting the evolution of the entire landslide sketched in Figure 4.3b. (Crosta et al. 2006).
A superimposition of displacement and water table levels is shown in Figure 4.4a, highlighting that the landslide displacement is characterized, during the data recording time interval, by roughly linear segments when the lowest water table levels are recorded. According to the procedure described in the previous section, the diagram is partitioned in 14 different intervals with clear correlation observed between displacement rate and groundwater level, the latter essentially related to rainfall (Secondi et al. 2011). In Figure 4.4b, the dimensionless displacement values achieved in each time interval are graphically shown.

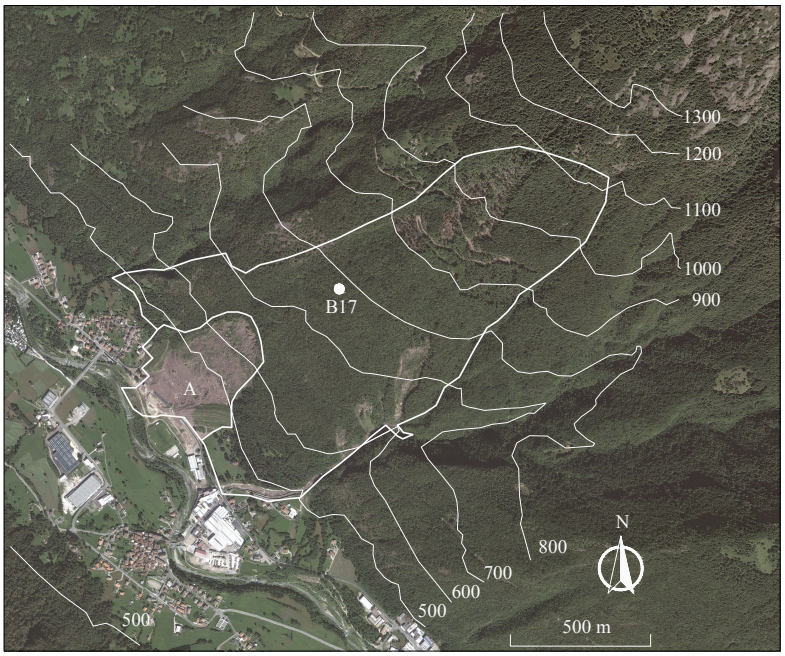

a)

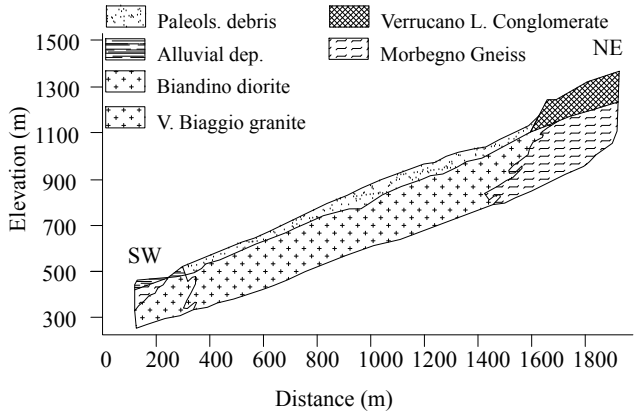

b)

Figure 4.3: a) Satellite imagine of Bindo-Cortenova landslide (Google Earth, 2009) with the indication of the instability area and monitoring optical target B17 (simplified from Secondi et al. 2011). Letter "A" refers to slope failure occurred in November-December 2012. b) Schematic cross section (simplified from Crosta et al. 2006).

It is noteworthy that even though the time duration of intervals are different, spanning from about two up to about six months, the dimensionless data lie in the upper part or close to the diagonal of the unit square in Figure 4.4b. The total displacements of the landslide are similarly bounded in a range spanning from few

centimetres up to little more than one meter. The displacement, rescaled with respect to the length of the landslide, does not exceed 1.3×10^{-3} in any activity stage (Table 4.2).

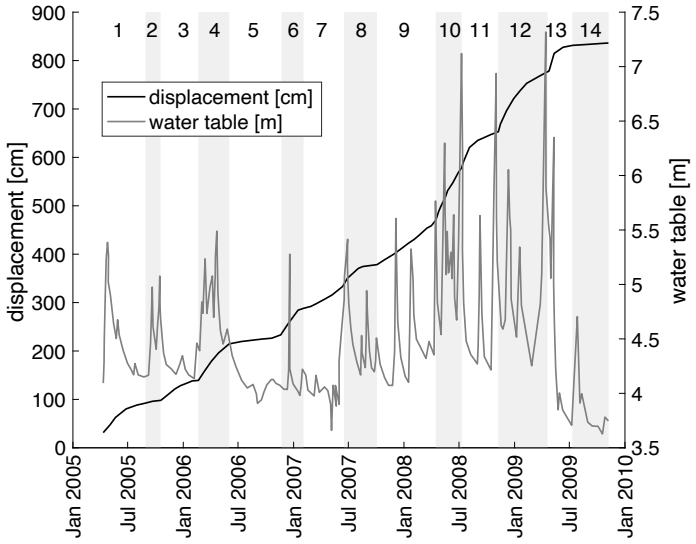

a)

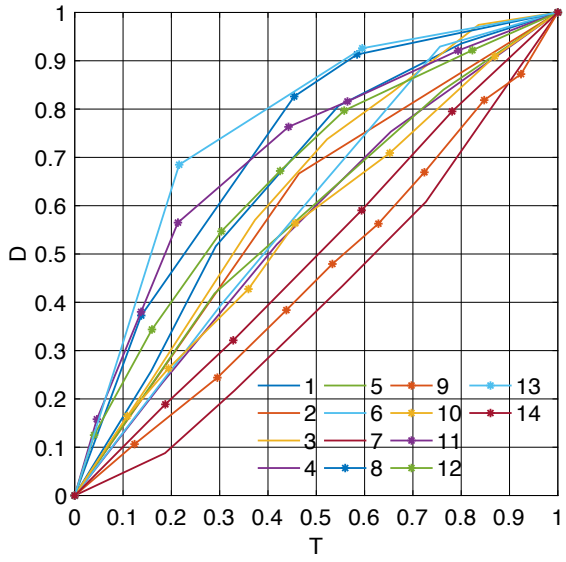

b)

Figure 4.4: Bindo-Cortenova landslide: monitoring data of cumulative displacements and water level (a) with the indication of the detected time intervals used for the computation of dimensionless diagrams (b).

Table 4.2: Bindo-Cortenova landslide: time interval, total travelled displacement and rescaled displacement for each activity stage.

Stage number	Time interval (days)	Total displacement (cm)	Rescaled displacements (-)
1	130	60.8	6.1E-04
2	52	5.9	5.9E-05
3	124	41.2	4.1E-04
4	102	75.5	7.5E-04
5	141	11.8	1.2E-04
6	76	54.9	5.5E-04
7	129	45.1	4.5E-04
8	114	45.1	4.5E-04
9	195	92.2	9.2E-04
10	85	107.8	1.1E-03
11	121	74.5	7.5E-04
12	168	125.5	1.3E-03
13	78	52.9	5.3E-04
14	119	4.9	4.9E-05

4.3.2 La Clapière landslide

La Clapière landslide is located in the southern French Alps and it mobilizes a volume of approximately 55 Mm^3 in a gneissic rock slope covered by a forest. This landslide shows a complicated sequence of active stages and occasional reactivations related to the river level flowing at the toe and other triggering factors (Helmstetter et al. 2004). It probably started to move before the beginning of the 20^{th} century, although the first changes in slope geometry were highlighted only in the period 1950-1980, through an aerial photogrammetric survey. A slope displacement survey started in 1982 with the aid of topographic measurements suggesting a correlation between slope displacements and river flow fluctuations and snow melting, possibly accompanied by heavy precipitation. Follacci et al. (1988, 1993) relate the acceleration recorded in the period 1986-1987 with the failure of the gneissic bedrock in the north-western block.

Figure 4.5a provides a map of the landslide referring to monitoring point 10, which is representative of the evolution of the landslide, for which a cross section is reported in Figure 4.5b.

In Figure 4.6a, the whole displacement data record is superimposed on the river flow record (representative of the triggering causes, not examining rainfall and snow melting data) to identify the activity stages. The resulting nine phases are not seasonal nor periodic and are usually longer than one year, in agreement with the

occurrence of triggering factors.

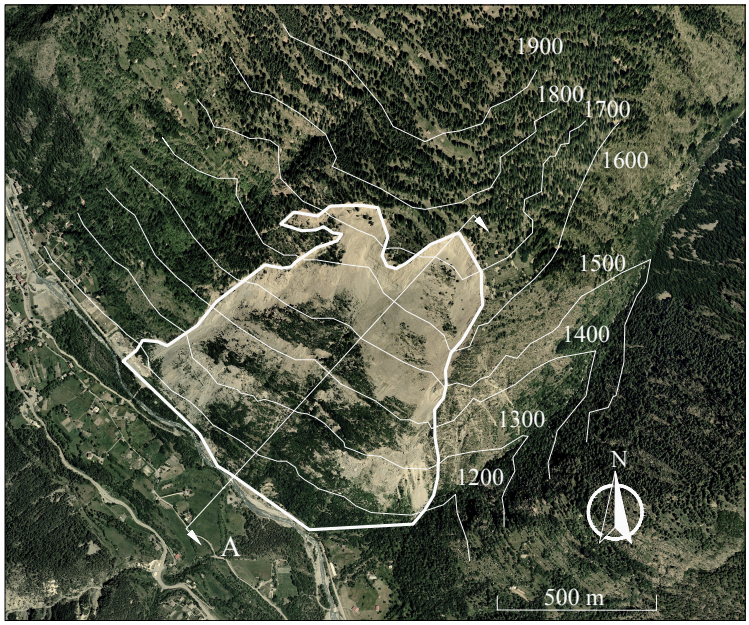

a)

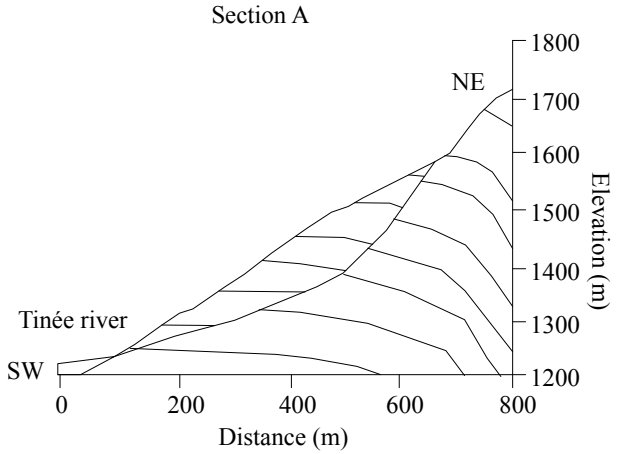

b)

Figure 4.5: a) Satellite imagine of La Clapière landslide (Google Earth, 2004) with the indication of the instability area and cross-section plane (Bouissou et al., 2012 and Bigot-Cormier et al 2005) b) Cross section (modified from Bouissou et al., 2012). For further detail, e.g. qualitative indication of monitoring stations, we refer to Helmstetter et al. (2004) and to Figure 6 therein.

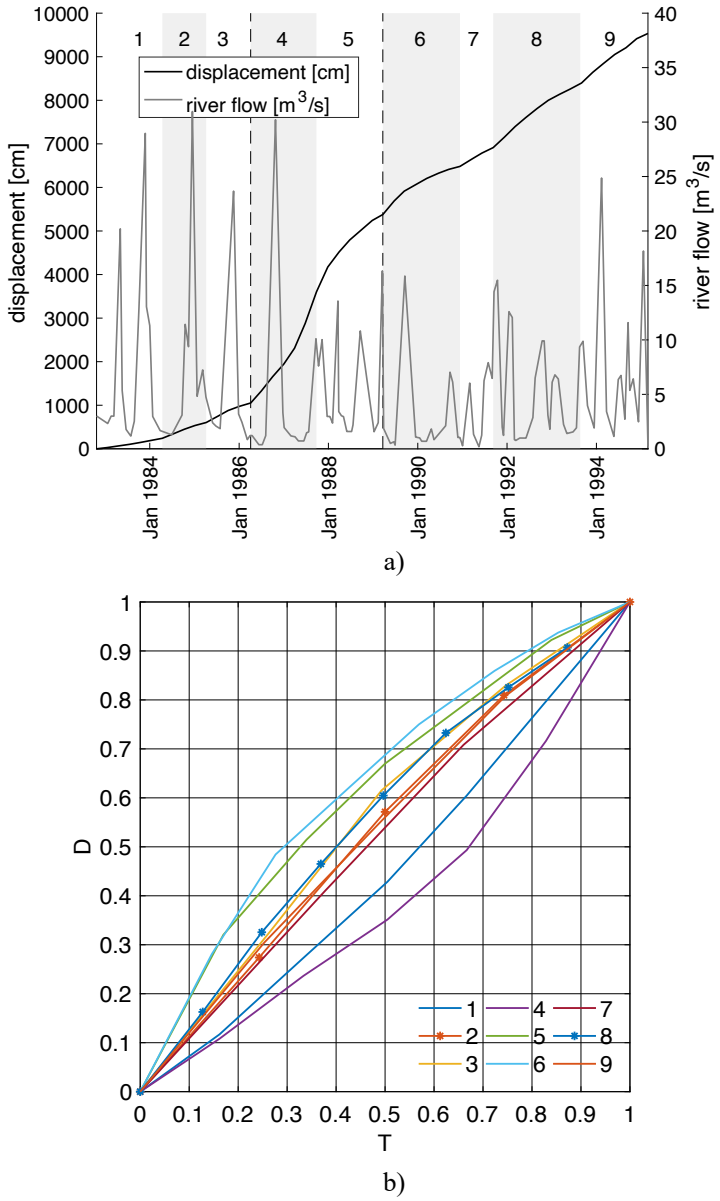

Figure 4.6: La Clapière landslide: monitoring data of cumulative displacements and river flow (a) with the indication of the detected time intervals used for the computation of dimensionless diagrams (b).

The presence of linear, concave and convex branches in the dimensionless diagram reported in Figure 4.6b highlight the complexity of this landslide. The results agree with the interpretation suggested by Follacci et al. (1988, 1993), especially for the acceleration recorded in the period 1986-1987 (stage 4 in Figure 4.6a and the lowest

convex curve in Figure 4.6b). These are typical of an occasional reactivation that is not connected to the fluctuation in river flow. The complexity of the landslide is also confirmed by the values of the rescaled displacements of the landslide body (Table 4.3), which have different orders of magnitude in case of concave or convex trends (10^{-3} or 10^{-2}, respectively). However, regardless of the activity stage, the final steady configuration after a more or less long transient phase shows that the whole landslide system is in condition to balance external forces due to triggering factors.

Table 4.3: La Clapière landslide: time interval, total travelled displacement and rescaled displacement for each activity stage.

Stage number	Time interval (days)	Total displacement (cm)	Rescaled displacement (-)
1	538	241.4	2.7E-03
2	358	362.1	4.0E-03
3	364	448.3	5.0E-03
4	538	2552.7	2.8E-02
5	543	1776.9	2.0E-02
6	630	1103.4	1.2E-02
7	272	431.0	4.8E-03
8	630	1344.8	1.5E-02
9	364	810.3	9.0E-03

4.3.3 Vajont landslide

The Vajont stream was blocked between the 50s and 60s of the 20th century by a concrete dam near the confluence of the Piave River in the Italian Alps. Following the first two fillings of the reservoir, the new boundary condition at the toe of the slope caused two accelerating stages of a complex existing landslide along Monte Toc. On 9 October 1963, following a further increase in the reservoir level, the third fatal landslide reactivation mobilized 270×10^6 m^3 of rock that, flooding into the reservoir, generated a 220 m high wave that overpassed the dam and caused approximately 2000 causalities in the valley below.

The literature on the Vajont landslide is so extensive that it is not possible to quote all the available references here; however, among many others, the contributions of Nonveiller (1987), Kilburn and Petley (2003), Semenza (2001), and Alonso et al. (2010) are worthy of note, since they focus on several interesting issues. Starting from the geological evolution of the valley, Alonso et al. (2010) analyse the landslide mechanism referring to two interacting wedges, the upper unstable and the lower resisting ones, and assuming that the residual and the peak shear strengths act at the base of the wedges and at their mutual interface, respectively. This highlights that the phenomenon was an occasional reactivation.

Figure 4.7a provides an overview of the landslide, showing the location of those monitoring stations where similar trends were recorded. Figure 4.7b sketches the cross section of both the *palaeo*-landslide (*old sliding surface*) and the recent landslide that we analysed, with reference to monitoring station 4.

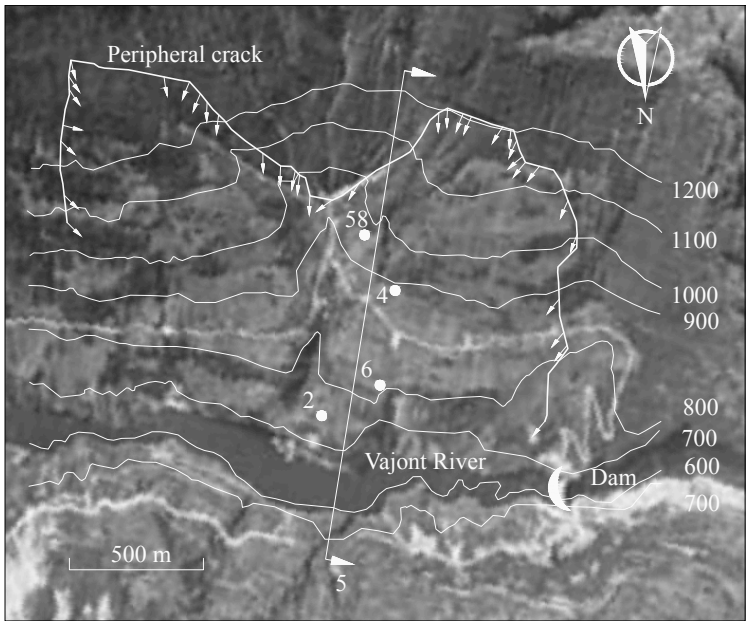

a)

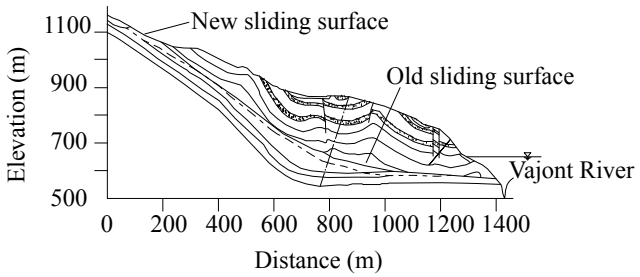

b)

Figure 4.7: Aeral imagine of Vajont landslide (IGM, the italian Military Geographical Institute, 1960) with the indication of monitoring surface markers, vector field of motion of the landslide front and cross-section plane, and b) cross section (modified from Alonso et al. 2010).

The available data (Figure 4.8a) show an alternation of linear segments and convex-concave curves until July 1963; these changes are related to the lowest and the highest values of the reservoir level, respectively, that confirms the phenomenon was

an occasionally reactivated landslide. Figure 4.8b reports the obtained dimensionless trends referring, for stage 6, to a displacement of approximately 3m, that was recorded when the monitoring device stopped working.

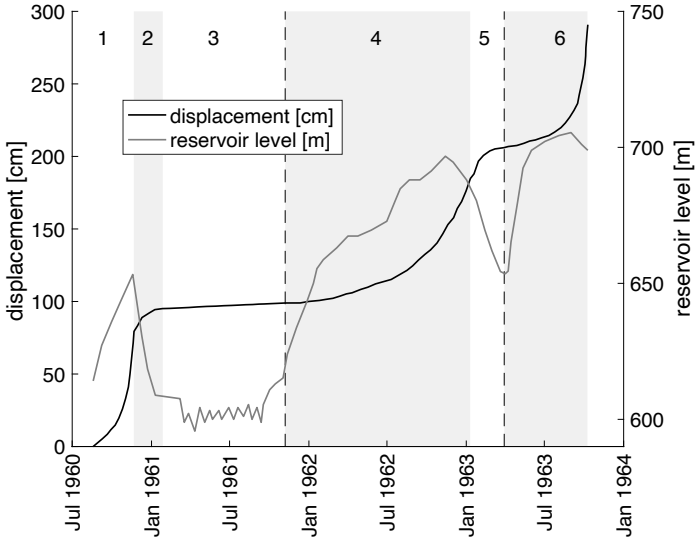

a)

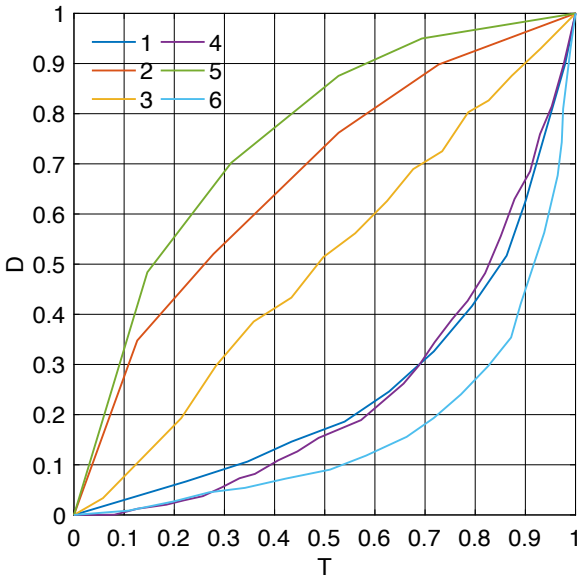

b)

Figure 4.8: Vajont landslide: monitoring data of cumulative displacements at station 4 and reservoir level (a) with the indication of the detected time intervals used for the computation of dimensionless diagrams (b).

The total and rescaled displacements are listed in Table 4.4 that also refers, for stage 6, to the maximum estimated landslide displacement of 500m (Kilburn and Petley 2003). It is worth noting that this value significantly affects position and curvature of the dimensionless displacement curve in the unit square chart, Figure 4.9, so highlighting the different response of the landslide with respect to the third fatal filling of the reservoir.

Table 4.4: Vajont landslide: time interval, total travelled displacement and rescaled displacement for each activity stage.

Stage number	Time interval (days)	Total displacement (cm)	Rescaled displacement (-)
1	95	79.39	6.6E-04
2	66	22.99	1.9E-04
3	285	3.85	3.2E-05
4	429	85.84	7.2E-04
5	70	18.10	1.5E-04
6 (last measured displacement)	185	83.98	7.0E-04
6 (last real displacement)	185	≅50000	4.1E-01

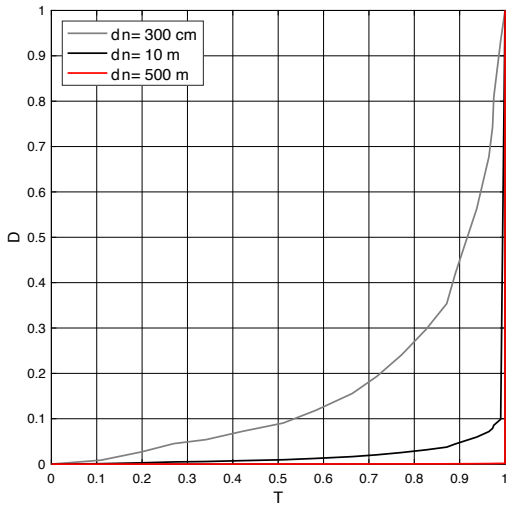

Figure 4.9: Dimensionless curve for the Trend IV of the Vajont landslide, computed by increasing the final value of displacement, d_n.

4.4 Results and discussion

All the eighteen landslides in the dataset were analysed through the procedure earlier described, obtaining the dimensionless curves plotted in Figure 4.10, where all the analysed activity stages are grouped in Trends from I to IV. The number of each trend type for all case studies is reported in Table 4.5.

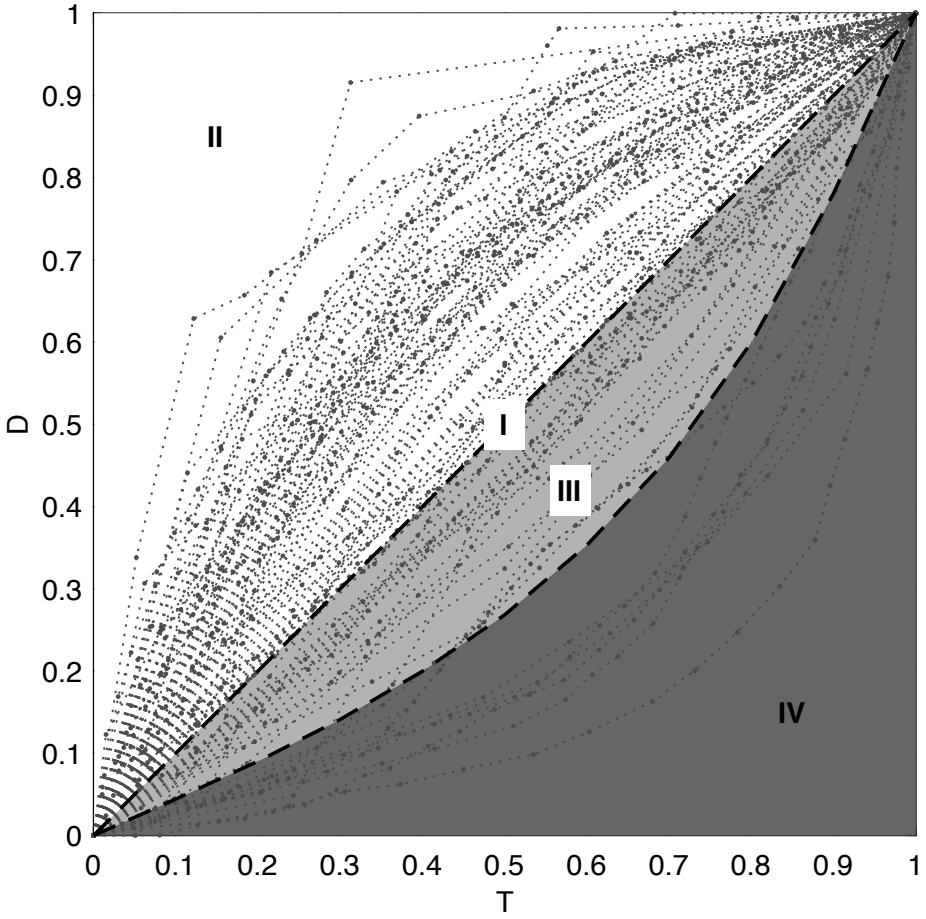

Figure 4.10: Unit-square chart of displacement curves vs time in dimensionless form.

Table 4.5: Number of trend types for all the landslides in the dataset.

Landslide	I	II	III	IV
Bindo-Cortenova	1	11	2	-
Castelrotto	1	4	-	-
Chuquicamata	2	-	1	1
Fosso San Martino	-	5	-	-
Kunimi	-	2	2	-
La Clapière	-	7	2	-
La Frasse	-	5	-	-
La Saxe	-	5	2	-
Montaldo di Cosola	2	2	-	-
Otho	1	-	-	1
Porta Cassia	-	3	-	-
Ragoleto	-	5	-	-
Rosone	-	2	2	-
Ruinon	1	3	5	-
Vallcebre	-	7	-	-
Val Pola	1	1	1	1
Vajont	1	2	2*	1
Xintan	1	2	1	1
Total trends	**11**	**66**	**20**	**5**

* These stages differ from all the other Trends III and call for further investigations.

Curves characterized by a Trend I have a linear behaviour associated to a steady-state movement.

The upper triangle of the square diagram, above the linear boundary, represents the area of Trend II and collects all the curves representing decelerating movement of active landslides or recorded after Trends III.

The area of Trend III includes all the curves of the occasionally reactivated landslides, as they can be defined according to the description provided in the quoted references.

The area of Trend IV collects the five failure stage contained in dataset. It also includes the first two stages of the Vajont landslide, which cannot be uniquely defined on the basis of the available literature and differ significantly from all the other Trends III identified in this study.

Finally, in Table 4.6 the maximum rescaled displacements recorded for each case study is reported and the three graphs in Figure 4.11 show the corresponding plot.

From the analysed displacement data, it is possible to conclude that Trend I is characterized by rescaled displacements of the order of 10^{-6}, Trend II are associated with values smaller than 10^{-3}, Trend III are related to values of the order of 10^{-2} while in correspondence of Trend IV the rescaled displacements are in the range between 10^{-1} and 1 (Cascini et al., 2020).

Table 4.6: Curve types and deformation values for the analysed landslides.

Landslide	**Maximum rescaled Displacements (-)**	**Corresponding curve type**
Fosso San Martino	3.8E-06	Linear -Trend I
Castelrotto	2.5E-07	Concave - Trend II
Montaldo di Cosola	4.3E-06	
Porta Cassia	4.8E-06	
Rosone	8.3E-06	
Vallcebre	1.9E-05	
La Frasse	9.6E-04	
Bindo-Cortenova	1.3E-03	
Ragoleto	1.4E-03	
Kunimi	2.7E-05	Convex (followed by concave) – Trend III
Ruinon	9.2E-03	
La Saxe	1.7E-02	
La Clapière	2.8E-02	
Vajont	4.1E-01	Convex (failure) – Trend IV
Val Pola	≅1	
Chuquicamata	-	
Ohto	-	
Xintan	-	

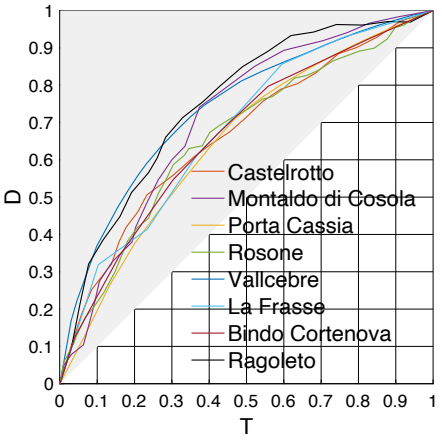

a)

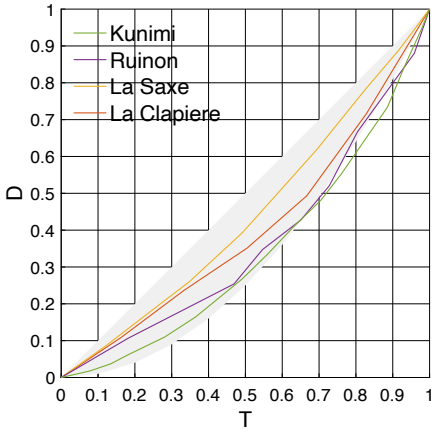

b)

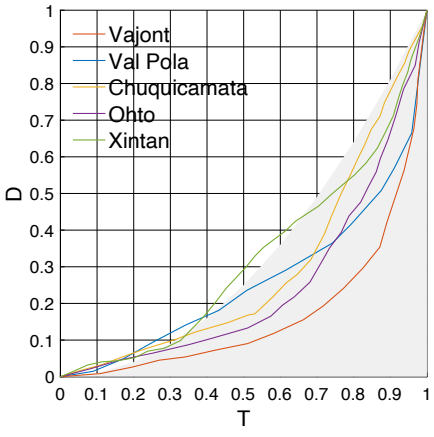

c)

Figure 4.11: Dimensionless trends for the activity stages reported in Table 4.6 for different shapes: a) concave (Trend II), b) convex (Trend III), and c) convex with failure (Trend IV).

With reference to the analysed literature, the method well describes both active landslides and occasional reactivations, identifying the most important accelerating stages, also in the case of failure.
Moreover, we observe that active landslides (Trend II) are often related to an ordinary triggering factor, such as a seasonal increase in pore water pressure induced by rainfall. In such a case, soon after a sudden acceleration, the velocity reduces until a new steady state is reached.
Slopes exposed to not-seasonal events, both natural as earthquakes or due to anthropic activity or specific variations in boundary conditions (i.e. those related to the presence of a new water reservoir at the toe of the slope), the velocity clearly increases, in the case of both an occasional reactivation and a first failure stage (Trends III and IV).
However, in Trend III cases, after the triggering cause has ceased, the landslide undergoes a Trend II deceleration process up to a constant value of the velocity characterizing a new stable condition of the slope (Trend I).
On the contrary, a landslide developing a Trend IV behaviour tends to naturally gain kinetic energy with increasing velocity until collapse occurs, except in rare cases, when specific external conditions slow down the landslide. This is the case of the Vajont landslides that decelerated on 1960 and 1962 just after lowering of the water level of the reservoir (Figure 4.8a).
It is interesting to observe that when the landslide evolves into a catastrophic event (e.g., stage 6 of the Vajont landslide, in Figure 4.8a), the dimensionless displacement curves tend to approach the bottom right corner of the unit square (Figure 4.11c), with the possibility of localized sharp curvature in the more extreme cases.
Indeed, shape and position of dimensionless curves indicate the possibility of establishing a criterion to interpret the evolution of a landslide and to distinguish stable from potentially unstable phenomena on the basis of displacement measurements only.
To this end, the displacement trends and the associated kinematic characteristics are investigated in the following chapter together with the techniques able to improve the construction of the dimensionless curves through the proper selection of the initial and final points of the activity stages.

.

5. Assessing the kinematic characteristics of displacement trends

The landslide displacement behaviour is determined by a large number of factors that can be strictly related to triggering causes and/or to the characteristics of the landslides (geometry, materials, dimensions, movement type, etc.). In addition, the quality of monitoring data depends on the specific acquisition device and is unavoidably affected by noises.
All these elements do not allow recognizing common features shared by different landslides in the available database that was implemented collecting eighteen well documented case studies in the literature. For this reason, each activity stage in the database was represented in a dimensionless displacement vs. time diagram, thus observing typical trends characterized by a well-defined shape and position of the corresponding curves.
This chapter examines these trends in order to individuate their kinematic characteristics, if any, able to quantitatively describe each of them.

5.1 Typical behaviours of displacement derivatives

A proper analysis and description of evolutive trends can be carried out through the derivatives of displacements. To this end, for each activity stage the derivatives up to the third order of cumulative displacement namely velocity (derivative of the first order), acceleration (derivative of the second order) and jerk (derivative of the third order) are computed, turning out to be particularly helpful for recognizing features of the recognized trends.
First of all, it is important to clarify the used nomenclature. The present work deals with scalar quantities, that are the intensity of kinematic vector acting on the slope. Therefore the term *displacement* indicates the intensity of displacement vector, *speed*, *velocity* or *displacement rate* the intensity of velocity vector; *acceleration* or *velocity rate* the intensity of the acceleration vector; *jerk* or *acceleration rate* the intensity of the derivative of the acceleration with respect to time.
Focusing on the physical meaning of each of these quantities, displacement and velocity represent kinematic features, characterizing the evolution of landslide motion, acceleration provides information about the system of forces that globally

affects the slope and jerk is related to the time variation of such a system. The forces acting on landslide body are divided in external, due to dead weights and boundary conditions, and internal, that are more difficult to determine. According to Newton' Second Law (Plastino e Muzzio, 1992), inertial force acting on a moving body is directly proportional to its acceleration, completely describing dynamics of several systems. However, in some cases dynamic behaviour is described with differential equations that make explicit jerk function. Despite it is not commonly used in structural and geotechnical engineering, some contributions highlighting role of jerk are available (Chase et al., 2003, He et al., 2015, Noda et al., 2013).

In Figure 5.1 qualitative derivatives of three schematic sequences of displacement trends are reported referring to typically observed behaviours, derived from displacement data series of Vallcebre (Figure 5.1a) (Corominas et al., 2005), Kunimi (Figure 5.1b) (Shuzui, 2001) and Vajont (Figure 5.1c) (Nonveiller, 1987).

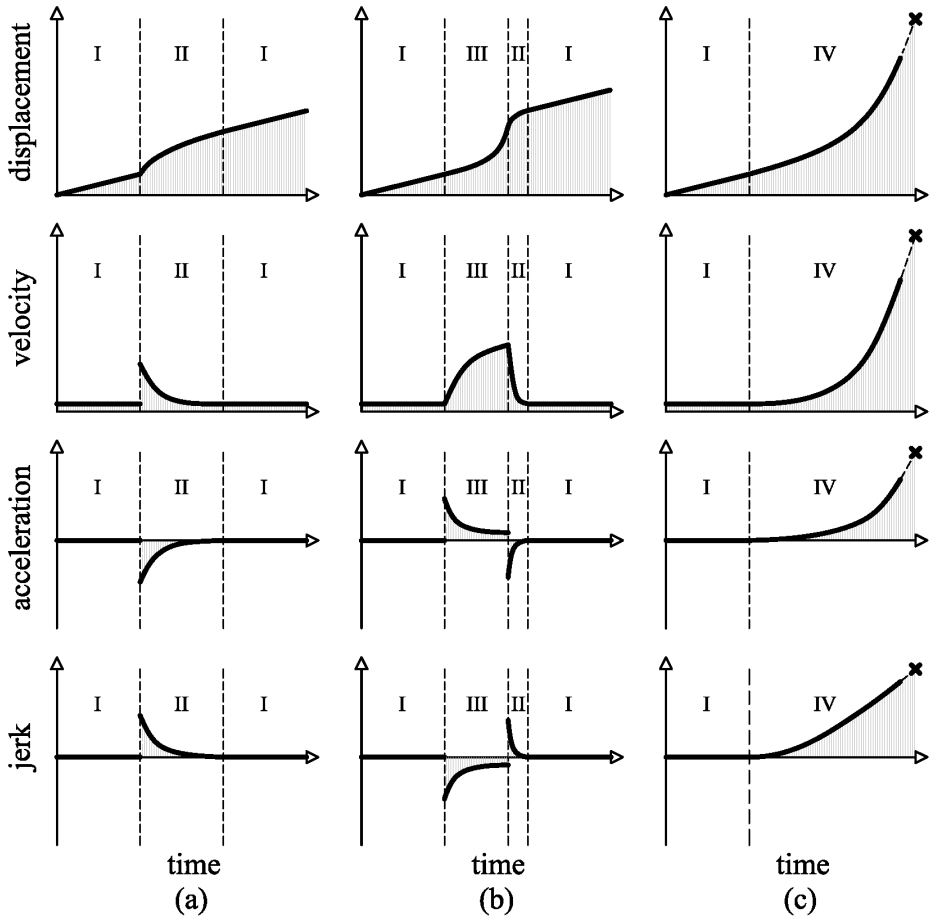

Figure 5.1: Schemes of displacement behaviours and corresponding derivatives of first, second and third orders for some typical sequences.

Additionally, in Table 5.1 a summary of the adopted framework is reported, indicating for each trend and order of derivatives (0th being the order of displacements) changes in positivity and growth. Upward arrows ("↑") indicate increasing functions, downward arrows ("↓") for decreasing functions, while functions constant over time are marked with horizontal two-headed arrows ("↔").

Table 5.1:Schematic synthesis of trends in terms of sign and growth proprieties of the derivatives up to third order.

	Order	**I**	**II**	**III**	**IVa**	**IVb**
displacement	0	$d > 0$ ↑	$d > 0$ ↑	$d > 0$ ↑	$d > 0$ ↑	$d > 0$ ↑
velocity	1	$\dot{d} > 0$ ↔	$\dot{d} > 0$ ↓	$\dot{d} > 0$ ↑	$\dot{d} > 0$ ↑	$\dot{d} > 0$ ↑
acceleration	2	$\ddot{d} = 0$ ↔	$\ddot{d} < 0$ ↑	$\ddot{d} > 0$ ↓	$\ddot{d} > 0$ ↑	$\ddot{d} > 0$ ↑
jerk	3	$\dddot{d} = 0$ ↔	$\dddot{d} > 0$ ↓	$\dddot{d} < 0$ ↑	$\dddot{d} > 0$ ↓	$\dddot{d} > 0$ ↑

Observing this synthetic scheme, it is possible to state some proprieties of each trend. Trend I can be defined as a dynamic equilibrium condition, in which all the functions are constant but the displacements, in particular acceleration and jerk are equal to zero. Trend II is characterized by negative acceleration and decreasing jerk.

Hence, Trend I represents the boundary between the stable Trend II and the Trend III, which is the *least* unstable among the accelerating trends. Indeed, the unstable trends are characterized by positive acceleration (which implies disequilibrium of forces). The recovery phase characterizing certain accelerative stages, which we call as Trend III, is due to the fact that the acceleration decreases over time, being the jerk not positive.

Trend IV, introduced in Chapter 4, is here further divided in Trends IVa and IVb on the base of growth proprieties of the jerk. This distinction is physically related to the final evolution of Trend IVa (characterized by decreasing jerk) that, in some circumstances, can be followed by a deceleration, as a result of specific modifications of initial boundary conditions, e.g. in the case of Vajont landslide in correspondence to the first two lowering of the water level in 1960 and 1962. This cannot occur in case of Trend IVb, where the increasing behaviour of the jerk indicates the achievement of an unstable condition that definitely leads to failure, as in the case of the last accelerating stage of Vajont in 1963 (Figure 5.1c).

Hence, while for Trends I, II and III it is possible to observe significant differences just analysing the sign of acceleration and thus the growth of velocity, with regard to Trends IVa and IVb, the study of the jerk is essential.

From Table 5.1, it is possible to observe jerk behaviour in a theoretical sequence of patterns, from the most stable to the very unstable one. In particular, jerk starts to be positive and decreasing with trend II, goes to 0 in Trend I, becomes negative in Trend

III, but changes in order to return to 0 at the boundary between Trends III and IV, where at last remains positive, decreasing to a constant value or increasing further.
A final remark is related to apparent jumps in data or in their derivatives. Actually, for physical reasons, all the mentioned quantities cannot reach infinite values. As a consequence, the corresponding functions must be continuous and differentiable, at any order. However, due to data resolution, fast changes in functions could result in apparent jumps. To avoid to deal with infinite values is sufficient to discard small regions, whose size must be determined, around the apparent jumps.

5.2 Dimensionless derivative trends

Dimensionless diagrams derived from the elaboration of cumulative displacements over time allow to obtain monotone curves interpolating points $P_{i,j} \equiv (T_{i,j}; D_{i,j})$.
Analysing the cloud of dimensionless data as a whole it is possible to observe that the points are symmetric with respect to the diagonal from the top left to the right bottom corners of the square, represented by the equation: $D = 1 - T$.
It is immediately observable that the other diagonal of the square (with equation $D = T$) represents the stage of activity in which landslides move with a constant velocity. This line corresponds also to the boundary between the area of diagram in which are the curves characterized by a negative acceleration (upper triangle) and the area in which are located the curves with a positive acceleration (lower triangle). These observations point that a curve passing throw the diagonal should be considered as representative of more than a single activity phase and, as such, it should be further partitioned, except in the cases in which there is a small fluctuation around the diagonal itself due to data noise.
According to the procedure of selection of activity phases, changes in the behaviour of triggering factors need to be considered coupled with variation in curvature of displacement curves. However, it is desirable that the selection is improved with the aim of making the method more robust and applicable even in the case in which no information on triggering causes are available. Indeed, initial and final points of single phase can influence the results in terms of dimensionless analysis.
Moreover, it is worth noting that the frequency of measurement can affect the applicability of the method and it needs to be proportioned to the amplitude of the selected time interval for the activity stage. According with the sampling theorem, that established the minimum sampling frequency required to reconstruct the original signal, a recorded sample contains the higher frequency of the original signal if the sampling frequency is at least twice that of the signal itself (Marks, 1991).

All the mentioned aspects should be taken into account during the definition of the proposed theoretical model, since its strong dependence on the experimental data.
In the following sections, a dimensionless analysis of the displacement data of the eighteen case studies in the dataset is presented, based on the differential quantities previously mentioned.
To obtain continuous behaviours of the derivatives is possible to construct a proper function that interpolates the experimental data and that can be analytically derived. Clearly, the choice of the function that best fits data is not a trivial task and many different options – as for example power law or sine functions - can be taken into account, each with its advantages and its limitations.
Alternatively, the computation of the derivatives can be obtained numerically from the discrete displacement data constituting each trend, using various differential techniques. In this case the presence of noise in input data should be carefully considered, introducing some smoothing operations on the original signal. Otherwise, fluctuations in displacement data propagate to derivatives and increase with the order of differentiation, affecting the output.
For the purpose of this work, both analytical and numerical differentiation, through centred finite differences, have been employed to derive displacement trends: obtained results are thereafter compared.

5.2.1 Interpolating function

In this section an analysis of dimensionless displacement trends is carried out through the use of an interpolating function. Among all the possible functions that may be suitable to describe the trends power law has been chosen, due to the fact that combines a good fitting of experimental data and simple mathematical features. Power laws are often employed in many different fields related to physics or earth and planetary sciences, to biology, economics and finance, and even to social sciences, as highlighted by Newman (2005) or by Andriani and McKelvey (2007), which, in particular, listed a large number of power laws among natural and social phenomena. Particularly, according to Newman (2005), power law functions are represented by straight lines in log-log plot, that has both horizontal and vertical axes in logarithmic scale. This can represent a first way to recognize if the function is suitable to interpolate experimental data, but to assess with certainty whether the data set has a power law distribution is not an easy task. In fact, having straight lines on a log-log plot is a necessary condition but it is not a definitely sufficient condition. This aspect is analysed in detail by Clauset et al. (2009) who studied, through a statistical approach, power law behaviours in empirical data combining maximum-likelihood fitting methods with goodness-of-fit tests.

However, it is out of the scope of this contribution to ascertain whether cumulative displacements measured from landslides exactly follow power law functions. Following Cascini et al. (2014) the dimensionless cumulated displacement in the j^{th} stage of activity ($1 \leq j \leq N$) can be expressed by:

$$D = T^{x} \tag{5.1}$$

in which the exponent x is a positive real number and the index j has been dropped for conciseness.

Following this approach landslide behaviour is completely described by the value of the exponent x, that represents the only parameter of the model.

According to this approach, each of the 102 dimensionless curves obtained in Chapter 4 can be represented by a power law function and, through equation (5.1), by a value of the exponent x. The identification of the power law that better fits experimental data has been carried out through a procedure that minimizes the distance between input data and corresponding points on the interpolant, that is by minimizing the following relationship:

$$\sum_{i=2}^{n-1} \left(\left(\frac{T_{i+1,j} - T_{i-1,j}}{2} \right) \left(T_{i,j}^{x_j} - D_{i,j} \right) \right)^2 \tag{5.2}$$

in which $D_{i,j}$ and $T_{i,j}$ have been already introduced in Section 4.2.2, n is the total number of the points contained in the j^{th} stage and x_j is the unknown exponent.

By way of example the comparation between experimental data and interpolating function is showed referring to accelerating stage of Kunimi landslide in Figure 5.2. The value of the exponent x is equal to 1.8635.

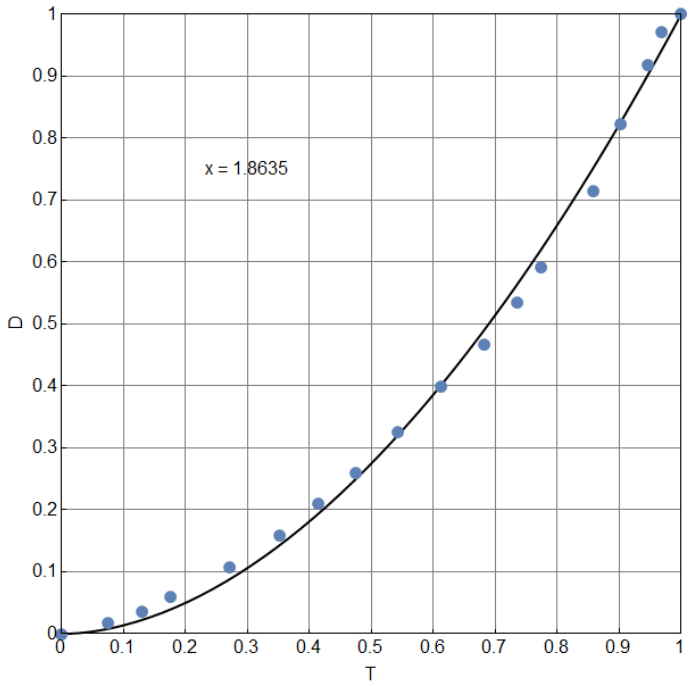

Figure 5.2: Interpolating power law function for accelerating stage of Kunimi landslide

Similar considerations have been made referring to the 102 dimensionless curves, observing a correspondence between the real evolution and the value of the exponent. Clearly the limits between trends are not so strict, thus a tolerance on the exponent value of $\pm 10^{-2}$ has been adopted.

5.2.2 Derivatives of the interpolating function

Assuming that each curve can be properly described with a power law, it is possible to analyse the derivatives of the interpolating function.
In particular, the derivatives of the function $D = D(T)$ up to the third order (velocity, acceleration, jerk) are readily computed as:

$$\dot{D} = x\,T^{x-1} \tag{5.3}$$

$$\ddot{D} = x\,(x-1)T^{x-2} \tag{5.4}$$

$$\dddot{D} = x\,(x-1)(x-2)T^{x-3} \tag{5.5}$$

Studying the sign and the growth proprieties of functions (5.3), (5.4) and (5.5), it is possible to associate each of the five trends to a range of values of exponent x (Figure 5.3):

- x=1 corresponds to Trend I, which characterizes any steady-speed motion with acceleration equal to zero (diagonal of the square D-T);
- $x \in (0,1)$ for Trend II, corresponding to negative acceleration (blue curves);
- $x \in (1,2]$ for Trend III, in which motion is governed by positive acceleration and negative jerk (green curves);
- $x \in (2,3]$ for Trend IVa, characterized by positive acceleration and positive decreasing jerk (orange curves);
- $x>3$ is related to Trend IVb, in which motion is characterized by all positive and increasing derivatives over time (red curves).

Dashed black curves represent the theoretical boundaries between trends: curve with x=1 corresponds to movement with constant velocity and zero acceleration, curve characterized by x=2 stands for motion with positive, constant acceleration, whereas curve with a value of exponent x equal to 3 is for motion with positive acceleration at constant jerk. The latter two curves are both associated to mechanical meanings: for a mass which is not dependent on time, x=2 and x=3 are respectively curves corresponding to inertia and rate of change of inertia which are held constant in the unit time slot.

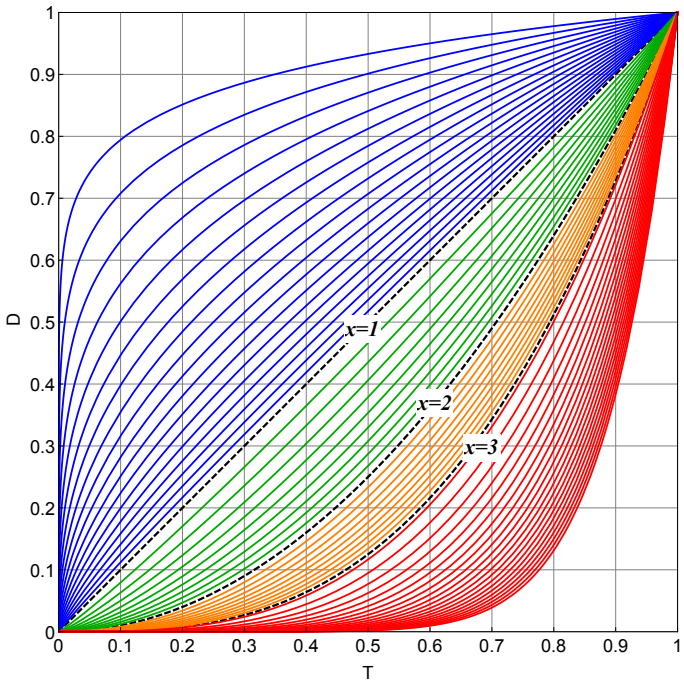

Figure 5.3: Dimensionless displacements D versus time T as power law functions. Color coding: blue curves (0<x<1); green curves (1<x<2); orange curves (2<x<3); red curves (x>3)

Finally, it is worth noting that both limits x=0 and $x \to \infty$ are not physically meaningful in case of moving landslides: the first one because it corresponds to a displacement reaching the maximum value in a vanishing time, at $T = 0$ and then getting constant for the remaining time, while the second one would give place to a movement characterized by vanishing displacement for any $0 \leq T < 1$ and reaching final maximum value instantaneously at $T = 1$.
In the practice it is possible to have a final value of the displacements some orders of magnitude higher than the previous monitored data. In such a case the dimensionless displacement curves reaches the boundary of the square and the exponent can be confusing with an infinite value: actually, this is only an issue in representation of experimental data. An example is the red curve reported in Figure 4.9 for the failure stage of Vajont landslide: in this case the final displacement is about 500 m while the previous displacements are in the order of 300 cm.

5.2.3 Numerical derivatives for landslides in database

In this Section, derivatives up to the third order are numerically computed. To reduce the noise of original records, derivatives have been estimated on manipulated input data.
For the sake of completeness, relationships (4.1) and (4.2) used for dimensionless displacements and time are here reported again:

$$D_{i,j} = \frac{d_{i,j} - d_{0,j}}{d_{n,j} - d_{0,j}} \tag{5.6}$$

$$T_{i,j} = \frac{t_{i,j} - t_{0,j}}{t_{n,j} - t_{0,j}} \tag{5.7}$$

Combining equations (5.6) and (5.7), relationship (5.1) can be rewritten as:

$$\frac{d_i - d_0}{d_n - d_0} = \left(\frac{t_i - t_0}{t_n - t_0}\right)^x \tag{5.8}$$

in which x is computed with the procedure described in Section 5.2.1.
The i^{th} displacement can thus be expressed as a function of the time t_i:

$$d_i = d_0 + \left(\frac{t_i - t_0}{t_n - t_0}\right)^x (d_n - d_0) \tag{5.9}$$

Therefore, for each value t_i within the j^{th} activity stage, it was possible to obtain the corresponding value of d_i.
The numerical differentiation of the new set of data (t_i, d_i) has been obtained using fourth order centred finite difference scheme, that for the i^{th} datum, is schematically expressed as:

$$\dot{d}_i = \frac{-d_{i+2}+8\,d_{i+1}-8\,d_{i-1}+d_{i-2}}{12\Delta t_i} \tag{5.10}$$

$$\ddot{d}_i = \frac{-\dot{d}_{i+2}+8\,\dot{d}_{i+1}-8\,\dot{d}_{i-1}+\dot{d}_{i-2}}{12\Delta t_i} \tag{5.11}$$

$$\dddot{d}_i = \frac{-\ddot{d}_{i+2}+8\,\ddot{d}_{i+1}-8\,\ddot{d}_{i-1}+\ddot{d}_{i-2}}{12\Delta t_i} \tag{5.12}$$

in which $i \in [3, n]$, where n is the total number of elements in the j^{th} interval.
As done for displacement, normalization procedures have been applied also to velocity, acceleration and jerk, in order to draw derivatives of data in a dimensionless diagram.
While the dimensionless time is the same as in equation (5.7), velocity, acceleration and jerk are respectively rescaled as:

$$\dot{D}_{i,j} = \begin{cases} sgn\left[\dot{d}_{\max,j}\right] \frac{\dot{d}_{i,j}-\dot{d}_{n,j}}{v_{max}}, & if\ v_{max} \neq 0 \\ \dot{d}_{i,j}, & otherwhise \end{cases} \tag{5.13}$$

$$\ddot{D}_{i,j} = \begin{cases} sgn\left[\ddot{d}_{\max,j}\right] \frac{\ddot{d}_{i,j}-\ddot{d}_{n,j}}{a_{max}}, & if\ a_{max} \neq 0 \\ \ddot{d}_{i,j}, & otherwhise \end{cases} \tag{5.14}$$

$$\dddot{D}_{i,j} = \begin{cases} sgn\left[\dddot{d}_{\max,j}\right] \frac{\dddot{d}_{i,j}-\dddot{d}_{n,j}}{j_{max}}, & if\ j_{max} \neq 0 \\ \dddot{d}_{i,j}, & otherwhise \end{cases} \tag{5.15}$$

in which:

$$v_{max} = max\left[\left|\dot{d}_{\min,j}\right|, \left|\dot{d}_{\max,j}\right|\right] \tag{5.16}$$

$$a_{max} = max\left[\left|\ddot{d}_{\min,j}\right|, \left|\ddot{d}_{\max,j}\right|\right] \tag{5.17}$$

$$j_{max} = max\left[\left|\dddot{d}_{\min,j}\right|, \left|\dddot{d}_{\max,j}\right|\right] \tag{5.18}$$

The terms $\dot{d}_{i,j}$, $\ddot{d}_{i,j}$, $\dddot{d}_{i,j}$ are velocity, acceleration, jerk included in the j^{th} stage, $\dot{d}_{\max,j}$, $\ddot{d}_{\max,j}$, $\dddot{d}_{\max,j}$ and $\dot{d}_{\min,j}$, $\ddot{d}_{\min,j}$, $\dddot{d}_{\min,j}$ are respectively the maximum and the minimum values of velocity, acceleration and jerk in considered activity stage, whereas $\dot{d}_{n,j}$, $\ddot{d}_{n,j}$, $\dddot{d}_{n,j}$ are the final values of derivatives.
Results are showed in Figure 5.4 that report dimensionless displacements (a), velocities (b), accelerations (c) and jerks (d) versus dimensionless time, using the following color coding:

- Black points (on the diagonal from the bottom left to the right corner in the displacement graph) represent Trend I, collecting any steady-speed motion;

- blue points refer to Trend II: displacements with negative dimensional acceleration;
- green points are for Trend III: motion with dimensional acceleration which is positive, but decreasing in time;
- orange points stand for Trend IVa: motion with positive dimensional acceleration and dimensional jerk decreasing with time;
- red points is for Trend IVb: motion with positive and increasing dimensional acceleration and jerk, corresponding to motion of landslides that are likely doomed to collapse.

Diagrams in Figure 5.4 have been plotted in a rescaled and translated form with the aim of obtaining square graphs, as in the case of displacement trends.

Thick, black, dashed curves represent possible boundaries between regions characterized by different trends. However, it must be noted that for a definition of boundaries, the uncertainty of data must be taken into account considering, in practical applications, a region of confidence between the different regions.

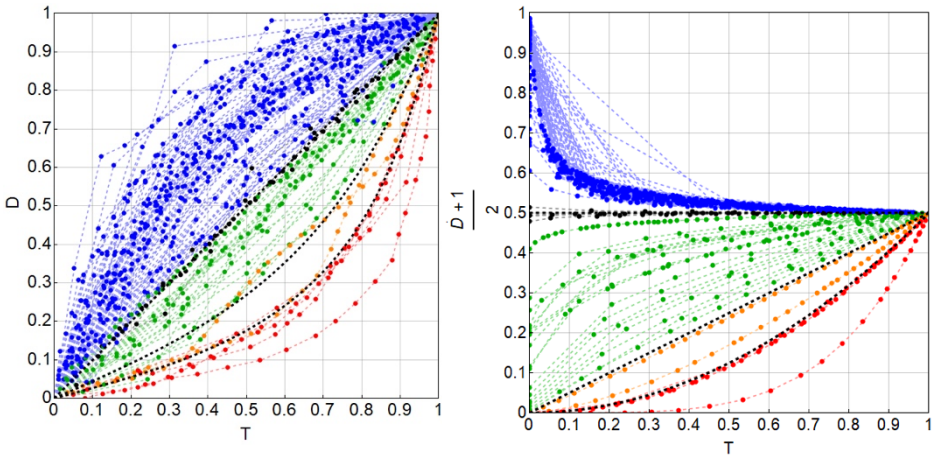

a) b)

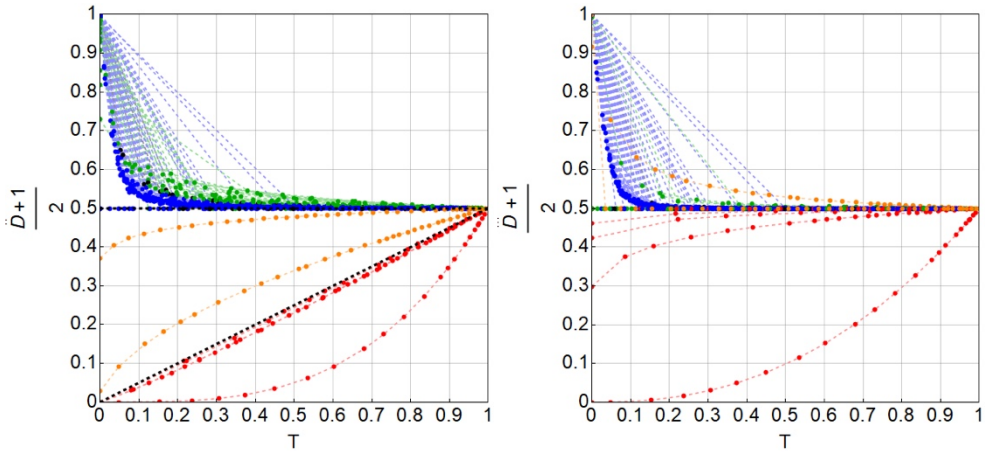

Figure 5.4: Dimensionless behaviours of displacements (a), velocities (b), accelerations (c), jerks (d) obtained for the case studies in the database. Velocity, acceleration and jerk diagrams have been rescaled and translated to obtain square plots.

Curves obtained for derivatives (Figures 5.4 b, c, d), as well as it has just observed for dimensionless displacement diagram (Figure 5.4a), are located in different regions depending on the trend which they are associated to, except for few data not satisfying growth property possibly because of poor quality of input or instrumental errors.
Finally, details about derivatives can be used to validate or improve the partitioning of original time series.

5.3 Discussion

In this chapter a distinction between the five dimensionless trends has been presented on the basis of the analysis of time derivatives of displacement up to the third order. The differentiation has been carried out both through an interpolating power function, analytically and numerically, leading to equivalent conclusions in terms of behavior.
Mathematically, the analysis of displacement, velocity, acceleration and jerk showed different sign and growth proprieties for each trend. These differences are related to physical characteristics, associated to kinematic and dynamic features of the landslides.
The results for the landslides presented in chapter 4, obtained in terms of displacements and derivatives, are in agreement with scientific literature and with the modelling of the phenomena provided by various authors.
By way of example it is possible to refer to the modelling of Vallcebre landslide proposed by Ferrari et al. (2011). Authors schematized landslide body through two

interacting sliding blocks for simulating the effects of mass accumulation at the toe of the slope, considering groundwater fluctuations as triggering factor and a viscous behaviour of the material along the sliding surface. Dynamic equation associated to this model has been solved discretizing time with finite difference approach, obtaining displacements and velocity trends describing the kinematic behaviour of the landslide, considering the influence of each of physical terms introduced in the model, e.g. the effects of groundwater fluctuations. The obtained displacement trends are characterized by a concave shape whose curvature depends on the viscosity parameters and on the dimensions of the two blocks. The corresponding velocity trends are characterized by a decreasing curve tending to zero, after a maximum value reached for the initial increase in water table. These results, obtained with a theoretical model, are consistent with the dimensionless trends computed on the basis of experimental data from Vallcebre case study, that is characterized by seven Trends II, defined as concave displacement and decreasing velocity curves.

Another interesting comparison can be made referring to the analysis carried out by Helmstetter et al. (2004) for the Vajont landslide. Authors considered a sliding block model and friction depending on state and velocity variations, simulating the final accelerative stage leading to the failure. The results are presented in terms of displacement and velocity, showing a trend with convex shape for displacements and an increasing velocity with an upward concavity. This represents the behaviour associated with Trend IV, that is the one recorded for Vajont paroxysmal stage according to the analysis proposed in this work.

More detailed considerations can be carried out analysing acceleration, that is directly proportional to the system of forces globally acting on the landslides body, and jerk, that is related to the variation of this system over time. The analysis of jerk allowed distinguishing, within Trend IV, between two different behaviours, called IVa and IVb. The first one is typical of stages close to the failure in which particular variation in boundary conditions can lead to a deceleration, whereas the second one, characterized by increasing jerk, is recorded in cases in which the failure of the slope is unavoidable.

The identification of the trend type of an activity stage has been simplified by the use of an interpolating function, consisting in a power law. As a result, each dimensionless curve can be associated to a value of the exponent and hence to a trend type.

Naturally, this procedure is based on mathematical approximations and on input data that can be affected by noise and acquisition errors. These aspects need to be considered in the assessment of the results. However, the method appears to be suitable to interpret the activity stages of the landslides in the dataset, providing a simple and informative remarks on the data.

Summarizing, through the computation of the exponent, it is possible to associate each displacement stage to a stability region in the dimensionless graph, providing information about the evolutive stage of the landslide.
This operation, that has been used in a posteriori analysis, can be implemented in a forecasting algorithm availing a near real time monitoring system. With this purpose, in Chapter 6 a study of the variation of the exponent over time is presented, with respect to case studies for which detailed displacement data are available.

6. A perspective on forecasting the evolution of slope movements

The previous chapters described a framework able to interpret the kinematic characteristics of all the activity stages that can affect a slope. This model derives from the analysis of well documented landslides in the literature and it introduces specific trends for the landslide displacement and their time derivatives, up to the third order.
The present chapter is devoted to investigate the application of such a method to forecast the evolution of a landslide. Although it must be acknowledged that the proposal is still in its early stage of development, it already seems to have the ability to predict the slope failure from displacement monitoring data in a near real time system.
To this end, a preliminary study was carried out on the functions that best interpret the displacement data of phenomena present in the available database. Current knowledge indicates that the power law function, introduced in Section 5.2.1, provides accurate interpolations of all identified displacement trends.
Indeed, this function has been used to investigate its ability to forecast the evolution for some landslides in the database and to compare its predictive skill with that of the method proposed by Fukuzono-Voight, that is the most used in the current practice.

6.1 The power law exponent method: basic concepts and explanatory examples

The power function is characterized by its exponent that assumes different values in the transition from one displacement trend to another, Section 5.2.2. Indeed, the exponent can be used as a forecasting tool especially when a near real time monitoring system is available.
To this end, the interpolation procedure of the experimental displacement data can be repeated every time a new datum is recorded by the system. Basically, the forecasting algorithm can apply the minimization procedure described in Section 5.2.1 for each set composed by displacement data, when progressively new points are acquired.

The procedure starts at the beginning of the any activity phase, with $x=1$ and then adjusts the value as the dataset increases with new entries. Particularly, the interpolating curve is computed firstly to a set of two elements, secondly to three elements and so on until the end of the stage. As the k^{th} datum is acquired, the exponent corresponding to the current data set is estimated as:

$$x_k = \min\left[\sum_{i=1}^{k}\left(\Delta t_i (T_i^x - D_i)\right)^2\right] \tag{6.1}$$

An example of the procedure is shown in Figure 6.1 for Kunimi landslide, reporting the interpolation carried out for k equal to 2, 6, 12 and 18 points, corresponding to the end of the stage.

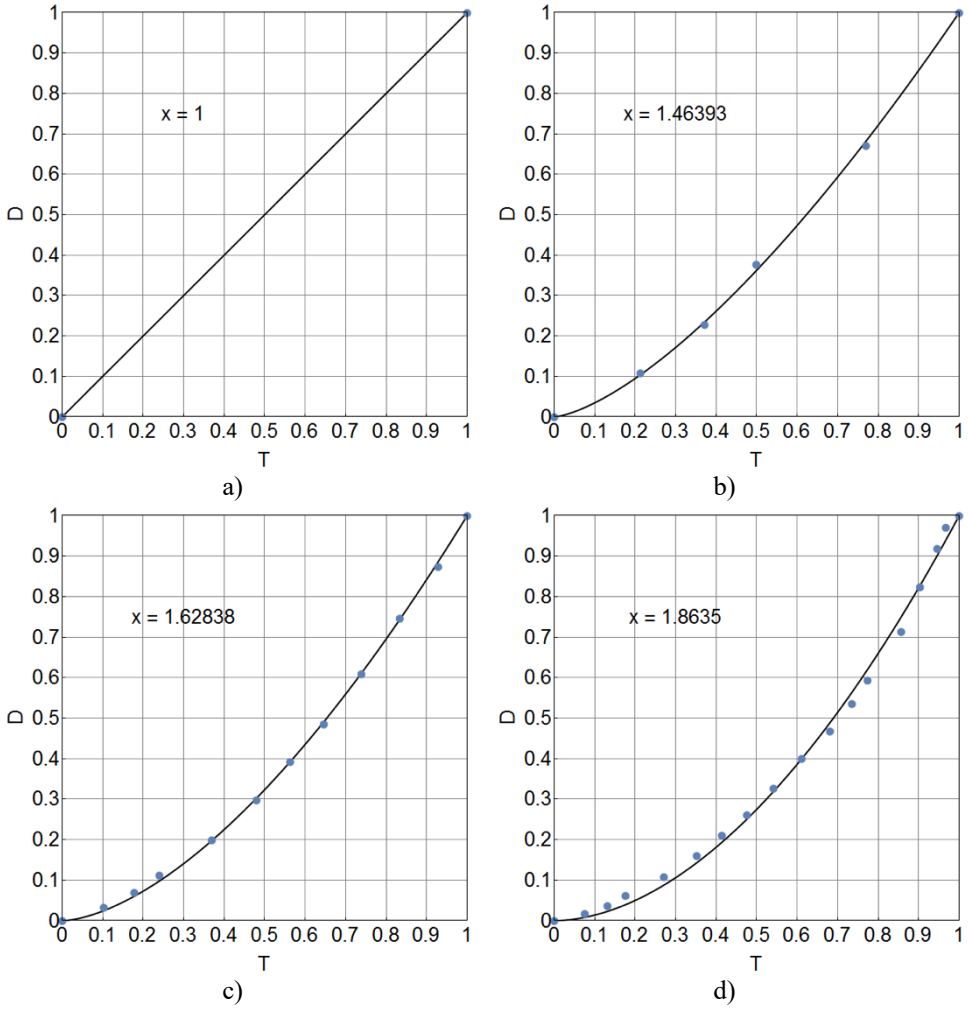

Figure 6.1: Evolution of displacement trend and related exponent for Kunimi accelerating stage computed for: a) 2 days (2 points), b) 8 days (6 points), c) 20 days (12 points) and d) 59 days (18 points) after the beginning of the stage.

Notice that the interpolating function when $k = 2$ is represented by a straight line, independently of the activity stage.

Equation (6.1) takes into account the variation of x as a discrete function of k. However, since the size of data set increases at a known and typically fixed time rate, equation (6.1) basically says how the exponent varies in time. Values reached by the exponent are compared with the thresholds between trends highlighted in Section 5.2.2, in order to monitor the transition of the stage from a stability region to a new one, associating alert levels when the exponent reaches values typical of Trend IVa and IVb.

As explanatory example, the procedure is here applied to an active landslide, an occasional reactivation and a slope failure. The first is represented by the stage 12 of Bindo Cortenova landslide (see Figure 4.4b), the second by the stage 4 of La Clapiere (see Figure 4.6b) and the third one by the stage 6 of Vajont (see Figure 4.8b). In all three cases we consider as if data were acquired one by one.

Figures 6.2a, 6.3a, 6.4a report the dimensionless trends obtained using the procedure showed in Chapter 4 and the final interpolating power laws: computed dimensionless points are indicated in blue, whereas the interpolating function is reported in black. Figures 6.2b, 6.3b, 6.4b show the corresponding variation of the exponent for the time interval corresponding to the selected activity phase. Dashed, red-coloured lines in Figure 6.4b indicate exponent thresholds, corresponding respectively to the transition from Trend III to Trend IVa and then to Trend IVb.

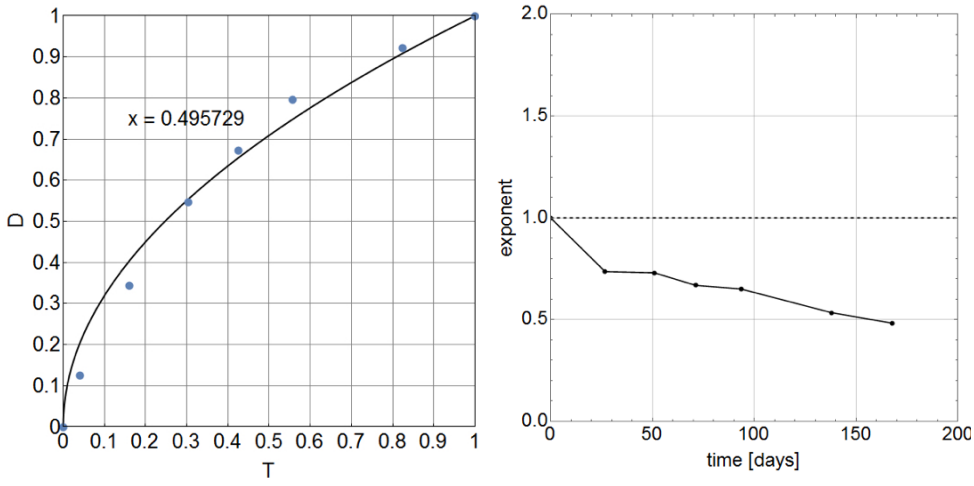

a) b)

Figure 6.2: a) Final dimensionless displacement points and interpolating function and b) variation of exponent over time for Trend II (Stage 12 of Bindo Cortenova landslide)

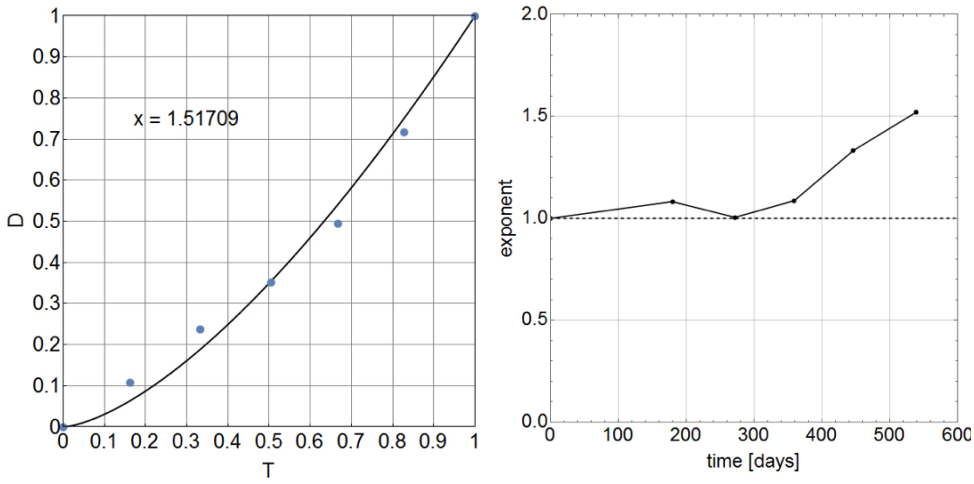

a) b)

Figure 6.3: a) Final dimensionless displacement points and interpolating function and b) variation of exponent over time for Trend III (Stage 4 of La Clapiere landslide)

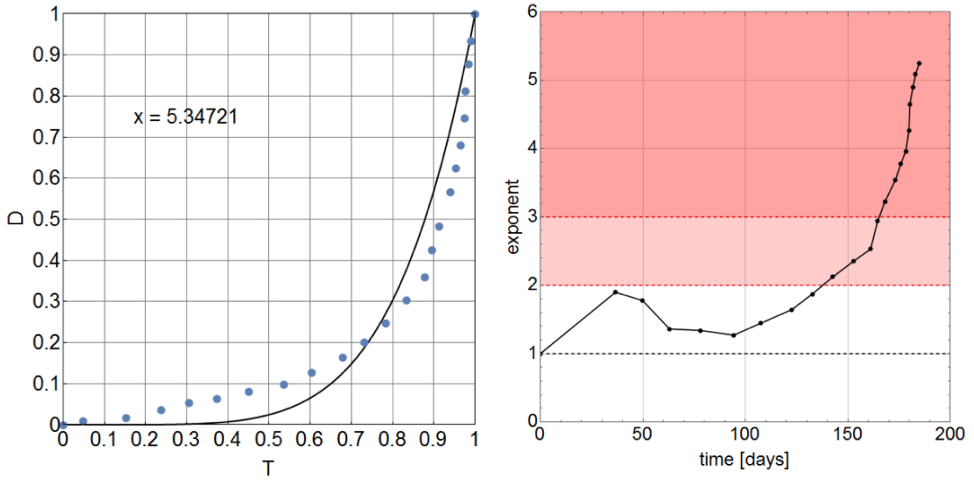

a) b)

Figure 6.4: a) Final dimensionless displacement points and interpolating function and b) variation of exponent over time for Trend IVb (Stage 6 of Vajont landslide). Red, dashed lines indicate the achievement of the first and second alert levels.

The 12th stage of Bindo Cortenova movement (from 8 March to 22 August 2013) is characterized by a final value of the exponent of the power law equal to 0.496, typical of Trend II ($0 < x < 1$). The evolution of the exponent shows that the value, starting from 1, decreases remaining almost constant until the last time step.

The 4th stage of La Clapiere landslide (from 5 April 1986 to 25 September 1987) is an accelerating stage that is followed by a decelerating one. The corresponding

dimensionless trend is interpolated by a power law of exponent $x = 1.517$, associated to Trend III ($1 < x \leq 2$). In this case the value of the exponent, again starting from 1, increases over time staying below the limit value $x = 2$.
Finally, stage 6 of Vajont landslide (from 8 April to the failure of 9 October 1963) is associated to a Trend IVb. In this case, the value of the exponent increases in time, exceeding the value $x = 2$ (transition from Trend III and Trend IVa) on 24 August and the value of $x = 3$ (transition from Trend Iva to Trend IVb) on 20 September. These values are respectively exceeded 46 and 19 days before the failure dated 9 October, when the exponent reaches the final value of 5.347.

6.2 Application of the proposed method to La Saxe rockslide

6.2.1 The case study

La Saxe rockslide is located in Valle d'Aosta Region, in the northern Italy, occupying the left hand side of Ferret Valley (Figure 6.5). The site is accurately monitored due to the high value of elements at risk, including Entreves and La Palud villages, in the Courmayeur municipality, and part of the route E25 near the access to Mont Blanc Tunnel, that represents a fundamental connection between Italy and France. Social and economic potential damage is very high, due to big losses in case of closure of the tunnel and for the touristic activities of Courmayeur area. For such a reason, after important mobilisations of the slope, in 2014 the Italian Civil Protection classified the landslide as a national emergency. An analysis of the emergency procedures and communication strategy is presented in Giordan et al. (2015).

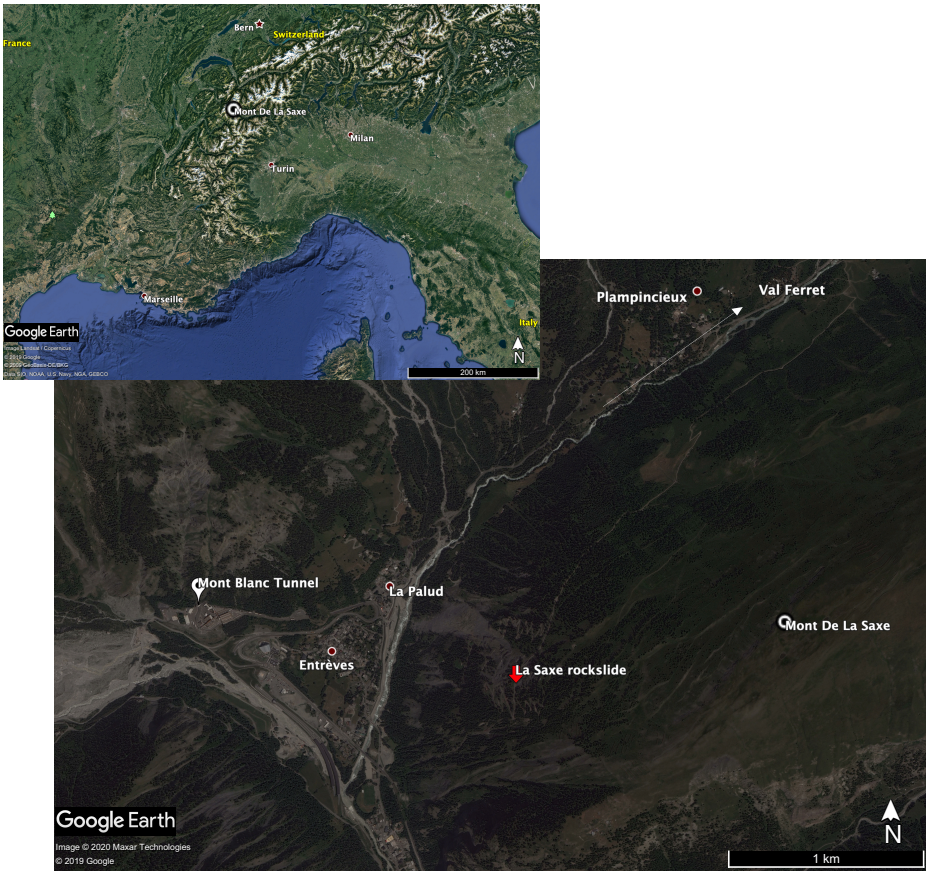

Figure 6.5: Location of La Saxe rockslide (Google Earth, 2020)

The rockslide, showed in Figure 6.6, is located on the side of a deep-seated gravitational slope deformation (DSGSD) and involves a total volume of about 8 millions of cubic meters and a surface area of about 15000 m^2. It is characterized by a maximum length of 550 m and a maximum width of 420 m, extending between 1400 and 1870 m a.s.l. with an average slope gradient of 37° (Crosta et al., 2014).

Figure 6.6: La Saxe rockslide

Mont de La Saxe is constituted by metamorphic rock, i.e. marls, argillaceous schists, black schists, mica-schists and calc-schists with quartzarenite and graphite.
These rocks are part of Ultra-Helvetic Basal Decollement units near to south of the Mt. Blanc crystalline Massif. Cover layers are constituted by rock deposits altered by gravitational processes.
The crown of the landslide is characterized by two scarps that show the presence of carbonate schists. On the other hand, at the toe of the landslide is recognizable the presence of deposits due to the instability phenomena occurred on the slope.
Landslide body is usually divided in five sectors, useful to schematically distinguish between different kinematic behaviours present on the slope:

1. Active sector;
2. Sector that is dragged from the active one;
3. Upper sector;
4. Lower sector;
5. External sector.

The movement of the rock mass is mainly associated to snow melting that occurs during Spring season, causing water infiltration and fluctuations in groundwater level. A cross section of La Saxe rockslide is reported in Figure 6.7, with the indication about sliding surface and the DSGSD.

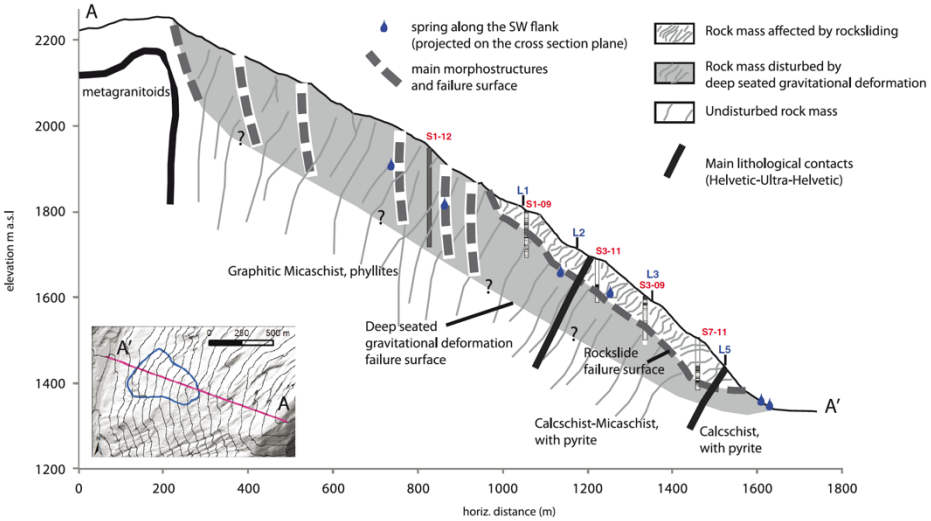

Figure 6.7: Cross section of La Saxe rockslide (Crosta et al., 2014)

6.2.2 Monitoring system

Even though aerial photos testified that landslide was active already in 1980, detailed information about the motion of the landslide are available from 2002 when a monitoring activity started using topographic measurements (Broccolato et al., 2011). Thereafter, since 2009, a complex monitoring system has been developed, due to the significant acceleration in the movement. Particularly, the system collects information about displacements, using both superficial and deep instruments, triggering factors such as groundwater level and snow melting and other physical quantities related to slope movement, including temperature and frost level. All the data collected are regularly upload in a website designed by Valle d'Aosta Region and available for early warning use.

More specifically, the system is composed by 6 boreholes with 3 inclinometers and wire-extensometers, 8 water pressure transducers in open-pipe piezometers (with depths between 16 to 50 m), 5 Differential Monitoring System (DMS) columns (CSG s.r.l.), 5 GPS network devices (with a frequency between 1h to 24h), 1 permanent GB-InSAR LiSALab™ system (Ellegi s.r.l.), a high-frames camera and a Leica TCA robotic total station, surveying 31 optical targets (Alberti, 2019). Finally, on the top

of Mont De La Saxe there is a weather station, aimed to the monitoring of rainfall, temperature, snow depth.

The monitoring network is continuously checked to detect eventual damages and variations in location of the instruments. Figure 6.8a and 6.8b respectively show a synthetic image of the report about the position of optical targets on October 2014, and optical target A1, whereas Figure 6.8c reports the Leica TCA robotic total station, located in front of the landslide.

a)

b) c)

Figure 6.8: La Saxe monitoring system: a) report on the optical targets on October 2014; b) detailed view of target A1; c) Leica TCA robotic total station.

6.2.3 Analysis of monitoring data and description of rockslide activity

Figure 6.9 reports cumulative displacements for the period between October 2010 and January 2019 for five optical targets, one for each sector.

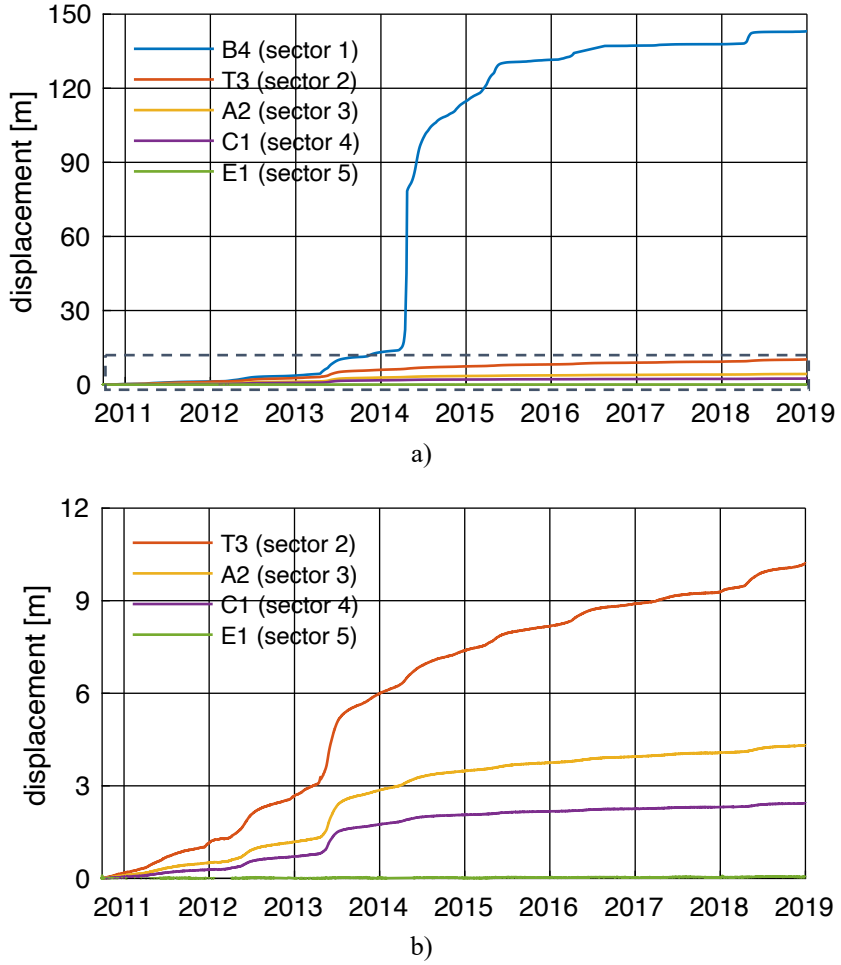

Figure 6.9: Cumulative displacement over time for optical targets B4, T3, A2, C1, E1 (a) with close-up of T3, A2, C1, E1 (b), indicated with dashed lines in (a) . High displacement recorded by target B4 corresponds to the collapse of April 2014

From displacement plots it is possible to observe the common shape of diagrams, even if a significant difference characterizes the cumulated displacement.
The first reactivation was recorded on May 2012, when 650,000 m^3 of rock accelerated, then decelerated and stopped. On Spring 2013 another reactivation occurred, due to snow melting and on 21 April a failure event was recorded. Due to the high risk one hundred people was evacuated from April to June.

The more important events occurred in 2014. Since the end of March a sector of the slopes accelerated leading to two collapses: the first one on 17 April at 20:00 CET, affecting 5,000 m^3 of rock mass and the second one 21 April at 23:00 CET involving 30,000 m^3 of material (Manconi and Jordan, 2015).
Observing the whole time series, it is evident the high displacement value associated to target B4 that corresponds to collapse occurred in Spring 2014. It was installed in the area affected by the collapse of 2014, showing an instantaneous displacement of about 30 m; then it has been recovered and is still employed in monitoring.
After 2014 events, accelerations are recorded every Spring, but the values has been very low, also due to stabilization works carried out on the slope (i.e. drainage systems). On Spring 2018 a new small reactivation has been recorded.
Figure 6.10 shows the situation of the slope on October 2019.

Figure 6.10: Details of the slope after instability events

Referring to the period from January to July 2018, Figure 6.11 reports monitoring data for displacement, velocity, groundwater level (GWL), rainfall and snow depth. Displacement and velocity are from optical targets; groundwater level is derived from two piezometers (P4 and P5) and a DMS column (DMSS3BIS).
The comparison between monitoring data of kinematic features and triggering factor highlights a strict relation between velocity and the variation in groundwater level. It is interesting to observe that the acceleration occurred in late Spring is related to an increase in groundwater level, mainly caused by the snow melting (testified by decrease in snow depth).

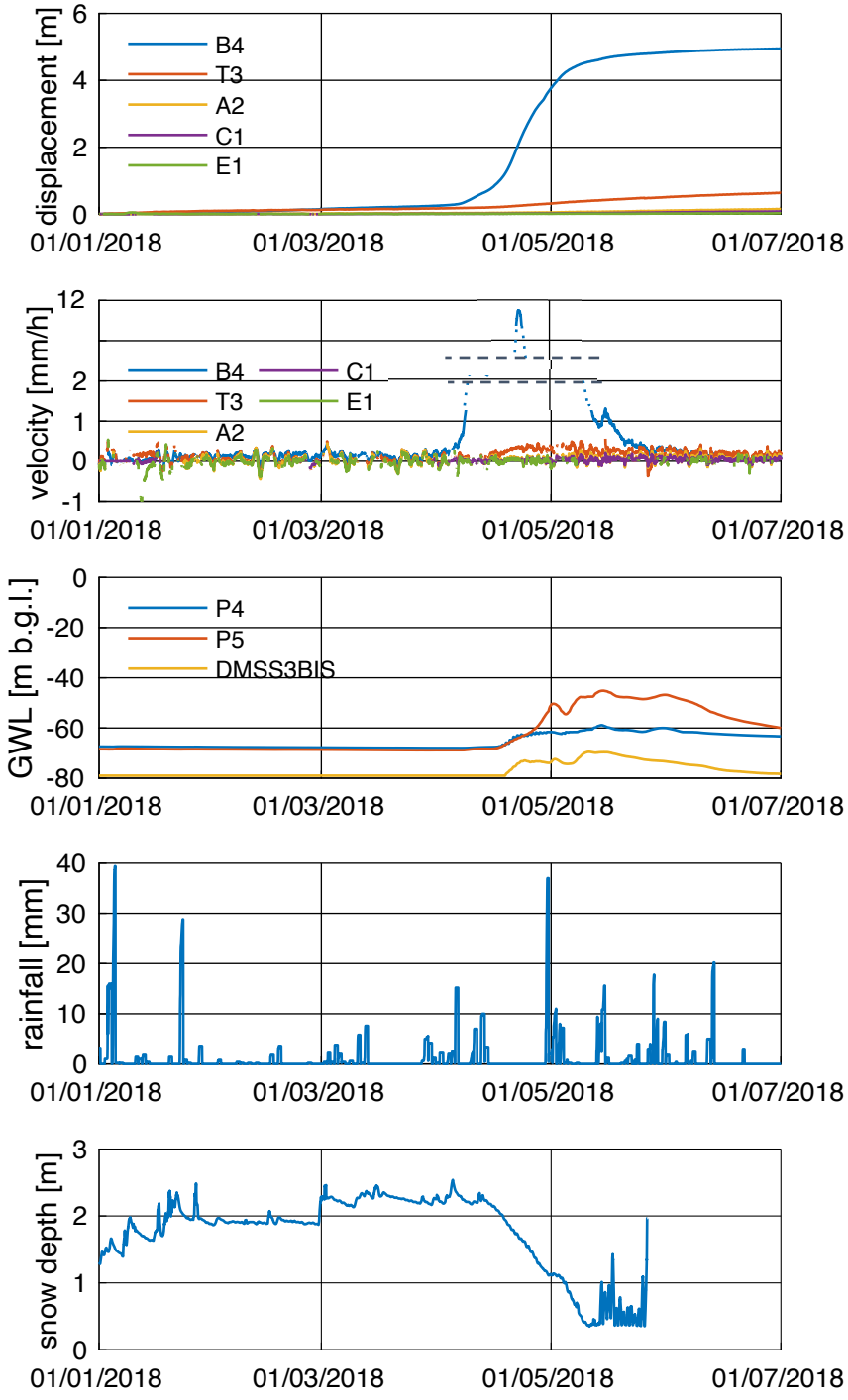

Figure 6.11: La Saxe monitoring data from January to July 2018

6.2.4 Results

For La Saxe rockslide the monitoring data used to investigate the potential of power law exponent method were provided by Geological Survey of Regione Autonoma Valle d'Aosta. Before presenting the obtained results, dimensionless curves in terms of displacements and derivatives, which have been computed according to the procedure described in Chapter 5, are showed in Figure 6.12. Data are acquired through the optical target B4, located in the active sector, from November 2010 to August 2018, extending the analysis developed in Chapters 4 and 5, in which the procedure was applied only till September 2012.
Diagrams contain 36 dimensionless trends, corresponding to the trend types reported in Table 6.1, obtained basing on exponent estimation.

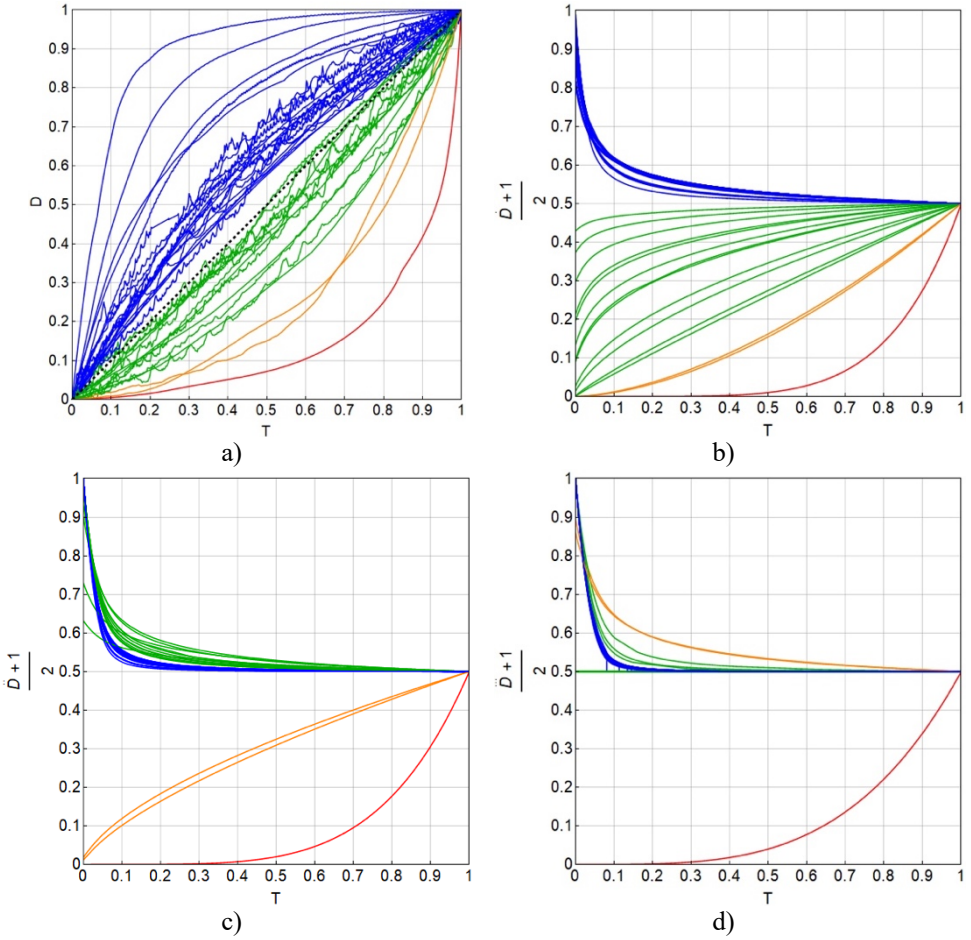

Figure 6.12:Dimensionless diagrams for La Saxe landslide in terms of displacements (a), velocities (b), accelerations (c) and jerks (d). Velocity, acceleration and jerk diagrams have been rescaled and translated to obtain square plots.

Table 6.1:Number of dimensionless curve for each trend type

Trend type	**I**	**II**	**III**	**IVa**	**IVb**
Number of curves	-	19	14	2	1

The results in terms of characteristic behaviours are satisfying, being the trends easily identifiable, even if some inaccuracies are recognizable due to data noise, responsible for wiggled profiles.

Recalling the adopted tolerance, Trend I should be associated to curves characterized by an exponent between 0.99 and 1.01. Actually, the analysis returns two curves with exponents lower than 1.05, that probably are definable as Trend I and, due to the high noise of input data, are here catalogued as Trend III. In such a case a larger tolerance for the exponent could be considered.

Trend IVa has been recorded during the snow melting seasons of 2013 and 2018, when two instabilities occurred. Particularly, these accelerating stages were recorded from 11 to 21 April 2013 and from 3 to 23 April 2018, reaching a value of the exponents respectively of 2.623 and 2.694.

Trend IVb was observed during Spring 2014, when, due to the snow melting, Mont de La Saxe was affected by an important acceleration that leads to the failure events of 17 and 21 April. During this event, the optical target B4 was involved in the collapse.

With the aim to validate the capability of the exponent method as forecasting tool, in the follows, the procedure is applied to three representative activity stages:

- Trend II recorded in the period between 3 April and 1 May 2015 (Figure 6.13);
- Trend III recorded in the period between 1 March and 10 May 2012 (Figure 6.14);
- Trend IVb recorded in the period between 16 March and 17 April 2014 (Figure 6.15).

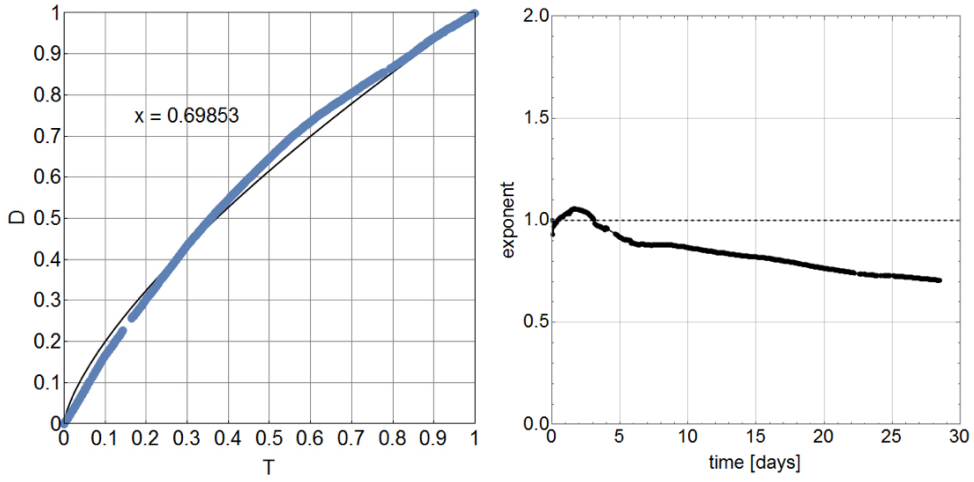

a) b)

Figure 6.13: Dimensionless displacement behaviour from a-posteriori analysis (a) and evolution of exponent over time (b) for the Trend II recorded in the period 3 April -1 May 2015.

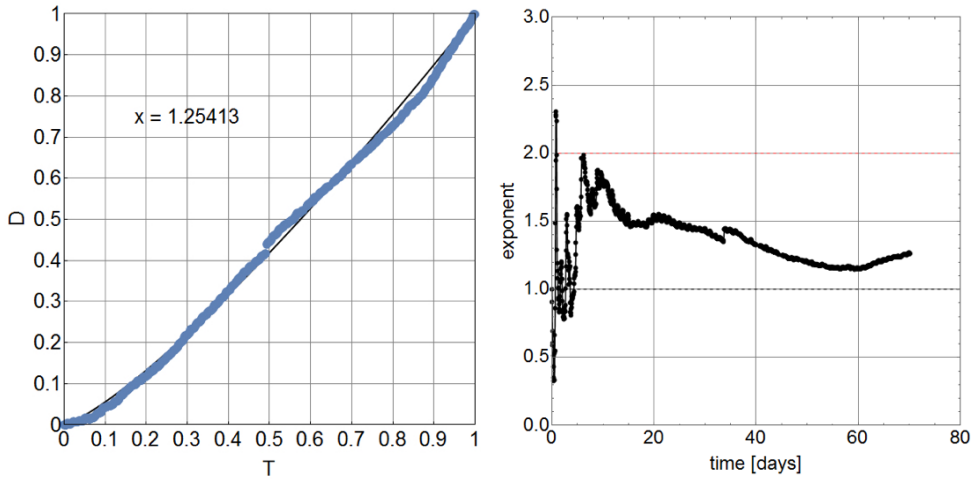

a) b)

Figure 6.14: Dimensionless displacement behaviour from a-posteriori analysis (a) and evolution of exponent over time (b) for the Trend III recorded in the period 1 March -10 May 2012

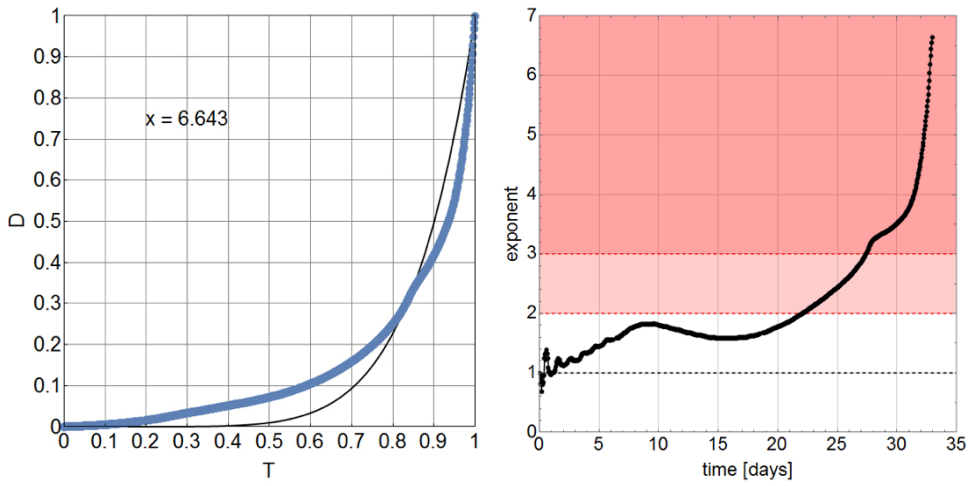

a) b)

Figure 6.15: Dimensionless displacement behaviour from a-posteriori analysis (a) and evolution of exponent over time (b) for the Trend IVb recorded 16 March- 17 April 2014. Red, dashed lines indicate the achievement of the first and second alert levels.

It is interesting to compare the results from Figure 6.14 and 6.15, since both data are referred to accelerations in the snow melting season. Acceleration recorded during Spring 2012 represents the first significant reactivation of La Saxe landslide. Actually, this accelerating stage did not represent a real emergency condition, in that rockslide then decelerated and stopped. This situation is appropriately described with the analysis of the exponent that remains under the value of 2 for all the analysed interval, except for large oscillations and errors likely due to noise in the input data. In the case of April 2014, the exponent increases in time, reaching the first and the second alert levels respectively 10 and 5 days before the local failure of sector 1.

6.3 Comparison with inverse-velocity method for an open pit mine

The proposed method is here compared with results obtained with Fukuzono-Voight inverse velocity method. For this purpose, data from an open pit mine in hard brittle rock have been considered.

The case study has been proposed by Carlà et al. (2017) which analysed 9 instable masses for the purpose of studying monitoring data and providing operational recommendations for the development of early warning systems.

Figure 6.16 shows an overview of the open pit mine, whose geographical position is not disclosed by the mine owner, with indications of identified instabilities (Carlà et al., 2017).

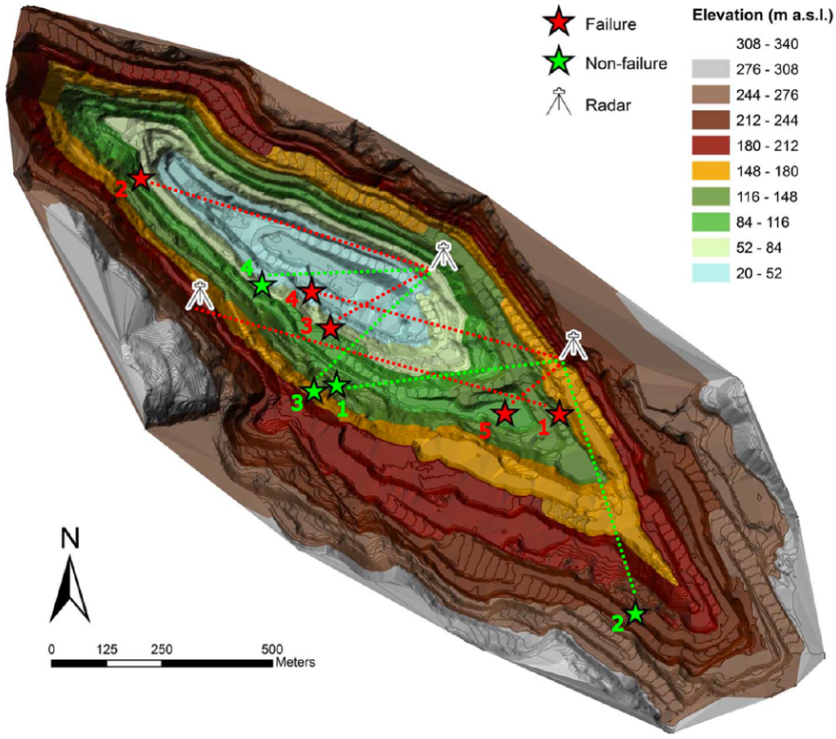

Figure 6.16: Overview of the open pit mine and of the instabilities (Carlà et al., 2017). This study focused on failures #3 and #4, reported in red.

For the purpose of this study, failures #3 and #4 – as reported in Figure 6.16 and in the original paper – have been analysed. Particularly, Authors applied inverse velocity method for the two instabilities, using 1-hour average velocities. It is worth noting that, in this case, time scale is of the order of few hours.
In Figures 6.17 and 6.19 displacement data, measured with ground-based radar, are reported, whereas in Figures 6.18 and 6.20 comparisons between results obtained with Fukuzono-Voight method (a) and proposed method (b) are shown.
Tables 6.2 and 6.3 report actual failure time and forecasting results obtained from the two methods.

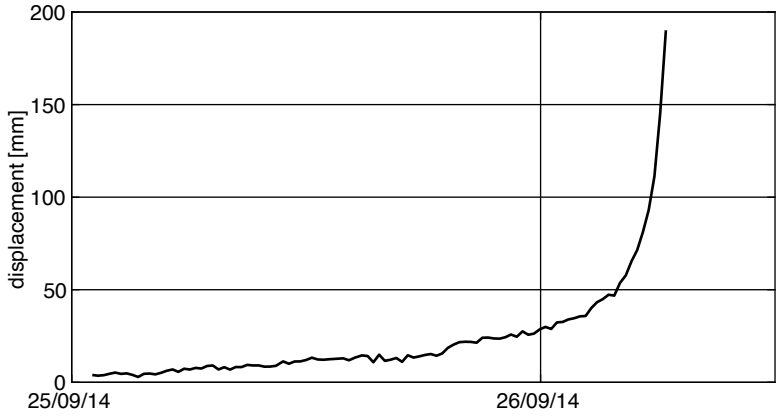

Figure 6.17: Displacement data for failure #3 (modified from Carlà et al., 2017)

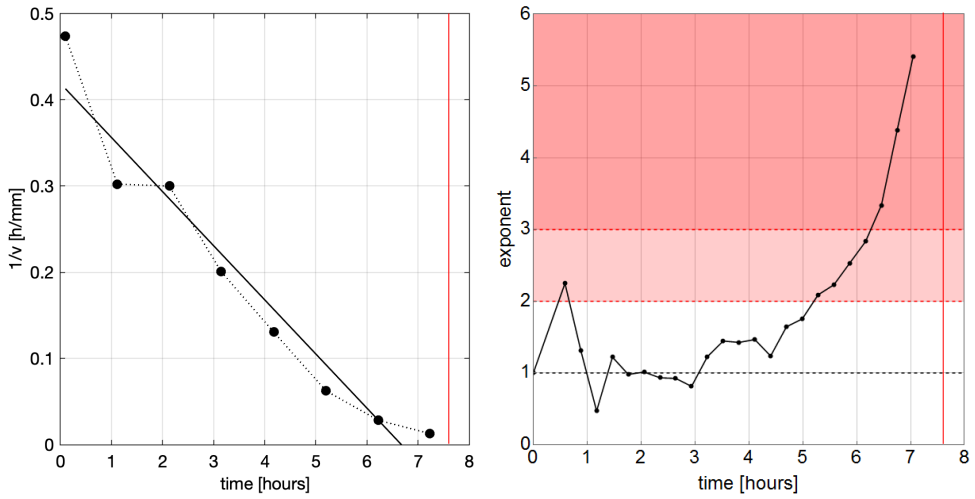

a) b)

Figure 6.18: Failure #3: a) Inverse velocity method (modified from Carlà et al., 2017); b) exponent method. Red-coloured lines mark the time of failure. Different number of points in the 2 figures is due to the fact that in (a) 1-hour average velocities have been used.

Table 6.2: Failure #3: comparison of results from Fukuzono–Voight inverse velocity method and the proposed one.

Monitored records	**Inverse velocity method**	**Proposed method**	
Failure time (hours)	Estimated failure (hours)	First alert threshold at: (hours)	Second alert threshold at: (hours)
7.63	6.68	5.00	6.30

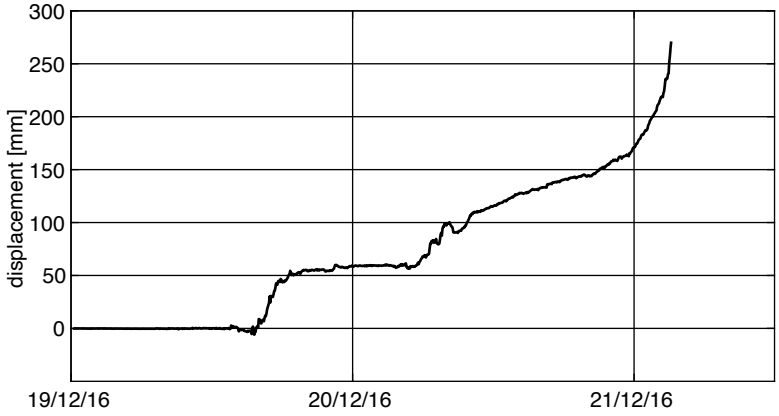

Figure 6.19: Displacement data for failure #4 (modified from Carlà et al., 2017)

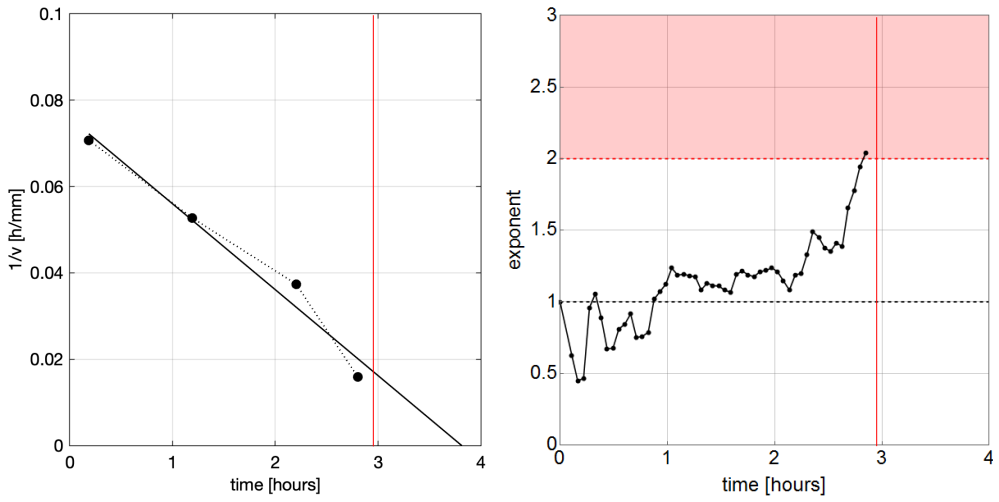

a) b)

Figure 6.20: Failure #4: a) Inverse velocity method (modified from Carlà et al., 2017); b) exponent method. Red-coloured lines mark the time of failure. Different number of points in the 2 figures is due to the fact that in (a) 1-hour average velocities have been used.

Table 6.3: Failure #4: comparison of results from Fukuzono–Voight inverse velocity method and the proposed one.

Monitored records	Inverse velocity method	Proposed method
Failure time (hours)	Estimated failure (hours)	First alert threshold at: (hours)
2.92	3.81	2.80

It is interesting to observe that if the starting point of the analysed accelerating stage is anticipated, forecasting results improve (Figure 6.21).

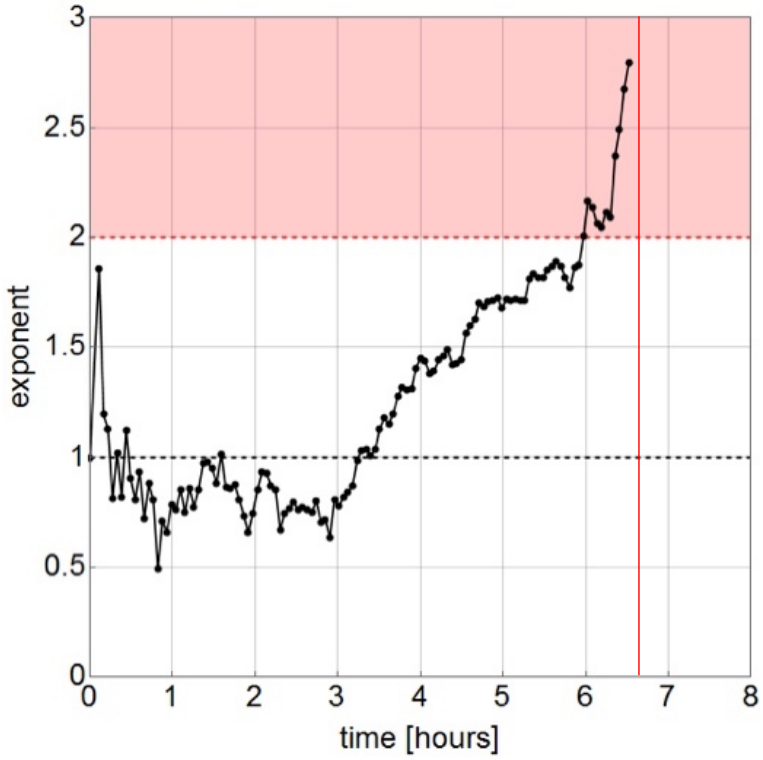

Figure 6.21: Failure #4: Exponent method applied to a time interval of 6.5 hours. Red-coloured line marks the time of failure.

Summarizing, the exponent method provided, at least in the investigated cases, satisfying information about the imminent failures.

Particularly, the analysis of failure #3 allows defining two alert thresholds both achieved before the failure time computed with inverse velocity method (Figure 6.18 and Table 6.2).

For failure #4 proposed method provides only the first alert level, whereas Fukuzono-Voight method fails the prediction (Figure 6.20 and Table 6.3).

Finally, the accelerating stage of failure #4 has been analysed considering a larger time interval, providing better results and highlighting the relevance in selecting the starting point.

6.4 Discussion

This chapter reports a perspective for forecasting landslide evolution on the basis of the approach presented in Chapters 4 and 5.
Time variation of the exponent of power law has been exploited with the aim of developing a forecasting tool able to define alert levels that are not dependent on the specific case study.
The transition from Trend III to IVa, corresponding to exponent set to $x = 2$, and from Trend IVa to IVb, at $x = 3$, appear effective for alarm procedures.
Proposed algorithm has been preliminarily applied to La Saxe rockslide, in particular to the failure of April 2014, providing satisfying results.
Moreover, a comparison between inverse velocity method has been carried out, referring to the forecasting of two failures in an open pit mine. In those cases, the results show the capability of the proposed algorithm to provide information about the landslide evolution and failure, with performances better than the Fukuzono-Voight method.
Concluding, proposed method provided satisfying results at least in the cases analysed so far, paving the way for the construction of a valid alert procedure, based on the analysis of displacement data. Alert levels have been defined through the evaluation of physical quantities, e.g. velocity, acceleration and jerk, in order to properly define dynamic characteristics of landslides.
Of course, it must be expected that there is room for improvements of the algorithm, which is not yet completely mature and whose reliability have to be tested with reference to a statistically meaningful number of case studies.
Nevertheless, results appear promising, especially considering that no smoothing techniques have been used on the data, making the method of immediate straightforward and fast application.

7. Future developments

Displacement trends have been described in Chapter 5 as those of a *stable* or an *unstable* landslide, depending on the behaviour of derivatives and, above all, the sign of the derivative of the second order, that is the landslide acceleration.
In particular, Trend I is characterized by a constant value of the velocity that represents a condition of dynamic equilibrium for the landslide. Trend II and Trend III are characterized the first by a concave displacement curve and the second by a convex displacement trait followed by a concave one. These trends are typical of a landslide that starts from a stable condition, undergoes an unbalanced system of forces and evolves towards a new dynamic equilibrium condition. Finally, trend IV is typical of an unstable landslides that in some cases (IVa) may evolve towards a new equilibrium condition, likely due to external factors, while in other cases (IVb) this possibility is inhibited, probably due to internal factors, leading to positive, growing jerk.
It is clear that the observed displacement trends are not casual being related to well defined mechanisms that probably can be explained by the stability theory of dynamic systems of Lyapunov.
This argument is outside the scope of the present PhD thesis. Nevertheless, it was considered interesting to develop some preliminary considerations in order to identify a possible development of the ongoing research.

7.1 Lyapunov's theory for landslide systems

The stability for linear and nonlinear systems in time domain can be studied with the Lyapunov's theory (1892) (Pignataro et al., 1991) under the assumption that an equilibrium state can be defined as stable if all the solutions of its dynamic equations starting at nearby states stay nearby (Nikravesh, 2013).
Interesting applications of Lyapunov's theory have been provided to describe landslide behaviour by Di Prisco and Flessati (2019), Chau et al. (1995), Kostic et al., (2014).
Hence, in the spirit of this theory, the stability of a slope movement, or generally of each dynamic system, can be investigated through the study of a set of autonomous ordinary differential equations.

The choice of such equations is not unique and many characteristics of the slope can be taken into account, as seen in Section 2.4.
If the model of a single rigid block on a surface inclined of an angle β is considered, assuming the pore water pressure on the basal plane $u(t)$ as the triggering external force, dynamic equation in the direction parallel to the movement can be expressed as:

$$\frac{dv(t)}{dt} = g\sin\beta - g\cos\beta\left(1 - \frac{u(t)}{\rho g H\cos^2\beta}\right)\left(tan\varphi'_0 + (tan\varphi'_1 - tan\,\varphi'_0)(1 - e^{-a\,v(t)})\right) \quad (7.1)$$

in which $v\,(t)$ is the displacement rate, ρ is the density of soil, g is the modulus of the gravitational acceleration and H is the height of the block. The equation has been enhanced with a strain-rate-dependent friction law (Scoppettuolo e Cascini, 2017).
In addition to the dynamic equilibrium, represented by equation (7.1), a further differential equation could be considered in order to describe the time variation of pore water pressure. A possible example could be introduced as:

$$\frac{du(t)}{dt} = \eta(u(t) - k) \quad (7.2)$$

in which η and k are two parameters, whose respective physical dimensions are T^{-1} and $ML^{-1}T^{-2}$.
Function $u(t)$ is showed in Figure 7.1, in which C (of same physical dimensions of k) is an integration constant.

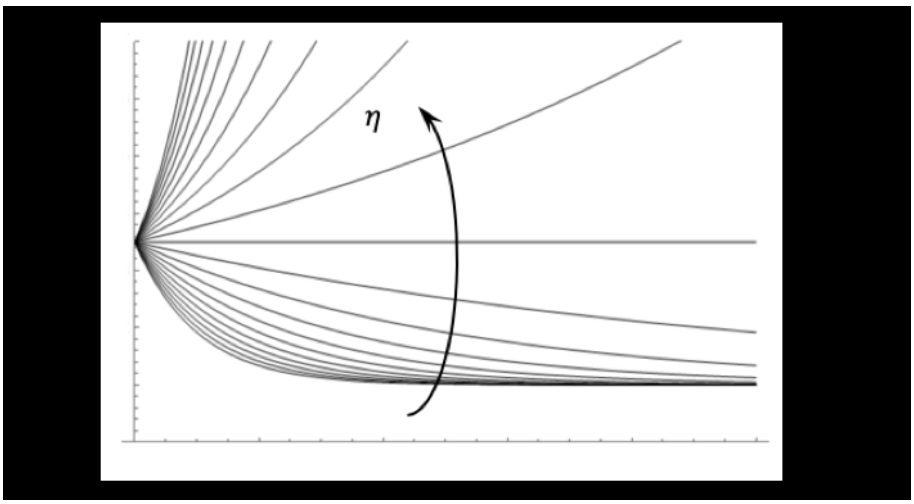

Figure 7.1: Behaviour of pore water pressure over time.

The stability of the system of nonlinear autonomous differential equation (7.1) and (7.2), can be analysed referring to its equilibrium configuration that is:

$$\begin{cases} v(t) = \frac{1}{a} ln \frac{(\rho g H \cos \beta - k \sec \beta)(\tan \varphi'_1 - \tan \varphi'_0)}{(\rho g H \cos \beta - k \sec \beta) \tan \varphi'_1 - \rho g H \sin \beta} \\ u(t) = k \end{cases} \quad (7.3)$$

Particularly, according to the so-called indirect method of Lyapunov, the stability of a nonlinear system can be investigated through the analysis of a linearized system (Hafstein, 2004; Pukdeboon, 2011). Operatively, the linearization is carried out introducing the Jacobian matrix:

$$A = \begin{pmatrix} -g\ a\ e^{-a\ v(t)} \cos \beta\ \left(\tan \varphi'_1 - \tan \varphi'_0\right)\left(1 - \frac{u(t) \sec^2 \beta}{\rho g H}\right) & 0 \\ \frac{\sec \beta \left(\tan \varphi'_0 + \left(1 - e^{-a\ v(t)}\right)\left(\tan \varphi'_1 - \tan \varphi'_0\right)\right)}{\rho H} & \eta \end{pmatrix} \quad (7.4)$$

The stability can be thus analysed finding the eigenvalues of *A,* computed for equilibrium configuration, that are:

$$\lambda_1 = \eta \quad (7.5)$$

$$\lambda_2 = a\left(g \sin \beta - g \cos \beta \tan \varphi'_1 + \frac{k \sec \beta \tan \varphi'_1}{\rho H}\right) \quad (7.6)$$

and the requirement for the stability is that the real part of eigenvalues (7.5) and (7.6) be negative.

In this perspective, the first condition corresponds to a decreasing behaviour of the pore water pressure ($\eta < 0$). The second condition, regarding equation (7.6), can be studied referring to the variation of parameter k, assumed as indicator of pore water pressure, and friction angle φ'_1, related to strain-rate friction effects.

7.2 Application to Vallcebre landslide

The Vallcebre case study is among the most investigated landslides in the literature (Corominas et al., 2005).

The landslide, located in North-Eastern Pyrenees,140 km from Barcelona (Spain), is included in the database reported in Section 4. For sake of completeness a cross section is showed in Figure 7.2, with indications about stratigraphy, location of sliding surface and location of the monitoring stations.

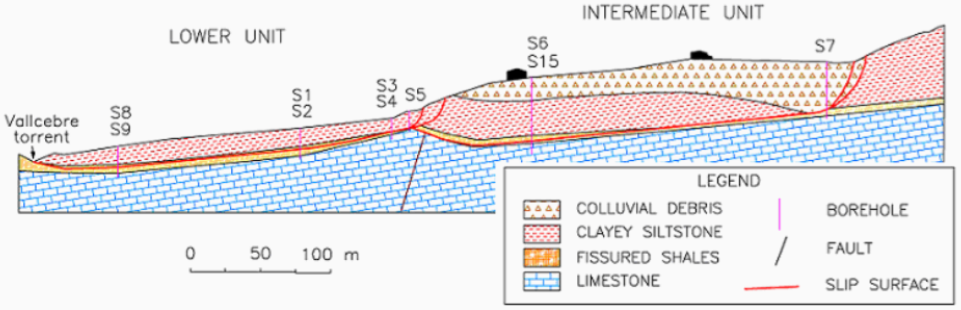

Figure 7.2: Cross section of Vallcebre landslide (Corominas et al., 2005)

Involved materials are stiff clays with shale and gypsium layers of Continental origin from Upper Cretaceous – Lower Palaeocene age, whereas the bedrock is constituted by limestone.

Monitoring data, derived from wire extensometers and electronic piezometers, show a strict correlation between displacement rate and groundwater level, itself associated with rainfall.

Referring to the lower unit, geometrical and material properties listed in Table 7.1 together with the parameter a of relationship between $\tan \varphi'$ and velocity. This last parameter was obtained through the numerical integration of equation (7.1) (Scoppettuolo and Cascini, 2017; Pinyol et al., 2017), that allowed fixing a maximum value of the mobilized friction angle φ'_{max} along the slip surface (Figure 7.3).

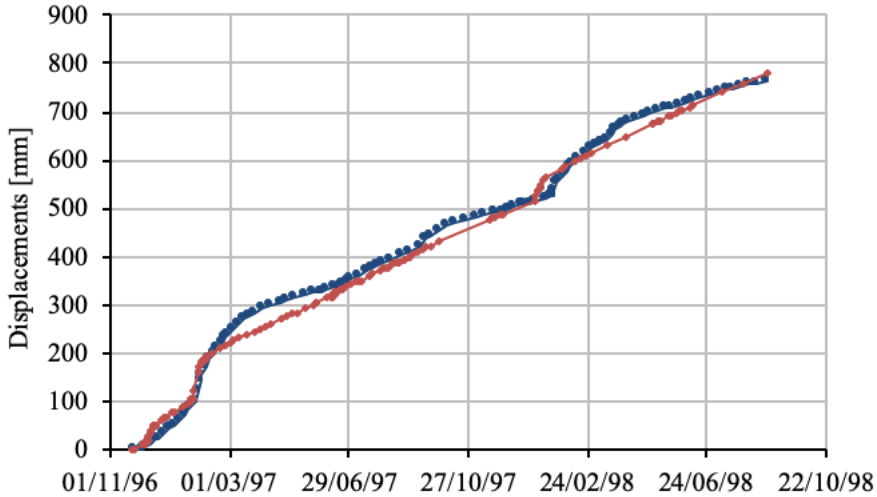

Figure 7.3: Computed (in red) and measured (in blue) displacement for vertical S2 of Vallcebre landslide (Scoppettuolo and Cascini, 2017; data from Corominas et al., 2005)

Table 7.1: Input parameters for Vallcebre landslide analysis

Height of rigid block	Slope angle	Density of soil	Residual friction angle	Maximum friction angle	Strain-rate friction parameter
H [m]	β [°]	ρ [kg/m^3]	φ'_0	φ'_{max}	a [s/m]
15.5	6.5	2000	7.8	12.3	3.85 10^7

The obtained results are reported in Figure 7.4. Black curve, corresponding to the condition $\lambda_2 = 0$, represents the boundary between stable (coloured region) and unstable domains. The two limit values of friction angle, φ'_0 (absence of strain-rate effects) and φ'_{max} (maximum allowed increment), are marked with red-coloured, dashed lines.

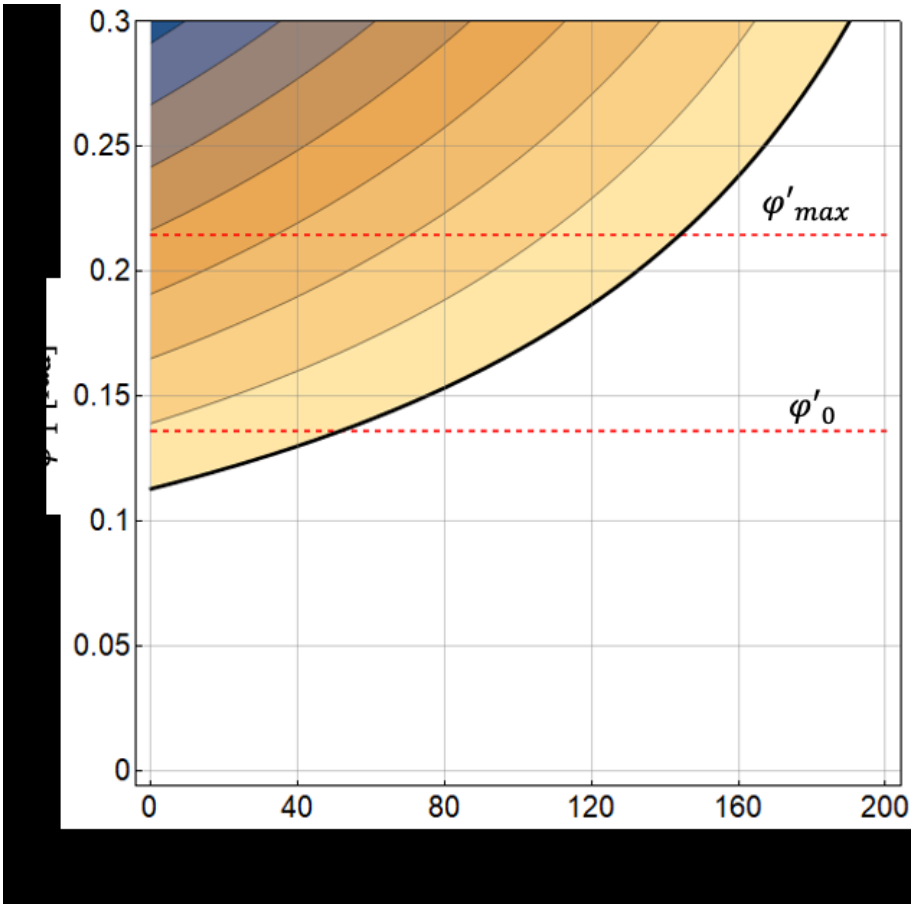

Figure 7.4: Stability region for Vallcebre landslide (coloured area). Red lines indicate φ'_0 and φ'_{max}

For $k = 0$, corresponding to a dry slope, the stability of the equilibrium is ensured by the mobilization of a friction angle equal to the slope angle β. In correspondence of the residual friction angle φ'_0 the value of k is 51.5 kPa.
It is possible to conclude that the equilibrium is stable with the mobilization of residual friction angle φ'_0 for values of pore water pressure between 0 and 51.5 kPa. Maximum value of φ'_{max} is needed when k reaches 144 kPa, thus representing the maximum admissible water pressure.
The results obtained for the Vallcebre landslide, although preliminary, highlight the potential of stability theory of dynamic systems to support on a mechanical basis the displacement trends described in this doctoral thesis.

8. Concluding remarks

Understanding and characterizing the landslide evolution is a complex topic that is deeply analysed in scientific literature even though the proposed approaches do not allow the quantitative identification of common displacement behaviours.
Considering the consequences of landslides and their diffusion all over the world, this PhD thesis makes a contribution on the subject through the implementation of a method that is composed of two parts. Part I is dedicated to finding common trends in the landslide displacement. Part II assesses the kinematic characteristics of the individuated displacement trends.
The method comes from the analysis of well-documented case studies in the scientific literature that encompass all the evolution stages classified by Leroueil et al. (1996) and five failure events.
In spite of the differences in soil properties, entity of displacement and many other factors, a dimensionless displacement versus time diagram reveals that each of them is essentially composed of linear, concave and convex curves.
These curves are combined in different ways but they originate only five displacement trends that have been characterized through the displacement derivatives up to the third order, e.g. velocity, acceleration and jerk. Displacement and velocity are clearly kinematic descriptors of the slope evolution, while the acceleration and jerk are strictly related to the stress field globally acting on the landslide through Newton's second law.
The analysis of the growth properties of derivatives shows precise characteristics associated to each trend, adequately reflecting the real evolution of case studies.
Trend I is represented by a straight line, observed in correspondence of equilibrium condition and characterized by a movement with a constant velocity.
Trend II is represented by a concave behaviour and it is recorded when, after a short time acceleration, the body decelerates (typical of active landslides).
In Trend III not ordinary boundary conditions occur, leading the landslide to accelerate; this trend is not particularly dangerous, being followed by a deceleration similar to Trend II.
On the contrary, Trend IV corresponds to a condition in which the landslide accelerates reaching high values of velocity, going toward the collapse.

In addition, Trend IV has been further subdivided in IVa and IVb, respectively characterized by decreasing or increasing jerk function, the latter condition associated to an unavoidable catastrophic evolution.
Starting from these trends the displacement data have been interpolated with a power law function that has been used to verify the possibility to forecast the evolution of the landslides. This capability has been investigated through the exponent of the power law that allows monitoring the transition from Trend III to Trend IVa and IVb, that is from a stable to an unstable condition.
The model has been applied to explanatory examples and after to the La Saxe rockslide (Courmayeur, Valle d'Aosta, Italy) and to collapses occurred in an open pit mine in brittle rock.
The obtained results highlight that the instability, when it occurs, can be individuated in advance and much earlier than the one provided by the inverse velocity method of Fukuzono-Voight, that is commonly used for this purpose.
Considering the potential of the proposed method, that seems able to identify common kinematic characteristics for different landslide phenomena, the ongoing research must be deepened in the future following two different paths.
First of all, the available database must be further enriched by other well documented landslides and it is hoped that the necessary data will be provided to the writer by those interested in further calibration of the method.
Moreover, it is essential to deepen the mechanisms behind the identified trends that can be profitably analysed with the stability of linear and non-linear systems in time domain. To this end, a first and preliminary example has been developed in this thesis strongly encouraging the further necessary investigation.

References

Alberti, S. (2019). Geological analysis and numerical modelling of La Saxe landslide (Courmayeur) to improve understanding of geomorphological and geotechnical mechanisms and of the potential landslide evolution. *PhD Thesis*, University of Milano Bicocca.

Alonso, E.E., Pinyol, N.M., Puzrin, A.M. (2010). Catastrophic Slide: Vaiont Landslide, Italy, In: *Geomechanics of failures. Advanced topics,* Springer Netherlands, Houten, 33-81.

Alonso, E.E., Zervos, A., Pinyol, N.M. (2016). Thermo-poro-mechanical analysis of landslides: from creeping behaviour to catastrophic failure. *Géotechnique, 66*(3), 202-219.

Andriani, P., McKelvey, B. (2007). Beyond gaussian averages: redirecting international business and management research toward extreme events and power laws. *Journal of International Business Studies, 38*(7), 1212–1230.

Asaoka, A. (1978). Observational procedure of settlement prediction. *Soils Found*, 18 (4), 87–101.

Azimi, C., Biarez, J., Desvarreux, P., Keime, F. (1988). Forecasting time of failure for a rockslide in gypsum. In: *Proceedings of 5th international symposium on landslides*, Lausanne, 531–536.

Berti, M. (2015). Atteso ma imprevedibile: il problema del dissesto idrogeologico in Italia. *Atteso ma imprevedibile: il problema del dissesto idrogeologico in Italia*, 95-114.

Bertini, T., Cugusi, F., D'Elia, B., Rossi-Doria, M. (1986). Lenti movimenti di versante nell'Abruzzo adriatico: caratteri e criteri di stabilizzazione. In: Associazione Geotecnica Italiana (ed), "La progettazione geotecnica per la stabilizzazione dei pendii", *Proceedings of 16th National Conference,* Bologna, Italy, 14-17 May, CLEUP, Rome, Italy, vol. 1, 91–100. (in Italian).

Binet, S., Mudry, J., Scavia, C., Campus, S., Bertrand, C., Guglielmi, Y. (2007). In situ characterization of flows in a fractured unstable slope. *Geomorphology, 86*(1-2), 193–203.

Blong R.J. (1973). A numerical classification of selected landslides of the debris slide- avalanche-flow type. *Engineering Geology, 7*, 99-144.

Bouissou, S., Darnault, R., Chemenda, A., Rolland, Y. (2012). Evolution of gravity-driven rock slope failure and associated fracturing: Geological analysis and numerical modelling. *Tectonophysics, 526*, 157-166.

Broccolato, M., Cancelli, P., Crosta, G., Tamburini, A., Alberto, W. (2011). Tecniche di rilievo e monitoraggio della frana di Mont de La Saxe (Courmayeur, AO). In: Associazione Geotecnica Italiana, *XXIV Convegno Nazionale di Geotecnica,* 2, 625-632.

Bucher, F. (1975). Die Restscherfestigkeit natürlicher Böden, ihre Einflussgrössen und Beziehungen als Ergebnis experimenteller Untersuchungen. *PhD Thesis*, ETH Zurich, Switzerland (in German).

Calvello, M. (2017). Early warning strategies to cope with landslide risk. *Rivista Italiana Geotecnica, 2*, 63–91.

Calvello, M., Pecoraro, G. (2018). FraneItalia: a catalog of recent Italian landslides. *Geoenvironmental Disasters, 5*, 13.

Carlà, T., Farina, P., Intrieri, E., Botsialas, K., Casagli, N. (2017). On the monitoring and early-warning of brittle slope failures in hard rock masses: Examples from an open-pit mine. *Engineering geology, 228*. 71-81.

Carlà, T., Intrieri, E., Di Traglia, F., Nolesini, T., Gigli, G., Casagli, N. (2017). Guidelines on the use of inverse velocity method as a tool for setting alarm thresholds and forecasting landslides and structure collapses. *Landslides, 14*(2), 517-534.

Cascini L., Bonnard Ch., Corominas J., Jibson R., Montero-Olarte J. (2005). Landslide hazard and risk zoning for urban planning and development. In: *Proceedings of the International Conference on Landslide Risk Management*, 31 May - 3 June, Vancouver, Canada, 199-235.

Cascini, , E., Babilio, E., Scoppettuolo, M.R. (2019). Forecasting first failure and evolution of landslides: a challenge to win**.** In: G. Frega, G., Macchione, F. (eds) *Technologies for Integrated River Basin Management 40,* ISBN 978-88-97181-71-2

Cascini, L., Calvello, M., Grimaldi, G.M. (2014). Displacement trends of slow-moving landslides: Classification and forecasting*. Journal of mountain science, 11*(3), 592-606.

Cascini, L., Scoppettuolo, M.R., Babilio, E. (2020). Un contributo alla caratterizzazione cinematica dei movimenti di versante. In: *Convegno Nazionale di Geotecnica (CNG).* Accepted. (in Italian)

Chase, J.G., Barroso, L.R. and Hunt, S. (2003). Quadratic jerk regulation and the seismic control of civil structures. *Earthquake Engineering & Structural Dynamics*, *32*, 2047–2062.

Chau, K. T. (1995). Landslides modeled as bifurcations of creeping slopes with nonlinear friction law. *International Journal of solids and Structures*, *32*(23), 3451-3464.

Clauset, A., Shalizi, C., Newman, M. (2009). Power-law distributions in empirical data. *SIAM Review, 51*(4), 661–703.

Cooper, M.R., Bromhead, E.N., Petley, D.J., Grant, D.I. (1998). The Selborne cutting stability experiment. *Geotechnique, 48*, 83–101.

Cornelius, R.R., and Scott, P.A. (1993). A materials failure relation of accelerating creep as empirical description of damage accumulation. *Rock Mechanics and Rock Engineering,* 26, 233–252.

Corominas, J., Moya, J., Ledesma, A., Lloret, A., Gili, J.A. (2005). Prediction of ground displacements and velocities from groundwater level changes at the Vallcebre landslide (Eastern Pyrenees, Spain). *Landslides, 2*, 83 – 96.

Crosta, G.B., Agliardi, F. (2003). Failure forecast for large rock slides by surface displacement measurements. *Canadian Geotechnical Journal, 40*(1), 176-191.

Crosta, G.B., Chen, H., Frattini, P. (2006). Forecasting hazard scenarios and implications for the evaluation of countermeasure efficiency for large debris avalanches. *Engineering Geology, 83*(1-3), 236-253.

Crosta, G.B., Chen, H., Lee, C.F. (2004). Replay of the 1987 Val Pola Landslide, Italian Alps. *Geomorphology, 60*, 127-146.

Crosta, G.B., di Prisco, C., Frattini, P., Frigerio, G., Castellanza, R., Agliardi, F. (2014). Chasing a complete understanding of the triggering mechanisms of a large rapidly evolving rockslide. *Landslides, 11*, 747–764.

Cruden D. M. (1991). A simple definition of a landslide. *Bulletin of Engineering Geology and the Environment, 43*(1), 27-29.

Cruden D.M., Varnes D.J. (1996). Landslide types and processes. In: Turner AK, Schuster RL (eds) Landslides investigation and mitigation. Transportation research board, US National Research Council. *Special Report* 247, Washington DC, USA, 36–75.

Davis, R. O., Desai, C. S., Smith, N. R. (1993). Stability of motions of translational landslides. *Journal of geotechnical engineering, 119*(3), 420-432.

Delle Piane, L., Fontan, D., Mancari, G. (2010). The Rosone landslide (Orco river valley, Western Italian Alps): an updated model. *Geografia Fisica e Dinamica Quaternaria, 33*, 165–177.

Di Prisco, C., Flessati, L. (2019). Progressive failure in elastic–viscoplastic media: from theory to practice. *Géotechnique,* 1-17. https://doi.org/10.1680/jgeot.19.P.045

Dick, G.J., Eberhardt, E., Cabrejo-Liévano, A.G., Stead, D., Rose, N.D. (2014). Development of an early-warning time-of-failure analysis methodology for open-

pit mine slopes utilizing ground-based slope stability radar monitoring data. *Canadian Geotechnical Journal 52*(4), 515-529.

Dieterich, J. H. (1979). Modeling of rock friction: 1. Experimental results and constitutive equations. *Journal of Geophysical Research: Solid Earth, 84*(B5), 2161-2168.

Eberhardt, E. (2008). Twenty-ninth Canadian Geotechnical Colloquium: The role of advanced numerical methods and geotechnical field measurements in understanding complex deep-seated rock slope failure mechanisms. *Canadian Geotechnical Journal, 45*(4), 484-510.

Emery J.J. (1979). Simulation of slope creep. In: Voight B (ed) *Developments in Geotechnical Engineering, Rock slides & avalanches,* 14A, 669–691. Elsevier, Amsterdam.

Emery, J. J. (1971). Finite element analysis of creep problems in soil mechanics. *PhD Thesis*, University of British Columbia.

Federico, A., Popescu, M., Elia, G., Fidelibus, C., Internò, G., & Murianni, A. (2012). Prediction of time to slope failure: a general framework. *Environmental earth sciences, 66*(1), 245-256.

Fell, R., Hungr, O., Leroueil, S., Riemer, W. (2000, November). Keynote lecture-geotechnical engineering of the stability of natural slopes, and cuts and fills in soil. In: *ISRM International Symposium*. International Society for Rock Mechanics and Rock Engineering.

Ferrari, A., Ledesma, A., González, D. A., Corominas, J. (2011). Effects of the foot evolution on the behaviour of slow-moving landslides. *Engineering geology, 117*(3-4), 217-228.

Follacci, J.P., Guardia, P., Ivaldi, J.P. (1988). La Clapière landslide in its geodynamical setting. In: Bonnard C (ed) *Proceedings of 5th International Symosium on Landslides*, Lausanne, Switzerland, 10-15 July, Balkema, Brookfield, USA. 3, 1323–1327.

Follacci, J.P., Rochet, L., Serratrice. J.F. (1993). Glissement de La Clapière, St Etienne de Tinée, Synthèse des connaissances et actualisation des risques, rapp. 92/PP/UN/I/DRM/03/AI/01, 76 pp., *Cent. Etud. Tech. de l'Equip.*, Nice, France (in French).

Froude, M. J., & Petley, D. (2018). Global fatal landslide occurrence from 2004 to 2016. *Natural Hazards and Earth System Sciences, 18*, 2161-2181.

Fukuzono T (1990) Recent studies on time prediction of slope failure. *Landslide News, 4*, 9–12.

Fukuzono T. (1985). A new method for predicting the failure time of slopes. In: Japan Landslide Society Committee for International Exchange of Landslide Technique (ed) *Proceedings of 4th International Conference and Field Workshop*

on Landslides, Tokyo, Japan, 23-31 August, 145–150.

Giordan, D., Manconi, A., Allasia, P., Bertolo, D. (2015). Brief Communication: On the rapid and efficient monitoring results dissemination in landslide emergency scenarios: the Mont de La Saxe case study. *Natural Hazards and Earth System Sciences, 15*(9), 2009-2017.

Grimaldi, G.M. (2008). Modelling the displacements of slow moving landslides. *PhD thesis*, University of Salerno, Fisciano, Italy.

Guglielmi, Y., Bertrand, C., Compagnon, F., Follacci, J.P., Mudry, J. (2000). Acquisition of water chemistry in a mobile fissured basement massif: its role in the hydrogeological knowledge of the La Clapière landslide (Mercantour massif, southern Alps, France). *Journal of Hydrology, 229*(3-4), 138-148.

Günther, A., Reichenbach, P., Malet, J. P., Van Den Eeckhaut, M., Hervás, J., Dashwood, C., Guzzetti, F. (2013). Tier-based approaches for landslide susceptibility assessment in Europe. *Landslides, 10*(5), 529-546.

Guzzetti, F., Cardinali, M., Reichenbach, P. (1994). The AVI Project: A bibliographical and archive inventory of landslides and floods in Italy. *Environmental Management, 18*(4), 623-633.

Hafstein, S. F. (2004). A constructive converse Lyapunov theorem on exponential stability. *Discrete and Continuous Dynamical Systems*, *10*(3), 657-678.

Haque, U., Blum, P., Da Silva, P.F., Andersen, P., Pilz, J., Chalov, S.R., Malet, J.P., Jemec Auflič, M., Andres, N., Poyiadji, E., Lamas, P.C., Zhang, W., Peshevski, I., Pétursson, H.G., Kurt, T., Dobrev, N., García-Davalillo, J.C., Halkia, M., Ferri, S., Gaprindashvili, G., Engström, J., Keellings, D. (2016). Fatal landslides in Europe. *Landslides, 13*(6), 1545–1554.

Hayashi, S., Komamura, F., Park, B., Yamamori, T. (1988). On theforecast of time to failure of slope—approximate forecast in the early period of the tertiary creep. *Journal of Japan Landslides Society, 25*(3), 11–16.

He, H., Li, R., Chen, K. (2015). Characteristics of Jerk Response Spectra for Elastic and Inelastic Systems. *Shock and Vibration, 2015*(46), 1–12.

Heim, A. (1932). Bergsturz und menschenleben (No. 20). Zürich. Fretz & Wasmuth. (in German).

Helmstetter, A., Sornette, D., Grasso, J.R., Andersen, J.V., Gluzman, S., Pisarenko, V. (2004). Slider block friction model for landslides: application to Vaiont and La Clapière landslides. *Journal of Geophysical Research, 109(B2)*.

Hungr, O., Leroueil, S., Picarelli, L. (2014). The Varnes classification of landslide types, an updat*e. Landslides, 11*, 167–194.

Hutchinson, J.N. (1988). Morphological and Geotechnical parameters of Landslides in relation to Geology and Hydrogeology. State of the art Report. In: *Proceedings V International Symposium on Landslides*, Lausanne, 1, 3–35.

International Conference on SMFE, 315-318.

Intrieri, E., Gigli, G., Mugnai, F., Fanti, R., Casagli, N. (2012). Design and implementation of a landslide early warning system. *Engineering Geology, 147*, 124-136.

ISPRA (2008). IFFI database. Rapporto sulle frane in Italia .

ISPRA (2018). ISPRA database. http://www.isprambiente.gov.it/it/pubblicazioni/rapporti/dissesto-idrogeologico-in-italia-pericolosita-e-indicatori-di-rischio-edizione-2018. Accessed 26 November 2019.

Jahns R.H. (1978). Landslides. *National Academy of Science; Geophysical Predictions,* 58-65.

Keqiang, H., Sijing, W. (2006). Double-parameter threshold and its formation mechanism of the colluvial landslide: Xintan landslide, China. *Environmental geology, 49*(5), 696-707.

Kilburn, C.R., Petley, D.N. (2003). Forecasting giant, catastrophic slope collapse: lessons from Vajont, Northern Italy. *Geomorphology, 54*(1-2), 21-32.

Kirschbaum D. B., Adler R., Hong Y., Hill S., Lerner-Lam A. (2010). A global landslide catalog for hazard applications: method, results, and limitations. *Natural Hazards, 52*(3), 561-575.

Kostić, S., Vasović, N., Franović, I., Jevremović, D., Mitrinovic, D., & Todorović, K. (2014). Dynamics of landslide model with time delay and periodic parameter perturbations. *Communications in Nonlinear Science and Numerical Simulation*, *19*(9), 3346-3361.

La Gatta, D.P. (1970). Residual strength of clays and clay shales by rotation shear tests. *Harvard Soil Mechanics Series, 86*, Cambridge.

La Gatta, D.P. (1971). The effect of rate of displacement on measuring the residual strength of clay. *Contract report 5-71-5*. Vicksburg: US Army Waterways Experiment Station.

Leroueil S., Locat J., Vaunat J., Picarelli L., Lee H., Faure R. (1996). Geotechnical characterization of slope movements. In: *Senneset K (ed), Landslides, Proceedings 7th International Symposium Landslides*, Trondheim, Norway, 17-21 June, Balkema, Rotterdam, The Netherlands, 1, 53-74.

Lollino, G., Arattano, M., Allasia, P., Giordan, D. (2006). Time response of a landslide to meteorological events. *Natural Hazards and Earth System Science 6*: 179–184.

Lyapunov, A.M. (1892). The general problem of the stability of motion. *Ph.D. thesis*, University of Kharkov. Kharkov, Russia (in Russian).

Manconi, A., Giordan, D. (2015). Landslide early warning based on failure forecast models: the example of the Mt. de La Saxe rockslide, northern Italy. *Natural Hazards and Earth System Sciences, 15*(7), 1639-1644.

Marks, R.J. (1991). Introduction to Shannon Sampling and Interpolation Theory. Springer texts in electrical engineering. Springer-Verlag.

Mitchell, J.K., Campanella, R.G., Singh, A. (1968). Soil creep as a rate process. *Journal of Soil Mechanics & Foundations Div*.

Munich Re (2014) NatCatSERVICE. https://www.munichre.com/en/reinsurance/business/non-life/natcatservice/index.html. Accessed 1 December 2019.

Musso, A. (1997). Limitazione nell'uso dei pendii con ridotto margine di sicurezza. In: Pellegrino A (ed) *Interventi di stabilizzazione dei pendii*, CISM Udine, 449-474 (in Italian).

Newcomen, W., Dick, G. (2015). An update to strain-based pit wall failure prediction method and a justification for slope monitoring. *Proceedings Slope Stability,* 139-150.

Newman, M.E.J. (2005). Power laws, Pareto distributions and Zipf's law. *Contemporary Physics, 46*(5), 323–351.

Nikravesh, S. K. Y. (2013). *Nonlinear systems stability analysis: Lyapunov-based approach*. CRC Press. ISBN 978-1-4665-6929-4.

Noda, T., Xu, B., Asaoka, A. 2013. Acceleration generation due to strain localization of saturated clay specimen based on dynamic soil-water coupled finite deformation analysis. *Soils and Foundations, 53*, 653–670.

Nonveiller, E. (1987). The Vajont reservoir slope failure. *Engineering Geology, 24*, 493−512.

Pecoraro G., Calvello M., Piciullo, L. (2019). Monitoring strategies for local landslide early warning systems. *Landslides, 16*, 213.

Petley D. (2012). Global patterns of loss of life from landslides. *Geology, 40*(10), 927–930.

Petley, D.N., Bulmer, M.H., & Murphy, W. (2002). Patterns of movement in rotational and translational landslides. *Geology*, *30*(8), 719-722.

Pignataro, M., Rizzi, N., Luongo, A. (1991). Stability, bifurcation and postcritical behaviour of elastic structures. Elsevier, Amsterdam. ISBN 0-444-88140-9.

Pinyol, N.M., Scoppettuolo, M.R., Alonso, E.E. (2017). Mecanismos que controlan la velocidad de los deslizamientos. In IX Simposio Nacional sobre Taludes y Laderas Inestables (pp. 52-55). International Centre for Numerical Methods in Engineering (CIMNE). (in Spanish).

Plastino, A.R.; Muzzio, J.C. 1992. On the use and abuse of Newton's second law for variable mass problems. *Celestial Mechanics and Dynamical Astronomy, 53 (3)*, 227–232

Popescu, M. E. (1994). A suggested method for reporting landslide causes. *Bulletin of the International Association of Engineering Geology-Bulletin de l'Association Internationale de Géologie de l'Ingénieur, 50*(1), 71-74.

Pukdeboon, C. (2011). A review of fundamentals of Lyapunov theory. *The Journal of Applied Science*, *10*(2), 55-61.

Rose, N.D., Hungr, O. (2007). Forecasting Potential Rock Slope Failure In Open Pit Mines Using the Inverse-velocity Method-Case Examples. In: *1st Canada-US Rock Mechanics Symposium*. American Rock Mechanics Association.

Ruina, A. (1983). Slip instability and state variable friction laws. *Journal of Geophysical Research: Solid Earth*, *88*(B12), 10359-10370.

SafeLand (2012). Deliverable D5.1. Compendium of tested and innovative structural, non-structural and risk-transfer mitigation measures for different landslide types (rev 2- Final dated April 2012) prepared by Studio Geotecnico Italiano S.r.l. (SGI).

Saito, M. (1969) Forecasting Time of Slope failure by Tertiary Creep. In: *Proceedings of the 7th International Conference on Soil Mechanics and Foundation Engineering*, Mexico City. 2, 677–683.

Saito, M., Uezawa M. (1961). Failure of soil due to creep. In: *Proceedings of the 5th*

Saito, M. (1965). Forecasting the time of occurrence of a slope failure. In: *Proceedings of 6th International Conference Soil Mechanics and Foundation Engineering*, 537-541.

Scoppettuolo, M.R., Cascini, L. Un modello attritivo dipendente dalla velocità di deformazione per la frana di Vallcebre. *Incontro annuale dei ricercatori di Geotecnica (IARG)*- Matera, 5-7 July 2017. (in Italian).

Scoppettuolo, M.R., Cascini, L., Babilio, E. (2020). Typical displacement behaviours of slope movements. *Landslides*. https://doi.org/10.1007/s10346-019-01327-z

Secondi, M.M., Crosta, G.B., di Prisco, C., Frigerio, G., Frattini, P., Agliardi, F. (2011). Landslide motion forecasting by a dynamic visco-plastic model. In: *Proceedings of Second World Landslide Forum (WLF 2).* Rome, 3-9 October 2011. Paper WLF2-(2011)-0571.

Segalini, A., Valletta, A., Carri, A. (2018). Landslide time-of-failure forecast and alert threshold assessment: A generalized criterion. *Engineering geology, 245*, 72-80.

Semenza, E. (2001). La storia del Vajont, raccontata dal geologo che ha scoperto la frana. Tecomproject, Ferrara. (in Italian)

Shuzui, H. (2001). Process of slip-surface development and formation of slipsurface clay in landslides in Tertiary volcanic rocks, Japan. *Engineering Geology, 61*, 199– 220.

Simeoni, L., Mongiovì, L., (2007). Inclinometer Monitoring of the Castelrotto Landslide in Italy. *Journal of Geotechnical and Geoenvironmental Engineering, 136*, 653-666.

Singh, A. (1966). Creep phenomena in soils. *PhD thesis,* University of California, Berkeley, California.

Skempton, A. W. (1953). Soil mechanics in relation to geology. *Proceedings of the Yorkshire Geological Society, 29*(1), 33-62.

Suwa, H., Mizuno, T., Ishii, T. (2010). Prediction of a landslide and analysis of slide motion with reference to the 2004 Ohto slide in Nara, Japan. *Geomorphology, 124*(3-4), 157-163.

Tacher, L., Bonnard, Ch., Laloui, L., Le Parriaux, A. (2005). Modelling the behaviour of a large landslide with respect to hydrogeological and geomechanical parameter heterogeneity. *Landslides, 2*, 3–14.

Terzaghi K. (1950). Mechanism of landslides. *Application of geology to engineering practice*, Geol. Soc. Am, 83-123.

Tika T. E., Vaughan P. R., Lemos, L. (1996). "Fast shearing of pre-existing shear zones in soil", *Géotechnique, 46*(2), 197–233.

Tommasi, P., Pellegrini, P., Boldini, D., Ribacchi, R. (2006). Influence of rainfall regime on hydraulic conditions and movement rates in the overconsolidated clayey slope of the Orvieto hill (central Italy). *Canadian geotechnical journal, 43*(1), 70-86.

U.S. Geological Survey. (2004). Landslides type and processes. https://pubs.usgs.gov/fs/2004/3072/fs-2004-3072.html. Accessed 2 December 2019.

Varnes D.J. (1984). Landslides Hazard Zonation: A Review of Principles and Practice. The UNESCO Press, Paris, *3*, 63 pp.

Varnes, D. J. (1978). Slope movement types and processes. *Special report,* 176, 11-33.

Voight, B. (1988). A method for prediction of volcanic eruptions. *Nature, 332*, 125–130.

Voight, B. (1989). A relation to describe rate-dependent material failure. *Science, 243* (4888), 200–203.

Voight, B., Kennedy, B.A. (1979). Slope failure of 1967–1969, Chuquicamata mine, Chile. *Developments in Geotechnical Engineering*, Rockslides and Avalanches 2 - Engineering sites, Elsevier, Amsterdam, *14B*, 595-632.

Walker, F., Blong, R.J., McGregor, J.P. (1987). Landslide classification, geomorphology, and site investigations. *Soil Slope Instability and Stabilisation,* Balkema, Rotterdam, 1-52.

Working Party on World Landslide Inventory (1990). A suggested method for reporting a landslide. *Bulletin of International Association of Engineering Geology, 41*, 5–12.

Working Party on World Landslide Inventory (1991). A suggested method for a landslide summary. *Bulletin of International Association of Engineering Geology, 43*, 101–110.

Working Party on World Landslide Inventory (1993). A suggested method for describing the activity of a landslide. *Bulletin of International Association of Engineering Geology, 47*, 53-57.